Skolkovo Institute of Science and Technology

ROLE OF LNCRNA LL35 IN HEPATOCYTE FUNCTION

Doctoral Thesis

by

EVGENIIA SHCHERBININA

DOCTORAL PROGRAM IN LIFE SCIENCES

Supervisor
Dr. Timofei Zatsepin

Moscow - 2022

I hereby declare that the work presented in this thesis was carried out by myself at Skolkovo Institute of Science and Technology, Moscow, except where due acknowledgement is made, and has not been submitted for any other degree.

Candidate (Evgeniia Shcherbinina)
Supervisor (Dr. Timofei Zatsepin)

Abstract

Glucose and lipid metabolism are an essential part of eukaryotic cell biogenesis and may be regulated *via* multiple cellular pathways and mechanisms. Multiple studies have shown that, along with other regulators, long non-coding RNAs play an important role in the regulation of glucose and lipid metabolism. Human lncRNA DEANR1 has been shown to regulate a variety of biological processes such as cell proliferation, apoptosis, glucose metabolism and tumorigenesis and even act as tumor suppressors in several cancer types. Murine lncRNA LL35/Falcor shares similar genomic locus as DEANR1 and was described as a possible functional analog of DEANR1 in lungs.

In this work we have shown that LL35 is the functional analog of DEANR1 in the liver and established the significance of LL35 for normal hepatocytes function *in vitro* and *in vivo*. We demonstrated that LL35 is downregulated in hepatocellular carcinoma and after partial hepatectomy, as well as in hepatoma cell lines in comparison to normal cells. Application of high throughput approaches like RNA-seq, LC-MS proteomics, lipidomics and metabolomics revealed changes caused by LL35 depletion in transcriptome, proteome, lipidome and metabolome of hepatocytes. Our data revealed that LL35 is involved in glycolysis and lipid biosynthesis in AML12 cells and a murine liver. Particularly, LL35 inhibition caused downregulation of plasmanyl-/plasmenylphosphatidylcholines (O-PC/P-PC) both *in vitro* and *in vivo*, while phosphatidylethanolamines (PE), hexosylceramides (HexCer) were increased only in cells, and diradylglycerols (DG), ceramides (Cer;O2) and lysophosphatidylcholines (LPC) – only in the liver. Moreover, LL35 affects Notch and NF-κB signaling pathways in normal hepatocytes. All observed changes result in the decrease of viability and migration of hepatocytes. We demonstrated similar phenotype changes between murine LL35 and human DEANR1 depletion *in vitro* and *in vivo* that opens the opportunity to translate the obtained results for LL35 in the murine liver to possible functions of human lncRNA DEANR1.

Publications

1. **Shcherbinina, E**., Abakumova, T., Bobrovskiy, D., Kurochkin, I., Deinichenko, K., Stekolshchikova, E., Anikanov, N., Ziganshin, N., Melnikov, P., Khrameeva, E., Logacheva, M., Zatsepin, T. & Sergeeva, O. (2022). Murine Falcor/LL35 lncRNA Contributes to Glucose and Lipid Metabolism In Vitro and In Vivo. Biomedicines. 10, 1397. https://doi.org/10.3390/biomedicines10061397

2. Sergeeva, O., Abakumova, T., Kurochkin, I., Ialchina, R., Kosyreva, A., Prikazchikova, T., Varlamova, V., **Shcherbinina, E.** & Zatsepin, T. (2021). Level of Murine DDX3 RNA Helicase Determines Phenotype Changes of Hepatocytes In Vitro and In Vivo. International journal of molecular sciences, 22(13), 6958. https://doi.org/10.3390/ijms22136958

3. Belicova, L., Repnik, U., Delpierre, J., Gralinska, E., Seifert, S., Valenzuela, J. I., Morales-Navarrete, H. A., Franke, C., Räägel, H., **Shcherbinina, E.**, Prikazchikova, T., Koteliansky, V., Vingron, M., Kalaidzidis, Y. L., Zatsepin, T., & Zerial, M. (2021). Anisotropic expansion of hepatocyte lumina enforced by apical bulkheads. The Journal of cell biology, 220(10), e202103003. https://doi.org/10.1083/jcb.202103003

4. Kovalenko, T. F., Yadav, B., Anufrieva, K. S., Rubtsov, Y. P., Zatsepin, T. S., **Shcherbinina, E. Y.**, Solyus, E. M., Staroverov, D. B., Larionova, T. D., Latyshev, Y. A., Shakhparonov, M. I., Pandey, A. K. & Pavlyukov, M. S. (2022). Functions of long non-coding RNA ROR in patient-derived glioblastoma cells. Biochimie, 200, 131–139. Advance online publication. https://doi.org/10.1016/j.biochi.2022.05.015

Table of Contents

List of Symbols, Abbreviations

3′ UTR – 3′ untranslated region

AML12 – alpha mouse liver 12 cell line established from hepatocytes

ASO – antisense oligonucleotide

ceRNA – competing endogenous RNA

CCND1 – cyclin D1

Cer – ceramides

DEANR1 – definitive endoderm-associated lncRNA1

DG (DAG) – diacylglycerol (diradyglycerol)

DNA – deoxyribonucleic acid

EMT – epithelial-mesenchymal transition

FOXO1 – forkhead box O1 protein

FOXO3 – forkhead box O3 protein

GalNAc – N-Acetylgalactosamine

HCC – hepatocellular carcinoma

KD – knockdown

LC-MS – liquid chromatography with mass spectrometric detetction

lncRNA – long non-coding RNA

lincRNA – long intergenic RNA

LPC – lysophosphatidylcholines

LSD1 – lysine-specific demethylase 1

LTBP3 – latent transforming growth factor-β (TGF-β)-binding protein 3

Luc – luciferase

Malat1 – metastasis-associated lung adenocarcinoma transcript 1

miRNA – microRNA

mRNA – messenger RNA

NAT – natural antisense transcript

NGS – next generation sequencing

NMD – nonsense-mediated mRNA decay

nt – nucleotides

PAGE – polyacrylamide gel electrophoresis

PCR – polymerase chain reaction

PC – phosphatidylcholin

PE – phosphatidylethanolamine

PI – propidium iodine

PRC1 – polycomb repressive complex 1

PRC2 – polycomb repressive complex 2

PS – phosphatidylserine

PTC – premature termination codon

PVDF – polyvinylidene difluoride

RFI – relative fluorescent intensity

RIP - RNA immunoprecipitation

RNA - ribonucleic acid

RNAi – RNA interference

RT-qPCR – reverse-transcription quantitative polymerase chain reaction

s.d. – standard deviation

siRNA – small interfering RNA

SOD2 – superoxide dismutase 2

TG (TAG) – triacylglycerol (triacylglyceride)

WT – wild-type

WB – western blot

Xist – X-inactive specific transcript

Chapter 1. Introduction

The overwhelming part of the mammalian genome consists of non-coding genes. Their transcription results in the formation of RNAs that in most cases do not encode any proteins or peptides. Long non-coding RNAs (lncRNAs) - RNA molecules longer than 200 nt, represent more than 50% of all non-coding transcripts and usually demonstrate tissue specific expression [1]. Along with proteins, lncRNAs regulate different processes within the cell, including disease development, moreover lncRNAs can serve as prognostic markers or participate in maintaining the normal cell biogenesis. Despite their important role in the processes of the eukaryotic cell, functions of the majority lncRNAs and the mechanism of their action remain unexplored [2]. We want to mention that their sequence conservation between different species is poor that significantly complicates their studies [3]. Investigation of murine analogues of human lncRNAs can help to uncover their roles in *in vivo* studies. Conditional knockout mice or tissue-specific knockdown can help to understand the influence of lncRNA on the development [4,5] or to study lncRNA roles in multiple disease models [6].

Human lncRNA DEANR1 is downregulated in multiple cancer types, such as hepatocellular carcinoma, endometrial carcinoma, prostate, pancreatic, breast and lung cancer and involved in many processes crucial for cancer development [7–12]. Acting as a tumor suppressor, DEANR1 can inhibit tumor growth by cell apoptosis stimulation and cell proliferation downregulation [13]. It also inhibits epithelial-mesenchymal transition (EMT), thus promoting the reduction of cancer cells invasiveness [14,15]. Moreover in pancreatic cancer DEANR1 could reduce glycolysis, thus, suppressing tumor growth [10].

It was also described that DEANR1 linked to the regulation of several signaling pathways, particularly, inhibits the activation of the Wnt pathway [16], interferes with p38 MAPK and Notch signaling pathways [12]. Despite its multiple roles in different diseases, the functional utility of DEANR1 in normal liver has never been investigated.

DEANR1 shares similar genomic locus with murine lncRNA LL35/Falcor (NCBI - 9030622O22Rik), which was proposed to be a possible functional analog of DEANR1 in lungs [5]. The promoter region, transcriptional start site and first exon of LL35 have strong conservation across all primates and placental mammals [5]. LL35 expression was predominantly observed in murine lung and liver tissues [5,17]. The functional significance of LL35 during regeneration after lung injury was already described by Swarr et al [5]. LL35 knockout disturbed the integrity of the epithelial airway barrier and impaired epithelial regeneration after injury in lungs *in vivo* [5]. However, significance, functions and mechanisms of action of LL35 in mouse liver remained unknown. This study is devoted to the establishing whether LL35 is a functional analog of DEANR1 in liver and to study the functional role of LL35 in normal hepatocytes *in vitro* and *in vivo.*

Chapter 2. Literature Review

2.1 LncRNAs: function, evolutionary conservation and mechanisms of action

Human and mouse genomes have only about 20,000 protein coding genes, while the number of total transcripts in their cells is more than 100,000. The rest of the genome consists of genes that do not encode proteins and pseudogenes. Several groups of non-coding transcripts, currently known as long non-coding RNAs (lncRNAs), form the majority (more than 50%) of all non-coding transcripts [1].

LncRNAs are transcripts between 200 nt and 100 kb in length, which predominantly do not code peptides or proteins. Nevertheless, some of them may have short open reading frames (ORFs.). Similar to protein-coding mRNAs, lncRNAs are transcribed by RNA polymerase II and may have cap structures and polyA tails [18]. Now several classes of lncRNAs are described: long intergenic non-coding RNAs, long non-coding antisense transcripts, long intronic non-coding RNAs, non-overlapping antisense lncRNAs [19]. The expression levels of lncRNAs are usually lower than expression of protein-coding mRNAs and are tissue specific [20].

LncRNAs are much less conserved between species than protein-coding genes [20]. The homology criteria for lncRNAs are still under consideration. Some studies revealed that conservation should be primarily preserved on secondary structure functional sites than on nucleotide sequences. Other publications claim that for lncRNAs homology the conservation of only their promoters is sufficient [21]. The presence of functional analogues of human lncRNA in other species, especially in mice, offers significant advantages to study them and to test potential therapies. Particularly, to avoid

creating complex xenografts models to study the influence of human lncRNA on organs development or their role in multiple diseases, it is less challenging to generate a mice with knockout of functional analogue of certain human lncRNA and further translate results of such research to human [4,5,22,23]. For example, lncRNA H19 is abundantly expressed in failing human hearts. Choong et al. generated H19 knockout mice and showed, that during cardiac remodeling process after infarction lncRNA H19 regulates fibrosis acting *via* YB-1 protein [24]. The presence of an analogue of human lncRNA HOTAIR in mice made it possible to study HOTAIR mechanism of action and function in cardiomyocytes after LPS-induced sepsis for better understanding of its role in cardiac diseases [6]. Thus, the presence of lncRNA animal analogues provides more opportunities to study their functions and to test potential therapies associated with them *in vivo*.

The function of most lncRNAs remains unknown, but rapid development of biotechnology helps this area to grow faster [3,18]. It has been shown that in mammals lncRNAs are able to regulate genes expression at many levels and by various mechanisms. They regulate gene transcription by mediating changes in chromatin modifications and DNA methylation or by direct binding to proteins, such as transcription factors, and/or DNA; post-transcriptional mRNA processing; mRNA translation and post-translational protein modification (**Figure 1**) [18].

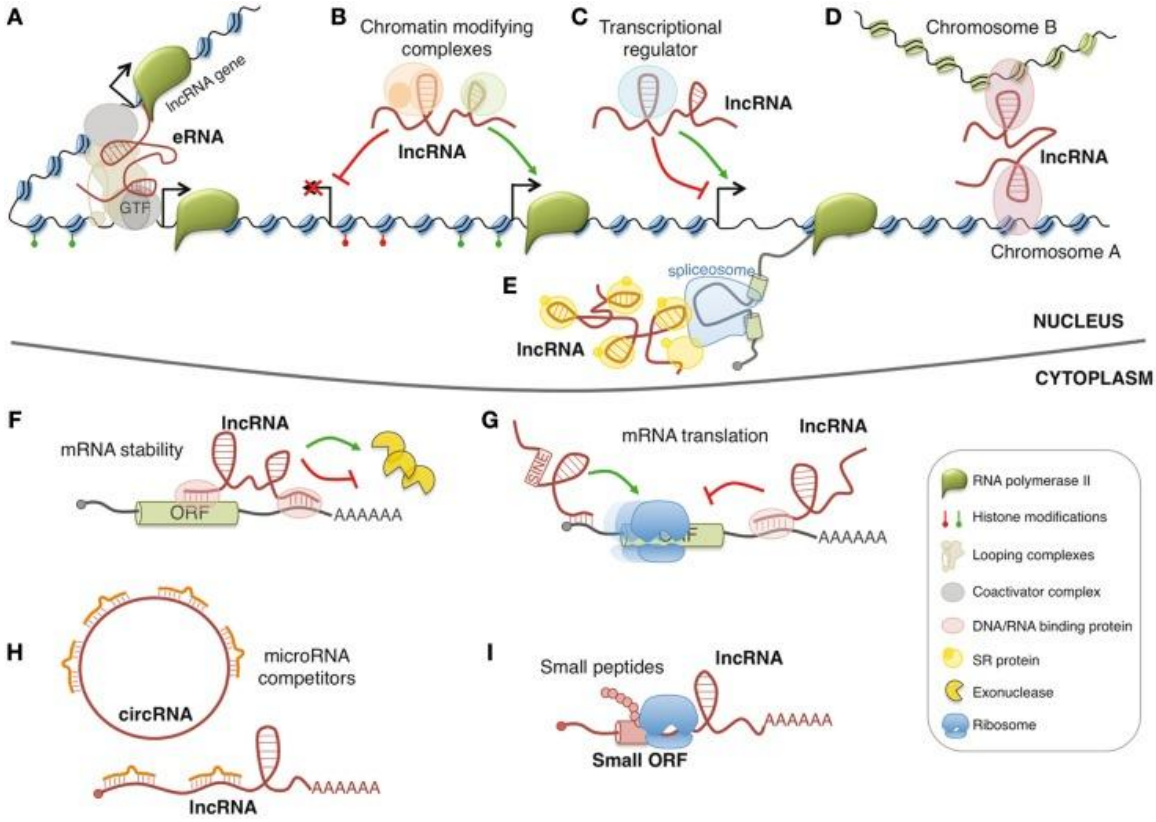

Figure 1. *Sketch of the main mechanisms of lncRNAs action. In nucleus lncRNAs (**A**) act as enhancer RNA (eRNA), (**B**) recruit chromatin modifying complexes, (**C**) regulate activity of transcription factors, (**D**) act on the spatial conformation of chromosomes or (**E**) influence pre-mRNA splicing. In cytoplasm lncRNAs (**F**) regulate mRNA stability, (**G**) mRNA translation, (**H**) compete for microRNA binding. (**I**) A small number of lncRNAs have short open reading frames (ORFs) and can be further translated in biological active peptides. Adapted from* [25].

2.1.1 LncRNAs regulate histone modifications on the chromatin level

Epigenetics is the key mechanism to modulate gene transcription without changes in DNA sequences. LncRNAs are important epigenetic regulators and can influence on the chromatin structure by different mechanisms, such as regulation of histone or DNA modifications, primarily methylation and acetylation, and chromatin remodeling [26].

Now we will consider the most studied examples of epigenetic regulation co-mediated by lncRNAs.

2.1.1.1 LncRNAs regulate histone methylation via binding to histone-modified enzymes or complexes

Histone methylation has an opposite effect on gene transcription depending on its localization. For example, methylation at H3K4, H3K36, H3K79 activates transcription, while H3K9, H3K27 and H4K20 downregulate gene expression [18,27]. Most common ways for modulation of histone modifications by lncRNAs are direct binding to histone methyltransferases or demethylases, thus, attracting chromatin-modifying complexes (**Figure 1B**) [18].

The lncRNA ST3Gal6-AS1 is transcribed in the opposite direction of ST3Gal6 gene from its promoter region. Expression of both transcripts are positively correlated and downregulated in colorectal cancer. Hu et al. showed that ST3Gal6-AS1 interacts with methyltransferase MLL1 and brings it to the promoter of ST3Gal6. MLL1 induces H3K4me3 modification, which activates transcription of ST3Gal6 [28].

Another lncRNA FEZF1-AS1 is overexpressed in gastric cancer that correlates with the poor prognosis for patients and larger size of tumors. Liu et al. found that elevated expression of FEZF1-AS1 leads to increased proliferation of gastric cancer cells due to cell cycle progression and downregulated apoptosis. RIP assay and RNA-pulldown assay showed that FEZF1-AS1 binds lysine-specific demethylase 1 (LSD1). LSD1 induces H3K4me2 demethylation at the p21 promoter, which leads to the inhibition of p21 transcription and, thus, cell cycle progression [29].

Interaction of mammalian lncRNAs with histone-modifying complexes in a greater extent exhibits itself in binding with polycomb repressive complexes, PRC2 and PRC1 [26]. PRC2 methylates lysine 27 in histone 3 (H3K27me), that is associated with repression of transcription, and PRC1 monoubiquitinates lysine 119 in histone H2A [30]. X-inactive specific transcript (Xist) ensures the same embryonic development for men and women due to silencing of the entire X chromosome in female embryos. Xist, which is highly expressed from the inactive X chromosome, interacts with PRC2 and recruits it to the X chromosome to silence genes expression [31]. P53 induced noncoding transcript (Pint) controls cell proliferation and survival by recruiting PRC2 to the target genes promoters, which provides genes silencing caused by promoters H3K27 trimethylation [32,33]. LncRNA HOTAIR is transcribed from the gene cluster HoxC and have an ability to regulate transcriptional silencing of genes located in another locus HoxD. The type of regulation when lncRNA influence distant genes is called *in trans* regulation. HOTAIR targets both PRC2 and histone H3K4me1/2 demethylase LSD1 to cause HoxD silencing [26,34].

2.1.1.2 LncRNAs regulate histone acetylation via binding to histone-modified enzymes or complexes

Histone methylation is a hallmark of transcription silencing, while histone acetylation activates genes transcription, and deacetylation turns it off. Acetylation occurs at lysine residues and is catalyzed by histone acetyltransferase (HAT), and deacetylation is mediated by histone deacetylase (HDAC). The most common sites of histone acetylation are H3K4Ac, H3K9Ac, H3K27Ac, H3K56Ac, and H4K16Ac. The

mechanism of the regulation of histone acetylation by lncRNAs is similar to the regulation of histone methylation by lncRNAs (**Figure 1B**). They activate or inhibit gene transcription by binding to histone acetyltransferases and deacetylases, such as HDAC, HAT, CREB-binding protein (CBP/p300), K acetyltransferase 2A (KAT2A), sirtuin 6 (SIRT6) [18].

Jain et al. were looking for p53-regulated lncRNAs with high expression in pluripotent human embryonic stem cells (hESC). They identified lncPRESS1 which controls a set of genes than induce pluripotency of hESC. The underlying mechanism is as follows: lncPRESS1 interacts with deacetylase SIRT6 and interferes with its binding to chromatin, thus, maintaining high levels of H3K56 and H3K9 acetylation at the promoter regions of genes responsible for cells pluripotency [35].

2.1.1.3 LncRNAs regulate histone methylation and acetylation remodeling

Besides binding with single protein to regulate histone methylation or acetylation, lncRNAs may act as molecular scaffolds and bind several proteins simultaneously (**Figure 2**) [18]. For example, gastric cancer-associated lncRNA 1 (GClnc1) forms a complex with KAT2A and H3K4 methyltransferase WDR5. This interaction causes an increase in H3K4me3 and H3K9ac in promoter regions of GClnc1 target genes. WDR5/KATA2 complex targets multiple genes in human genome, including superoxide dismutase 2 (SOD2). Most probably SOD2 transcriptional upregulation mediates GClnc1 positive correlation with gastric cancer cell proliferation, invasiveness and metastasis [36].

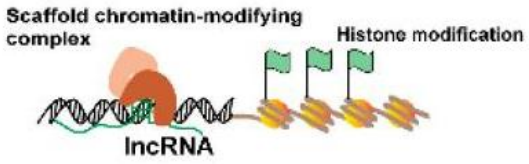

Figure 2. *LncRNAs act as a scaffold to regulate histone modifications Adapted from* [18].

2.1.2 LncRNAs regulate DNA methylation at the DNA level by interacting with DNA methylases

Another epigenetic mechanism to regulate gene expression besides histone modification is methylation of DNA itself. DNA methylation predominantly occurs at CpG islands located in the gene promoter region and is catalyzed by DNA methyltransferases. Such DNA methylation causes silencing of gene transcription. LncRNAs are able to recruit DNA methyltransferases to their target sites, providing an alternative solution for transcriptional regulation (**Figure 3**) [18].

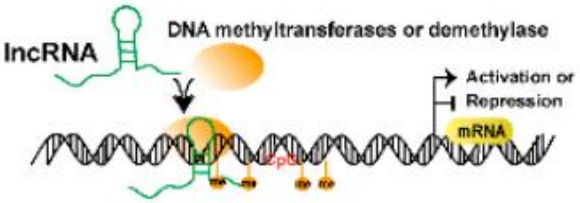

Figure 3. *LncRNAs regulate DNA methylation. Adapted from* [18].

For example, lncRNA ATB in renal carcinoma cells binds to the maintenance methyltransferase DNMT1 and recruits it to p53 promoter. DNMT1-mediated methylation of p53 promoter results in p53 silencing. Thus, cancer cells with activated ATB have showed increased proliferation and migration, and decreased apoptosis [37]. Moreover, some lncRNAs can bind to different DNA methyltransferases at once. So,

LINC00313 recruits both DNMT1 and DNMT3B to the promoter of aristaless-like homeobox 4 (ALX4) gene. Excess methylation of ALX4 promoter leads to gene transcription suppression and promotes thyroid cancer progression [18,38].

2.1.3 LncRNAs participate in the process of transcriptional regulation

Besides regulation of gene transcription through chromatin or DNA modification, lncRNAs can directly regulate this process by different mechanisms. The most common mechanisms that we would like to consider are: a) direct binding of lncRNAs to DNA followed by inhibition of transcription, and b) interaction with proteins, such as transcription factors, that regulate transcription (**Figure 4**) [18].

Figure 4. *LncRNAs activate or repress transcription via direct binding to transcription factors. Adapted from* [18].

LncRNA Malat1 (metastasis-associated lung adenocarcinoma transcript 1) is a multifunctional lncRNA. In genome MALAT-1 is located upstream to LTBP3 (latent transforming growth factor-β (TGF-β)-binding protein) gene, which controls TGF-β activation and bioavailability. Both Malat1 and LTBP3 expression is upregulated in mesenchymal stem cells in patients with myeloma. One of Malat1 mechanisms of action is direct binding to the transcription factor Sp1 together with the formation of a stable complex with LTBP3 promoter that facilitate the recruitment of Sp1 to LTBP3 promoter. Overexpression of LTBP3 results in the increased TGF-β secretion from patients'

mesenchymal stem cells [39]. LINC01355 serves as a good example of how lncRNA interaction with transcription factor may repress transcription of a target gene. The transcription factor forkhead box O3 (FOXO3) is a transcriptional repressor for cyclin D1 (CCND1) gene, which is involved in breast cancer cells proliferation. LINC01355 stabilizes FOXO3 by direct interaction with it. LINC01355 is downregulated in breast cancer, but its overexpression promotes FOXO3 enrichment at CCND1 promoter region, thus, repressing CCND1 gene expression, which results in cell cycle arrest at the G0/G1 phase [40].

2.1.4 LncRNAs are involved in post-transcriptional regulation

LncRNAs also carry out the post-transcriptional regulation of mRNAs, primarily by influencing the following processes in the cell: alternative splicing, binding of miRNA, RNA editing, protein translation and transport [18].

2.1.4.1 LncRNAs regulate alternative splicing

Alternative splicing is inherent in eukaryotes and expands protein diversity together with the regulation of gene expression [41]. Splicing consists of multiple steps and is catalyzed by a complex machine called spliceosome. Besides spliceosome a large number of RNA-binding proteins and splicing factors, which contain RNA-binding domains, participate in the regulation of splicing. LncRNAs can directly bind to these proteins, thus, regulating alternative splicing (**Figure 5**) [18].

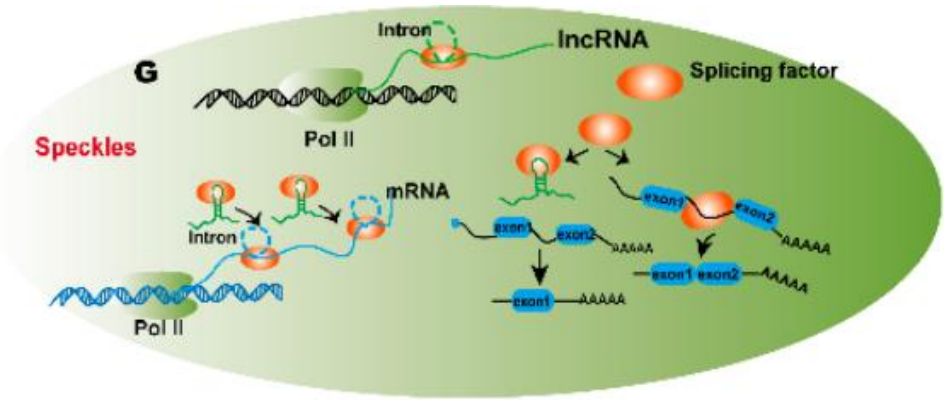

Figure 5. *LncRNAs can regulate alternative splicing. Adapted from* [18].

LncRNA MALAT1 localizes to nuclear speckles and interact with several serine/arginine rich proteins, which are involved in alternative splicing regulation. Binding with MALAT1 determines the distribution of SR proteins in nuclear speckles: attraction of SR proteins to the transcriptional active region by MALAT1 regulates cleavage of pre-mRNA [42]. LncRNA Morrbid (myeloid RNA repressor of Bcl2l11 induced death) interacts with SFPQ (splicing factor proline and glutamine rich) and NONO (non-POU domain-containing octamer-binding protein) splicing complex and regulates NRAS (neuroblastoma RAS viral oncogene homolog) splicing in hepatocytes. Morrbid expression promotes synthesis of NRAS isoform with inclusion of premature terminal codons (PTC), which serves as a signal for NRAS degradation via NMD (nonsense-mediated mRNA decay) pathway [43].

2.1.4.2 LncRNAs - molecular sponges for miRNAs

Some lncRNAs may act as sponges for microRNA (miRNA). Most often miRNA repress target mRNA translation or cause its degradation *via* binding to its 3′ UTR

(untranslated region). This binding depends on many factors, including the abundancy of both miRNA and target mRNA [44]. Some lncRNAs include specific sites complementary to miRNA sequences. Due to the complementarity of sequences they bind miRNA acting like a sponge and preventing miRNA from interaction with their targets (**Figure 6**) [45]. Single lncRNA can sponge several different miRNAs, while single miRNA can be bound by multiple lncRNAs. For example, the lncRNA IMFNCR competitively binds two different miRNAs: miR-128-3p and miR-27b-3p. PPARG (peroxisome proliferator-activated receptor-gamma) is a direct target for both miRNAs, which bind to its 3'UTR and *via* attracting of minimal miRNA-induced silencing complex (miRISC) cause PPARG mRNA cleavage. Thus, INFNCR activity increases PPARG expression by sequestering miR-128-3p and miR-27b-3p, preventing them from binding to PPARG mRNA for its silencing and promotes intramuscular adipocyte differentiation [46]. LncRNA TRPM2-AS serves as a sponge for tumor suppressive miR-612. TRPM2-AS is upregulated in gastric cancer and promotes cell proliferation and tumor progression. The underlying mechanism is the following: TRPM2-AS sequesters miR-612, which prevents its binding to IGF2BP1 and FOXM1 mRNAs for their further degradation. Upregulated IGF2BP2 increases expression of cMyc protein, thus promoting cell proliferation. Also, enhanced expression of FOXM1 promotes cells radioresistance [47].

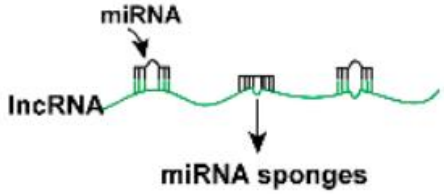

***Figure 6**. LncRNAs act as miRNAs sponge. Adopted from* [18].

2.1.4.3 LncRNAs mediate RNA decay

mRNA redundancy directly influences on the protein production and is determined by either transcription amount or mRNA decay. LncRNAs can interfere with both transcription (described above) and decay of mRNA. The class of lncRNAs termed half-Staufen 1 (STAU1) – binding site RNAs (1/2-sbsRNAs) participate in STAU-1-mediated mRNA decay (SMD). These lncRNAs are involved in the formation of a STAU1-binding site (SBS) between their Alu element and the Alu element in the 3'-UTR of target mRNA. Functional SBS transactivates STAU1 facilitating its binding to target mRNA and promotes binding of UPF1 protein to STAU1 followed by mRNA degradation [48]. Another lncRNA MEG3 (maternal expression gene 3) binds to polypyrimidine tract-binding protein 1 (PTBP1) and facilitates PTBP1 interaction with CDS region of small heterodimer partner (SHP) mRNA. Overexpression of PTBP1 and MEG3 leads to SHP mRNA decay that promotes liver fibrosis [49].

2.1.5 LncRNAs encode peptides

Initially, lncRNAs were described as RNAs which do not encode proteins, but recently it was shown that functional micropeptides could be translated from some lncRNAs (**Figure 1I**). For example, conserved in vertebrates lncRNA LINC00948 has a

small ORF, which results in translation of 46 amino acids microprotein called myoregulin (MLN). MLN is expressed predominantly in skeletal muscle and regulates Ca^{2+} entering the sarcoplasmic reticulum [50]. LINC00116 encodes Mtln peptide, which is detected in mitochondria of mouse cell lines and tissues. The lack of Mtln decreases the activity of mitochondrial respiratory chain complex I. Mtln interacts with NADH-dependent cytochrome b5 reductase and stimulates complex I functioning most probably by providing a favorable lipid composition of the membrane [51].

2.1.6 LncRNAs are involved in translational regulation

Besides transcriptional and post-transcriptional regulation of gene expression, lncRNAs also participate in the regulation of mRNA translation (**Figure 7**). LincRNA-p21 was first described as a transcriptional repressor of p53 target genes *via* affecting p53-mediated apoptosis, but later its additional role as a translational modulator was determined. Linc-p21 association with RNA-binding protein HuR facilitates the recruitment of let-7/Ago2, which results in decrease of lincRNA-p21 stability and its further degradation. This event promotes HuR binding to β-catenin (CTNNB1) and JUNB mRNAs, thus increasing their translation. Hence, downregulated HuR promotes accumulation of lincRNA-p21 that stimulates interactions with CTNNB1 and JUNB mRNAs and decreases their translation [52].

LncRNA GAS5 can directly interact with translation initiation complex EIF4E, thus, decreasing cMyc translation [53]. Another lncRNA RP1-5O6.5 disrupts the interaction of eIF4E with eIF4G *via* binding to eIF4E. Thus, RP1-5O6.5 inhibits the translation of negative regulator of Snail protein in breast cancer cells – p27kip1 [54].

One more lncRNA involved in the regulation of translation is treRNA, which activity inhibits the translation of E-cadherin. TreRNA first binds to several ribonucleoproteins (RNPs), including SF3B3, hnRNP K, PUF60, FXR1 and FXR2, and then the formed complex interacts with eIF4G1 [55].

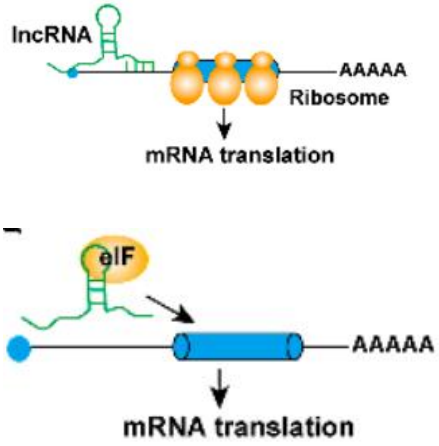

Figure 7. *LncRNAs affect mRNA translation via binding mRNA or the translation initiation complex eIF. Adopted from* [18].

2.1.7 LncRNAs regulate post-translational modifications of proteins

Post-translational modifications of proteins influence on diverse cell processes by regulating proteins activity, stability, conformation and interaction with other molecules. More than 20 types of proteins modifications are currently known, and lncRNAs are involved in many of them. Predominantly they regulate proteins phosphorylation, ubiquitination and acetylation (**Figure 8**) [18].

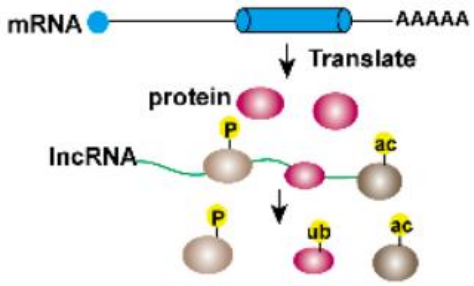

Figure 8. *LncRNAs interact with proteins and control protein phosphorylation, acetylation, and ubiquitination at the post-translation level. Adapted from* [18].

Protein phosphorylation of serine and tyrosine residues plays an important role in cellular signal transduction. LncRNA lnc-DC mediates human dendric cells differentiation *via* direct interaction with signal transducer and activator of transcription 3 (STAT3). Lnc-DC binds to STAT3 in cytoplasm and prevents its interaction with protein tyrosine phosphatase SHP1, which dephosphorylates STAT3. Thus, lnc-DC promotes STAT3 phosphorylation of Tyr705 and activates downstream transcriptional activity [56]. LncRNA HULC is upregulated in hepatocellular carcinoma and promotes malignant cell proliferation by inducing G1/S transition in the cell cycle. HULC specifically interacts with Y-box binding protein 1 (YB-1), which as a part of translationally inactive messenger ribonucleoprotein particles keeps mRNA in a silent state. Increase in HULC expression leads to YB-1 phosphorylation by activating ERK pathway and its release from complexes with oncogenic mRNAs, such as cyclin D1, cyclin E1 and MMP11. Reinforced translation of these mRNAs results in increased cell proliferation and tumor progression [57].

Protein ubiquitination serves as a label for protein degradation in proteasome with the involvement of three enzymes: ubiquitin-activating enzyme (E1), ubiquitin-binding

enzyme (E2) and ubiquitin protein ligase (E3). Among others, one of the functions of lncRNA HOTAIR (HOX antisense intergenic RNA) is regulation of protein ubiquitination. HOTAIR plays a role of a scaffold molecule, which brings together E3 ubiquitin ligases Mex3b and Dzip3 with their substrates Snurportin-1 and Ataxin-1, resulting in substrate degradation [58]. LncRNA uc.134 binds to E3 ubiquitin ligase CUL4A, promoting its nuclear accumulation, while knockout of uc.134 causes the increase in CUL4A protein cytoplasmic level. CUL4A activates ubiquitination of LATS protein kinase – a member of the Hippo signaling pathway. Thus, active uc.134 binds to CUL4A and prevents its translocation to cytoplasm, which, in turn, decrease LATS1 degradation and induce Hippo signaling [59].

Non-histone protein acetylation and deacetylation play an important role in cellular signaling and can be regulated by lncRNAs. For instance, lncRNA MALAT1 regulates the activity of SIRT1 deacetylase through interaction with DBC1 (depleted breast cancer 1) protein, which binds to the catalytic domain of SIRT1 and inhibits its deacetylation activity. Active SIRT1 promotes p53 deacetylation, which inhibits its transcriptional activity [60].

2.2 LncRNAs regulate cellular metabolism

The relationship between cellular metabolism and lncRNAs was first observed during cancer progression, where lncRNAs changes its expression, which correlates with the induced metabolism of cancer cells. Thus, investigation of the nature of this relationship is an important task [61,62]. Liver is a central organ in the body, which coordinates multiple diverse metabolic processes, and glucose and lipid metabolism

among them. Multiple studies tried to uncover the role of lncRNAs in the regulation of these processes in the liver, as well as in different types of cancer [63]. In this review we will focus on lipid and glucose metabolism and their regulation by lncRNAs.

2.2.1 Liver lipid metabolism

Glucose serves as a main metabolic source for liver, and when the levels of carbohydrates in the liver are increased, glucose is converted into fatty acids. In addition, fatty acids enter the liver from the outside from the bloodstream, where they get from the adipose tissues or gastrointestinal tract after the food digestion. Fatty acids are precursors for triglyceride (TAG) and cholesterol esters. Newly synthesized TAG and cholesterol esters could be further secreted as very-low-density lipoprotein (VLDL) particles or accumulated inside hepatocytes in the form of lipid droplets. In addition, fatty acids are part of phospholipids, VLDL, surface layers of lipid droplets, bile particles. Under the fasting conditions, fatty acids enter mitochondria, where undergo oxidation for energy generation and ketone bodies formation [64].

When carbohydrates are abundant, the hepatic lipogenic program is arranged as follows (**Figure 9**). Glucose is converted into pyruvate *via* glycolysis pathway. Pyruvate then enters mitochondria and utilizes by pyruvate dehydrogenase complex (PDC) to form acetyl-CoA. Citrate synthase (CS) catalyzes the reaction of citrate synthesis from acetyl-CoA and oxaloacetate. Citrate is then secreted into the cytoplasm, where it breaks down by ATP-citrate lyase (ACL) into acetyl-CoA and oxaloacetate, which further forms malat. Malic enzyme converts malate into pyruvate, which is accompanied by the release of NADPH. Newly synthesized pyruvate again enters mitochondria, where undergo

carboxylation by pyruvate carboxylase (PC). The oxaloacetate formed in this pathway drives continuous citrate synthesis. In the cytoplasm, acetyl-CoA carboxylase (ACC) converts acetyl-CoA to form malonyl-CoA. Synthesized in the course of these reactions NADPH and malonyl-CoA serves as precursors to 16-carbon palmitic acid synthesis by fatty acid synthase (FAS). Family members of fatty acyl-CoA elongase (Elovl) elongates palmitic acid to generate long-chain fatty acids (LCFAs) with chains longer than 16 carbons. After, stearoyl-CoA desaturases (SCDs) catalyzes desaturation of LCFAs with formation of mono- and poly-unsaturated LCFAs [64].

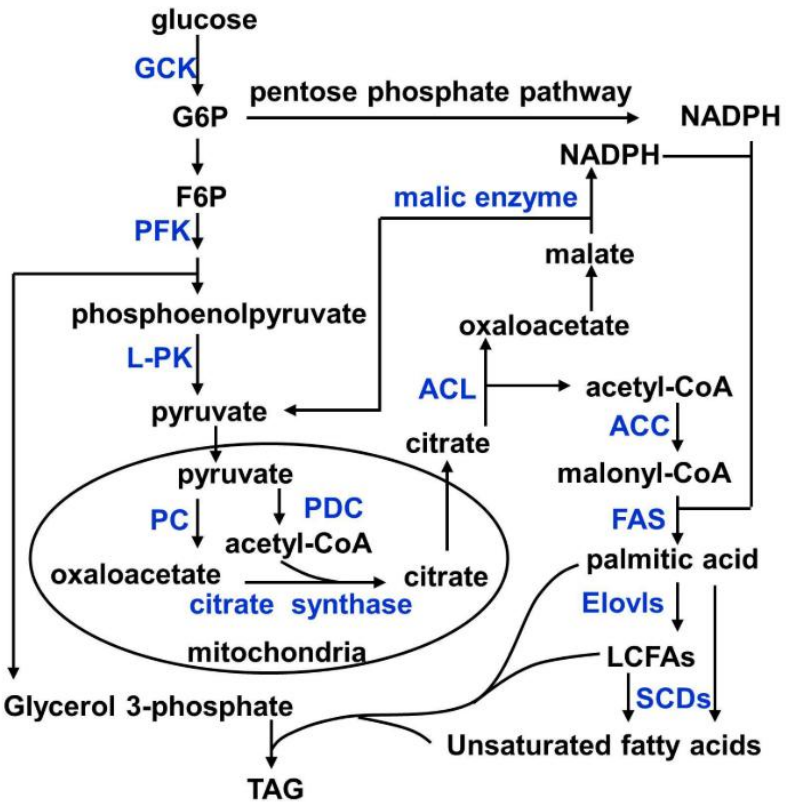

Figure 9. *Lipogenic pathways. Lipogenic enzymes are marked in blue. ACL: ATP-citrate lyase; ACC: acetyl-CoA carboxylase; FAS: fatty acid synthase; Elovls: fatty acyl-CoA elongases; SCDs: stearoyl- CoA desaturases. Adapted from [64].*

Under normal conditions, the liver stores little TAG and exports them in VLDL particles to deliver fatty acids to muscle and fat tissues. At the same time the increased TAG storage and VLDL secretion play a protective role against hepatotoxicity mediated by fatty acids. In most mammalian cells the main pathway of TAG synthesis is the glycerol-3-phosphate (G3P) pathway. G3P pathway starts with a rate-limiting step, when a long-chain acyl-CoA esterified to G3P by G3P acyltransferase (GPAT) enzyme. Lysophosphatidic acid (LPA), which is formed during this step, is then acylated by the acylglycerol-3-phosphate acyltransferases (AGPAT) to produce a phosphatidic acid (PA). PA can further participate in the synthesis of glycerolphospholipids and cardiolipins or convert to diacylglycerol (DG) by dephosphorylation by phosphatidate phosphohydrolase (PAP). DG serves as a precursor for TAG, phosphatidylcholine (PC) and phosphatidylethanolamine (PE) (PC and PE synthesis and function will be discussed further in this review). DG acylation to TAG is catalyzed by DG acyltransferase (DGAT). Newly formed TAG is then from cytosolic lipid droplets or VLDL [65]. It is important to notice that DG can promote insulin resistance in hepatocytes *via* activation of protein kinase C epsilon (PKCε), which phosphorylates insulin receptor substrate (IRS) proteins [64].

The process of lipogenesis can be controlled by various mechanisms and we will focus on some of them, such as availability of lipogenic substrates, control by multiple transcription factors and co-regulators and stimulation by insulin [64]. Pyruvate is a main carbon source for lipogenesis and links this process with glycolysis. Availability of pyruvate is regulated by multiple glycolytic enzymes, primarily by glucokinase (GCK),

which catalyzes the first step of glycolysis and which activity is regulated by GCKR (GCK regulator). Mutations in GCKR are associated with hepatic steatosis and hyperglycemia in patients with obesity [66]. Deletion of liver receptor homologue 1 (LRH-1) downregulates GCK, leading to reduced glycolysis and lipogenesis on liver [67]. Another substrate, which drives lipogenesis, is NADPH that can be synthesized not from malate, but also come from pentose phosphate pathway. Glucose-6-phosphate dehydrogenase and 6-phosphogluconate dehydrogenase participate in the lipogenesis regulation.

Lipogenesis is also controlled by various transcription factors and their co-regulators through the transcriptional regulation of glycolytic and lypogenic genes. We would like to highlight the following factors: ChREPB, SREBP, LXR, FXR, PPARγ and PPARδ. They will be discussed in the next chapter, since they are also involved in the regulation of glucose metabolism. Moreover, insulin activates mTORC1 *via* the PI3K/AKT pathway. Meanwhile, mTORC1 mediates insulin stimulation of the expression of SREBP-1 and lipogenesis. Also, insulin stimulates glycolysis, thus, providing pyruvate available for lipogenesis [64].

In the next sections of this literature review we would like to focus on the lipid classes which turned out to be important for our research.

2.2.2 Phosphatidylcholine and phosphatidylethanolamine metabolism and function in liver

Phosphatidylcholine (PC) and phosphatidylethanolamine (PE) belong to the class of phospholipids, which are a key component of eukaryotic cell membranes. Moreover,

metabolism of phospholipids plays an important role in the regulation of lipid, lipoprotein and whole-body energy metabolism and its abnormal functioning may be associated with the development and progression of various diseases [68].

To prevent lipotoxicity TAGs-incorporated excess intracellular fatty acids are accumulated in cytosolic lipid droplets. Lipid droplets consist of neutral lipids surrounded by a monolayer of phospholipids, including PC and PE. Their relative abundance on the lipid droplets surface plays a crucial role for the dynamics of lipid droplets. For example, a higher relative quantity of PE promotes fusion of smaller lipid droplets. On the other hand, downregulation of PC biosynthesis leads to the increase of lipid droplets size [68].

SREBP-1a and SREBP-1c transcription factors regulate genes involved in cholesterol, fatty acid, phospholipid and TAG biosynthesis. Despite that insulin is the main regulator of SREBP-1 processing, there is some evidence, that phospholipids also regulate the SREBP-1 pathway of lipogenesis. For example, in mammalian cells PC can suppress the activation of SREBP-1. Particularly, in human hepatoma cells and murine liver with inhibited PC synthesis due to depletion of crucial for its synthesis enzymes, increased level of mature SREBP-1 was observed [69].

Speaking about the importance of PC and PE in proper liver function, we would like to note that the molar ratio between PC and PE is a key determinant of liver health. It was shown that alterations in the hepatic PC/PE molar ratio clearly correlate with the development of non-alcoholic fatty liver disease (NAFLD) in humans, liver failure and impaired liver regeneration [68].

2.2.2.1 Phosphatidylcholine synthesis in the liver

In mammalian cells biosynthesis of PC occurs *via* CDP-choline or the Kennedy pathway (**Figure 10**). Three classes of choline transporters (the high-affinity transporter, the intermediate-affinity transporters, the low-affinity organic cation transporters) help choline to enter the cell. Inside the cell choline is immediately phosphorylated to phosphocholine by the choline kinase (CK) using ATP. Then CTP:phosphocholine cytidylyltransferase (CT) (encoded in mice by Pcyt1a and Pcyt1b genes) converts phosphocholine to CDP-choline. This reaction is the rate-limiting for PC synthesis *via* the Kennedy pathway. During the last reaction of CDP-choline pathway two enzymes: CDP-choline:1,2-diacylglycerol cholinephosphotransferase (CPT) (encoded by Chpt1 gene) and CDP-choline:1,2-diacylglycerol choline/ethanolamine phosphotransferase (CEPT) (encoded by Cept1 gene) transfer phosphocholine from CDP-choline to diacylglycerol (DAG), thus, producing PC [68].

In the liver one more pathway for PC synthesis exists in addition to the described above CDP-choline pathway. The enzyme phosphatidylethanolamine N-methyltransferase (PEMT) uses S-adenosylmethionine (AdoMet) as a methyl group donor and catalyzes the methylation of PE to form PC. In mouse PEMT has high expression only in the liver. Summarizing, in murine liver approximately 70% of PC is synthesized by the CDP-choline pathway, while the rest 30% of PC is generated by PEMT [70].

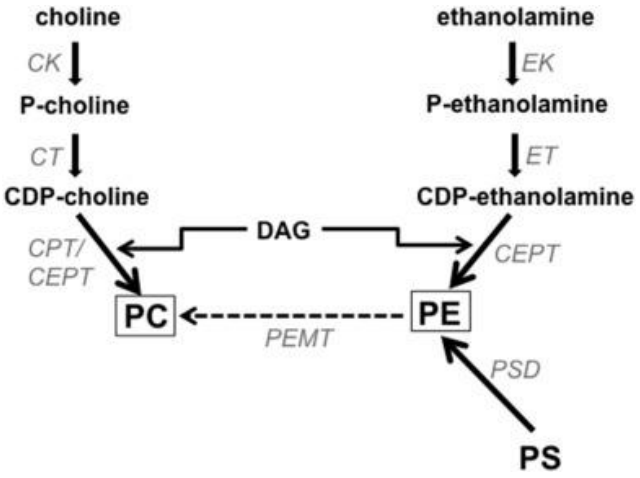

Figure 10. *Phosphatidylcholine (PC) and phosphatidylethanolamine (PE) synthesis pathways. CK: choline kinase; CT: phosphocholine cytidylyltransferase; CTP: CDP-choline:1,2-diacylglycerol cholinephosphotransferase (CPT); CEPT: CDP-choline:1,2-diacylglycerol choline/ethanolamine phosphotransferase; EK: ethanolamine kinase; ET: CTP:phosphoethanolamine cytidylyltransferase; PEMT: phosphatidylethanolamine N-methyltransferase; PSD: phosphatidylserine decarboxylase. Adapted from* [68].

2.2.2.2 Phosphatidylethanolamine synthesis in the liver

There are two major pathways of PE biosynthesis occurred in ER and mitochondria that mammalian cells utilize. The first CDP-ethanolamine pathway is similar to CDP-choline pathway and occurs in ER. After entering the cell ethanolamine is phosphorylated by cytosolic ethanolamine kinase (EK), encoded by Etnk1 and Etnk2 genes and abundant in the liver (**Figure 10**). Then phosphoethanolamine is converted to CDP-ethanolamine with the formation of pyrophosphate by the enzyme called enzyme CTP:phosphoethanolamine cytidylyltransferase (ET). This reaction is a rate-limiting for CDP-ethanolamine pathway. The last step of PE synthesis in CDP-ethanolamine pathway, when CDP-ethanolamine and DAG are converted to PE, is mediated by CEPT or CDP-ethanolamine:1,2-ethanolaminephosphotransferase [68].

The second pathway of PE synthesis occurs on the outer aspect of mitochondrial inner membranes and is called the PSD pathway. In the PSD pathway phosphatidylserine (PS) serves as a substrate for PE synthesis and is converted by phosphatidylserine decarboxylase (PSD), encoded by Pisd gene. PS translocation from ER to the mitochondria inner membrane is a rate-limiting step of PSD pathway [68].

2.2.2.3 Lysophosphatidylcholine synthesis and function

Lysophosphatidylcholine (LPC) is another class of phospholipids, changes in the synthesis of which occur in various diseases, including diabetes and cancer. In the liver tissue LPC participates in the downregulation of genes involved in hepatic fatty acid oxidation and meanwhile upregulates genes of cholesterol biosynthesis. An increase in LPC concentration in hepatocytes disrupts mitochondrial integrity and enhances cytochrome C release. LPC is synthesized *via* two pathways. First, phospholipase A2 (PLA2) enzyme cleaves PC to form LPC, that can be reversed by lysophosphatidylcholine acyltransferase (LPCAT), which converts LPC back to PC in the presence of Acyl-CoA. Second, LPC is formed during the transfer of fatty acids to free cholesterol by lecithin-cholesterol acyltransferase (LCAT) [71].

2.2.3 Production and function of ceramide in the liver

Ceramide belongs to sphingolipids, which mediate many cellular functions as bioactive signaling molecules. Ceramide, in particular, regulates cell apoptosis, cell cycle arrest and stress response. Ceramide synthesis may be induced by multiple stimuli, such as tumor necrosis factor-α (TNF-α), heat stress, oxidative stress, Fas ligand and etc. [72]

There are several pathways of ceramide synthesis inside the cell (**Figure 11**). The de novo synthesis of ceramide utilizes serine and palmitoyl-CoA and can be stimulated by oxidative stress, metabolic loading with serine, and oxidized LDL. Ceramide de novo synthesis involves four steps, as a result of which serine and palmitoyl-CoA converts to ceramide by the sequential action of the following enzymes: serine palmitoyl-CoA transferase (SPT), 3-oxosphinganine reductase, sphingosine N-acyltransferase and dihydroceramide desaturase. The reaction catalyzed by SPT is a rate-limiting step of ceramide de novo synthesis. Redox status of the cell can regulate ceramide synthesis *via* inhibition of dihydroceramide desaturase by glutathione (GSH) [73].

Another way to generate ceramide occurs by the hydrolysis of sphingomyelin in cell membranes catalyzed by neutral sphingomyelinase (N-SMase) (encoded by Smpd1 gene). Inflammation upregulates both de novo pathway and N-SMase activity. In contrary, GSH can inhibit N-SMase activity and reduce ceramide synthesis from sphingomyelin. Finally, in salvage pathway the ceramide synthase (encoded by Asah1 gene) induces reacylation of sphingosine generated from catabolism of complex sphingolipids to form ceramide [73].

Liver is a key site for ceramide production, aberrations in ceramide synthesis are linked to liver pathological conditions, such as liver steatosis, fibrosis and NAFLD. Moreover, ceramides promote insulin resistance by inhibiting AKT activation [73].

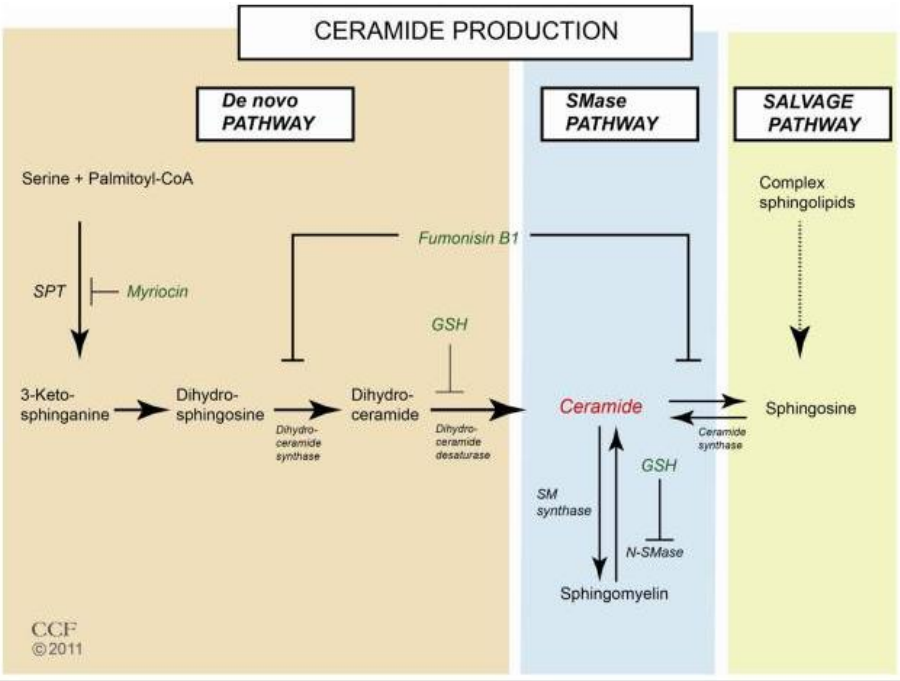

Figure 11. *Three pathways of ceramide production. SPT: serine palmitoyl-CoA transferase; GSH: glutathione. Adapted from* [73].

2.2.4 LncRNAs participate in lipid biosynthesis

In tumor cells increased lipid synthesis results in excessive amount of membrane phospholipids, which serve as a material for cell proliferation and division, and in a large number of lipid signaling molecules, participating in cancer progression, like phosphatidylinositol, sphingomyelin and others [74]. FASN serves as a main rate-limiting enzyme in the pathway of fatty acid biosynthesis, and it has been observed that some lncRNAs can regulate its activity. LncRNA HAGLR (or HOXD-AS1), is upregulated in NSCLC (non-small cell lung carcinoma) and is usually associated with the poor prognosis for patients. Knockdown of HAGLR results in the arrest of cell cycle in G1 phase, which decreases the invasion ability and proliferation of NSCLC cells. Moreover,

downregulation of HAGLR reduces the free fatty acids amount and downregulated FASN expression level [75]. Another lncRNA HOTAIR is upregulated in human nasopharyngeal carcinoma cells, which correlates with high levels of FASN in this cancer type. Meanwhile, HOTAIR knockdown downregulates FASN expression at both transcriptional and post-transcriptional levels, and reduces the amount of free fatty acid [76]. In osteosarcoma cells, lncRNA Pvt1 sequesters miR-195, which leads to the upregulation of expression levels of FASN, Cyclin D1 and Bcl2 (B-cell lymphoma 2) [77]. LINC01138 interacts with protein arginine methyltransferase 5 and increases the methylation of SREBP1 at arginine, thus, LINC01138 participates in the regulation of lipid desaturation and renal cell carcinoma growth. (**Figure 12**) [78].

2.2.5 LncRNAs regulate lipolysis

The first step of lipid catabolism is fat mobilization, which is predominantly catalyzed by adipose triglyceride lipase (ATGL). Expression levels of ATGL vary in several types of cancer, such as NSCLC, pancreatic adenocarcinoma and hepatocellular carcinoma (HCC) [74]. Upregulation of ATGL in HCC induced production of DG and free fatty acids, leading to cancer cells growth. Liu et al. showed that lncRNA NEAT1 (Nuclear paraspeckle assembly transcript 1) could regulate ATGL expression *via* sponging miR-124-3p, thus, increasing ATGL level and HCC progression [79].

The most important pathway of fatty acid decomposition is β-oxidation of fatty acids (FAO), thus, lncRNAs, which regulate FAO also regulate lipolysis. The rate-limiting step of fatty acid oxidation is catalyzed by Acyl-CoA synthetase (ACS). LncRNA HULC, which expression is significantly elevated in hepatocellular carcinoma

can regulate lipogenesis by sequestring miR-9, which normally inhibits peroxisome proliferator-activated receptor alpha (PPARA), which in turn activatea ACS long-chain family members 1 (ACSL1) (**Figure 12**) [80].

In gastric cancer lncRNA MACC1-AS1 is significantly upregulated compared with healthy tissue. This occurs due to the activity of transforming growth factor β1. MACC1-AS1 sequesters miR-145-5p, preventing its inhibitory effect on FAO, which promotes stemness and chemoresistance of gastric cancer cells [74].

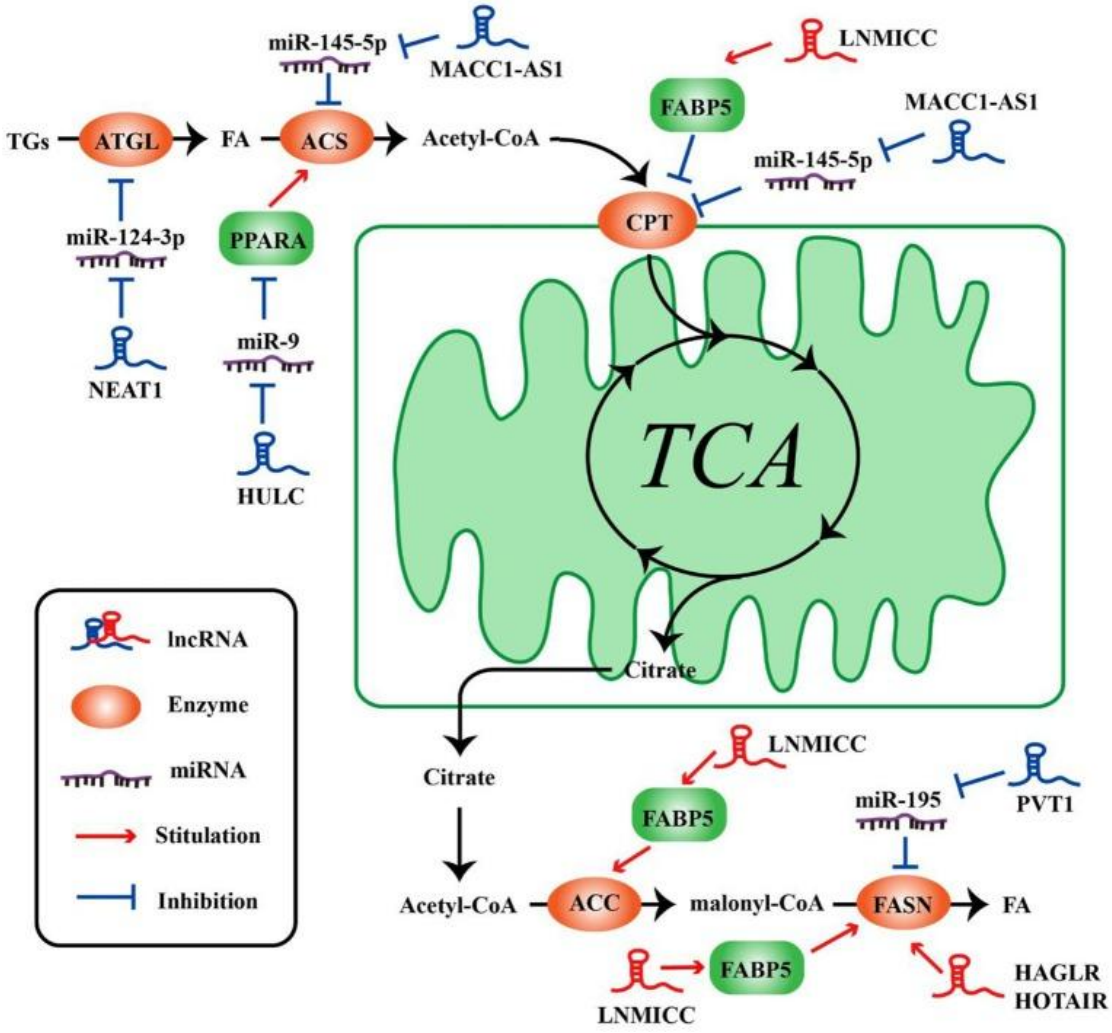

Figure 12. LncR*NAs regulate lipid metabolism in cancer cells. Adapted from* [74].

Inhibition of lncRNA MALAT1 prevents hepatic lipid accumulation *via* its ability to interact with nuclear SREBP-1c protein, which regulates transcription of crucial enzymes involved in lipid metabolism, such as SCD1, FAS, ACC1 and ACLY. Another lncRNA lncHR1 has an opposite effect on SREBP-1c expression unlike MALAT1. Overexpression of lncHR1 suppressed activation of SREBP-1c and FAS, leading to decrease TAG synthesis and lipid droplet formation in hepatocytes. Similarly, another lncRNA called Gm16551 negatively regulates SREBP-1c expression in murine liver. Yang et al. found that overexpression of SREBP-1c led to upregulation of Gm16551 and at the same time upregulation of Gm16551 inhibited elevated circulation of TAG and lipogenic genes, such as SCD1, FAS and ACLY, induced by SREBP-1c. Summing up, a negative loop between SREBP-1c and Gm1655 exists and is involved in the regulation of lipolysis [81].

It was demonstrated, that one of the mechanisms of apoptosis inhibition in cancer cells by lncRNAs is alteration of lipid metabolism and lipid toxicity. LncRNA SPRY4-IT1 (Sprouty4-intronic transcript 1) expression level is significantly higher in melanoma cells compared with normal melanocytes and its depletion promoted apoptosis and inhibited tumor cell proliferation and invasion. It was suggested that SPRY4-IT inhibits apoptosis *via* binding to lipid phosphatase LPIN2 leading to decrease in fatty acyl chains and TAG [82].

2.2.6 LncRNAs and phospholipids

Lu et al. demonstrated that lncRNA LOC100506036 can regulate expression of N-SMase, which converts sphingomyelin to ceramide, thus, driving the inflammatory process in Rheumatoid arthritis [83]. Phospholipase D (PLD) catalyzes the hydrolysis of PC to form PA. In different cancer types upregulation of phospholipase D (PLD) stimulates tumor growth by suppressing aberrant apoptotic programs. PLD inhibitor destabilizes mTOR to promote cell autophagy and has anti-tumor properties. In lung cancer lncRNA ANRIL (antisense non-coding RNA in the INK4 locus) is responsible for anti-tumor effect of PLD inhibitor. Moreover, the depletion of ANRIL suppresses tumor cell apoptosis induced by PLD inhibitor [84]. LncRNA SNHG14 (Small Nucleolar RNA Host Gene 14) activates phospholipase PLA2G4A, which is also involved in DG synthesis *via* sponging miR-145-5p. Thus, SNHG14 induces activation of microglia cells through modulating the miR-145-5p/PLA2G4A axis [84].

Finally, lncRNAs can modulate cellular processes by direct interaction with phospholipids. Phosphoinositide 3-kinase (PI3K) produces phosphatidylinositol-3,4,5-trisphosphate (PIP3), which acts as a second messenger in multiple signaling pathways. Moreover, aberrations in PI3K expression and abnormal activation of its downstream effector AKT protein are common in multiple diseases and cancers. LncRNA LINK-A (long intergenic noncoding RNA for kinase activation) directly binds to PIP3 and AKT, thus, promoting interaction between AKT and PIP3. Activation of AKT by LINK-A leads to the tumorigenesis and resistance to AKT inhibitors. Notably, depletion of PIP3-

binding motif in LINK-A results in breast cancer cells positive response to AKT inhibitors [85].

2.2.7 Glucose metabolism

Lipid and glucose metabolism ate tightly related to each other. Pyruvate is a product of glycolysis and is further decarboxylized to acetyl-CoA, which participates in tricarboxylic acid cycle (TCA). Glucose 6-phosphate after degradation in the pentose-phosphate shunt provides NADPH, which serves as a substrate for *de novo* lipogenesis. Moreover, both lipid and glucose metabolism are regulated by insulin *via* PI3K pathway and the same transcription factors regulate the expression of genes involved in both of these processes [86].

Glucose is the major source of carbon required for cellular biosynthesis and energy generation. Under feeding conditions, carbohydrates from food are digested in the gastrointestinal tract to monosaccharides, primarily glucose. Through the bloodstream, glucose is then transported to different tissues for further ATP generation. The process of glucose breakdown into pyruvate is named glycolysis and serves as a main pathway of ATP production in most mammalian tissues. In tissues with the large number of mitochondria, pyruvate dehydrogenase complex converts pyruvate into acetyl-CoA inside mitochondrial matrix. Acetyl-coA together with oxaloacetate enter tricarboxylic acid cycle. Tricarboxylic acid cycle, also known as citric acid cycle or the Krebs cycle, leads to the release of stored energy via generation of GTP – energy equivalent of ATP, NADH and FADH2. Electron transport chain-oxidative phosphorylation leads to ATP production, while NADH and FADH2 are significant electron carries during this process (**Figure 13**).

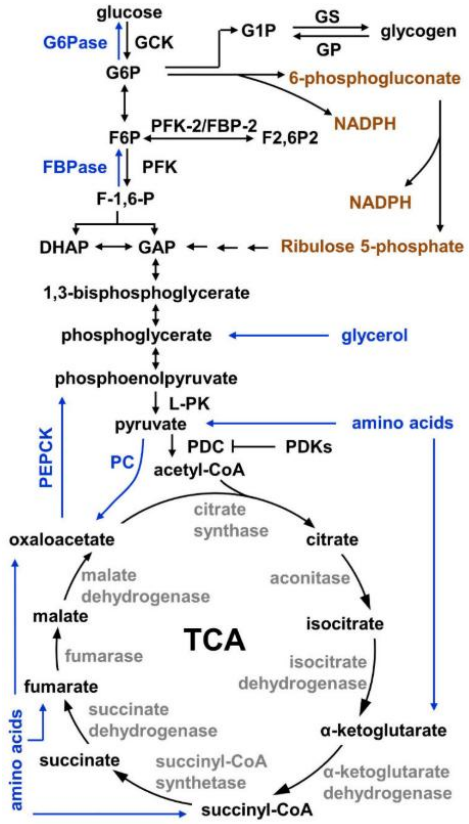

Figure 13. *Glucose metabolism pathways. Gluconeogenic pathways are marked in blue, and the pentose phosphate pathway is marked in orange. GCK: glucokinase; G6Pase: glucose-6-phosphatase; G6P: glucose 1-phosphate; G1P: glucose 1-phosphate; GP: glycogen phosphorylase; GS: glycogen synthase; PFK: 6- phosphofructo-1 kinase; FBPase: fructose 1,6 bisphosphatase; GAP: glyceraldehyde 3-phosphate; DHAP: dihydroxyacetone phosphate; L-PK: liver pyruvate kinase; PC: pyruvate carboxylase; PDC: pyruvate dehydrogenase complex; PDKs: pyruvate dehydrogenase kinases. Adapted from* [64].

Liver is a key metabolic organ that regulates energy metabolism in the body. As a result of glycogenesis in the liver excess of carbohydrates is converted into glycogen. Glycogen is a branched glucose polymer that serves for energy storage in animals. Another pathway of excessive carbohydrates processing is their conversion into fatty acids during lipogenesis. Acetyl-CoA formed from pyruvate is incorporated into very low density lipoproteins and then transported to white adipose tissue [87].

In the fasted state the liver generates glucose for other tissues. Overexpression of the pancreatic hormone glucagon after activation *via* cascade of kinases leads to the release of glucose from glycogen. The process of glycogen conversion into glucose is called glycogenolysis [88]. Stored glycogen provides normal glucose homeostasis at night during sleep and fasting. But longer period of fasting leads to the depletion of liver glycogen storage and glucose is then synthesized *via* gluconeogenesis from non-carbohydrate precursors. Lactate from skeletal muscles and red blood cells and glycerol from adipose tissues are the main precursors for glucose synthesis during gluconeogenesis [89]. Liver energy metabolism is tightly controlled and regulated by multiple signaling pathways. Dysfunction of liver metabolism leads to the development of different diseases, such as diabetes [64].

Hepatocytes are the main functional cells of the liver - they represent about 80% of the total liver volume and perform metabolic, endocrine and secretory functions [90]. Glucose transporter type 2 (GLUT2) mediates both hepatocytes glucose uptake from the bloodstream and glucose release from the liver. However, in the case of GLUT2 deletion other mechanisms compensate normal glucose release from hepatocytes by additional transporters, such as GLUT1, or by other mechanisms. After entering the liver cell glucose undergo phosphorylation and forms glucose 6-phosphate (G6P). This process is mediated by glucokinase enzyme and leads to increased glucose uptake due to reduction of intracellular glucose level. Under fasting conditions G6P serves as a source of glucose: it is dephosphorylated by G6Pase to form a glucose inside the endoplasmic reticulum (ER). Under feeding conditions G6P participates in several different metabolic pathways.

First, through glycolysis pathway G6P is converted to pyruvate, which either is oxidized in mitochondria to generate ATP during TCA and oxidative phosphorylation or participates in lipogenesis to synthesize fatty acids. Second, G6P serves as a precursor for glycogen synthesis. Third, G6P is utilized to generate NADH in pentose phosphate pathway (PPP) [64].

Under feeding conditions, increased levels of blood glucose, amino acids and fatty acids lead to insulin secretion in pancreatic β-cells. Insulin activates serine/threonine-protein kinase AKT, which in turn phosphorylates and inactivates GSK-3, thus leading to activation of glycogen synthase and increased glycogen synthesis. At the same time glycogenolysis is suppressed because of the following cascade of reactions: insulin causes acetylation of glycogen phosphorylase which promotes its dephosphorylation and suppression by protein phosphatase 1 [91]. Insulin also increases G6P synthesis by activation of glucokinase, which activity also stimulates glucose uptake in hepatocytes. G6P as previously mentioned by allosteric regulation inhibits glycogenolysis and activates glycogenesis [92].

2.2.8 Control of hepatic glycolysis

Glycolysis is the pathway of glucose catabolism, which serves as an energy source. Among all enzymes that catalyze glycolysis, several ones are called rate-limiting and regulate this pathway. These three enzymes are glucokinase (GCK), phosphofructokinase-1 (PFK-1) and liver piruvate kinase (L-PK). As mentioned above, GCK catalyzes the first step of glycolysis and converts glucose into glucose 6-phosphate. PFK-1 converts fructose 6-bisphosphate into fructose 1,6-bisphosphate and L-PK

converts phospoenolpyruvate into pyruvate. All these enzymes are subjected to the allosteric regulation and their activity induces glycolysis [64,89].

Besides the regulation by rate-limiting enzymes, glycolysis is still controlled by several transcriptional mechanisms. Sterol regulatory element binding protein 1c (SREBP-1c) and carbohydrate response element binding protein (ChREBP) are the main transcriptional factors responsible for transcriptional activation of glycolytic genes during feeding and genes participating in biosynthesis of fatty acids (**Figure 14**). SREBP-1c activates transcription of GCK gene, and knockout of SREBP-1c leads to impaired glycolysis activation [93]. SREBP-1c itself is regulated by various mechanisms. For instance, insulin and oxysterol-sensing transcriptional factor liver X receptor (LXR) control transcription of SREBP-1c. Another transcriptional factor ChREBP, responsible for glycolysis regulation, is increased in the liver under feeding conditions [89]. ChREBP activates L-PK expression via interaction with E-box motifs in its promoter region [94]. There are evidences that LXR may activate transcription of ChREBP, but this fact is debatable, because LXR knockout does not lead to changes in ChREBP expression [95,96]. Additionally, phosphorylation of ChREBP at different sites determine its activity and localization [89].

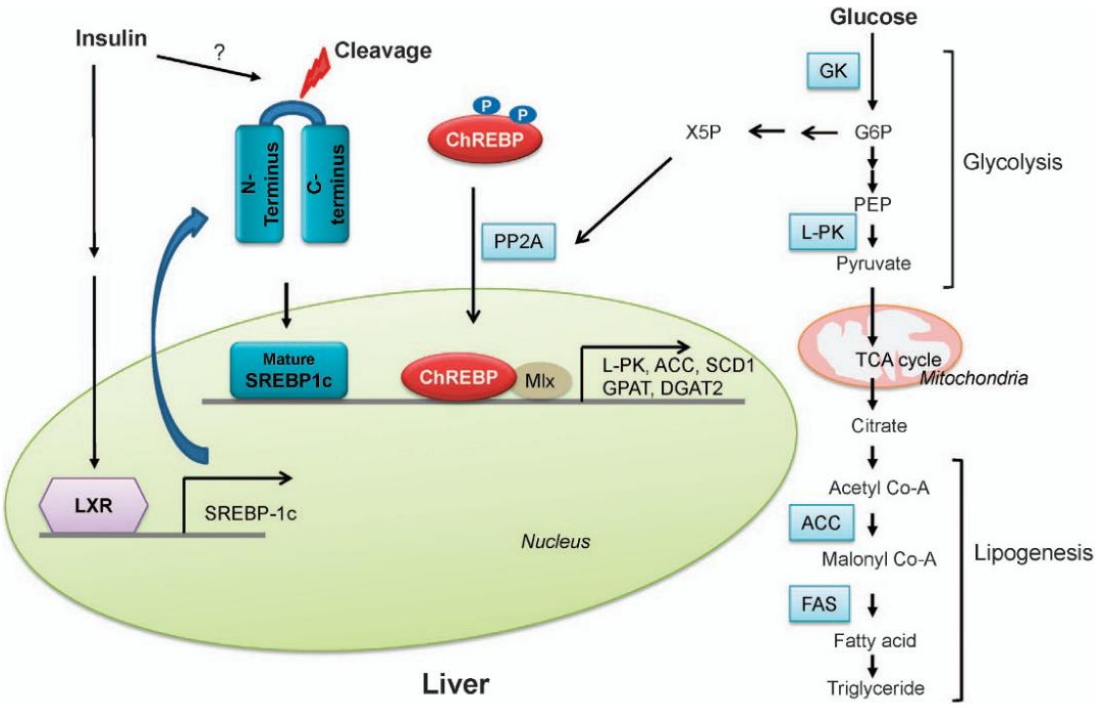

Figure 14. *Regulation of hepatic glycolysis. Adapted from* [89].

2.2.9 Control of hepatic gluconeogenesis

During a short period of fasting, glucose in the liver is produced by glycogenolysis pathway. During prolonged starvation, glycogen stores are not enough, therefore glucose in hepatocytes is synthesized through gluconeogenesis from lactate, pyruvate, glycerol and amino acids, which were produced inside the liver or delivered from other tissues. Schematically the gluconeogenesis pathway is as follows (**Figure 13**): lactate dehydrogenase oxidizes lactate to pyruvate, which is then converted by pyruvate carboxylase to oxaloacetate inside the mitochondria. Mitochondrial malate dehydrogenase reduces oxaloacetate to malate, which is then oxidized by cytoplasmic malate dehydrogenase back to oxaloacetate. The key step of gluconeogenesis is

conversion of oxaloacetate to phosphoenolpyruvate in cytoplasm catalyzed by cytoplasmic phosphoenolpyruvate carboxylase (PEPCK-C). A cascade of several reactions leads to the formation of fructose 1,6-bisphosphate from phosphoenolpyruvate. Dephosphorylation of fructose 1,6 bisphosphate by fructose 1,6-bisphosphatase results in the formation of fructose-6-phosphate, which is then converted to glucose-6-phosphate and goes to endoplasmic reticulum (ER) for glucose synthesis by glucose-6-phosphatase (G6Pase). Dephosphorylation of glucose-6-phospate by G6Pase is a second key rate-limiting step for gluconeogenesis and also for glycogenolysis. Other possible precursors for triggering gluconeogenesis are glycerate-3 phosphate formed from glycerol and α-ketoacids produced from amino acids [64,89].

There are multiple ways to regulate and control gluconeogenesis and I would like to focus on the main ones (**Figure 15**). First, gluconeogenesis can be regulated by accessibility of required substrates, primarily pyruvate. Pyruvate, produced through glycolysis and glycogenolysis under fasting conditions in skeletal muscles, may be used for acetyl-coA synthesis in mitochondria, which participates in TCA cycle, or it can be converted to lactate. Released lactate enters hepatocytes and is utilized in gluconeogenesis. Availability of pyruvate for gluconeogenesis is regulated by pyruvate dehydrogenase complex, responsible for acetyl-coA synthesis [97]. Additionally, glycerol synthesis and release from adipose tissue and access of amino acids are regulators of gluconeogenesis [64].

Second, gluconeogenesis is controlled by gluconeogenic enzymes, which in turn are regulated allosterically or *via* posttranscriptional modifications, predominantly by

acetylation [98]. Under fasting conditions, deacetylation of PEPCK-C by sirtuin 2 (SIRT2) stimulates gluconeogenesis, while under feeding conditions, acetylation of PEPCK-C by p300 induced by glucose leads to PEPCK-C ubiquitination and degradation [99].

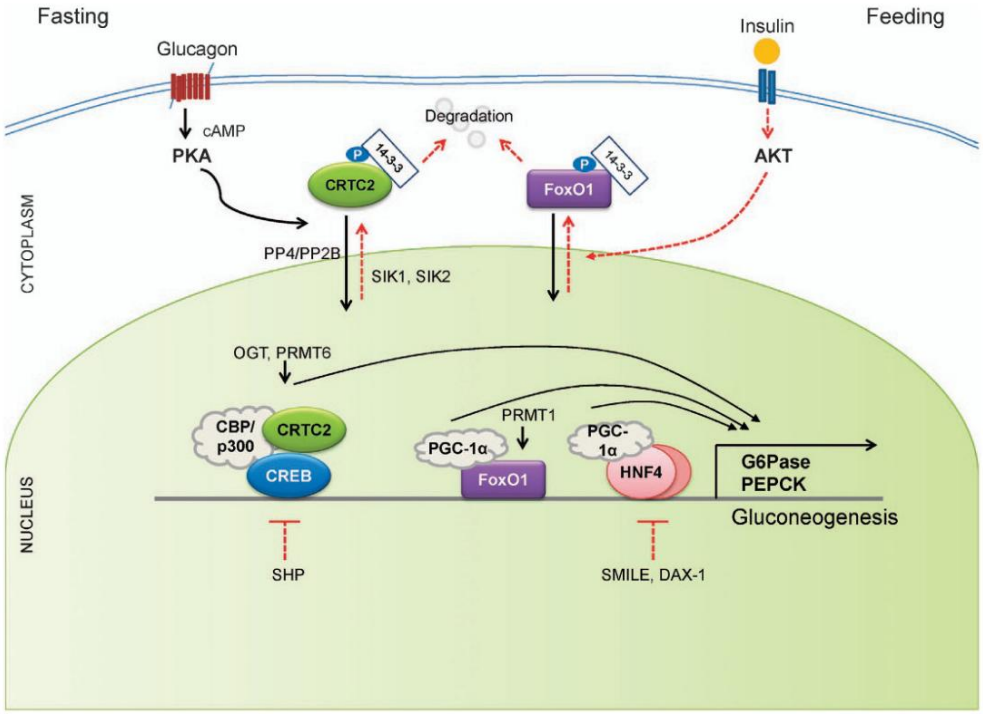

Figure 15. *Regulation of hepatic gluconeogenesis. Adapted from* [89].

Third, gluconeogenesis is tightly regulated by transcription factors that control the expression of key gluconeogenic genes. Transcription factor CREB (cAMP-response element (CRE) binding protein) interacts with CRE on gene promoter to promote the expression of target genes. PEPCK-C and G6Pase promoters contains CRE and are targeted by CREB transcription factor. CREB itself can be phosphorylated by protein kinase A (PKA), which becomes active after increased secretion of pancreatic glucagon

during fasting. Phosphorylated CREB has higher affinity to its co-activators, such as CBP/p300 and CRTC2, that leads to transcriptional activation of PEPCK-C and G6Pase [100]. Moreover, CREB regulates the activity of peroxisome proliferator γ-activated receptor coactivator 1-α (PGC1α), which activates gluconeogenic genes expression under prolonged fasting conditions [101,102]. Also, CREB activation mediates the expression of another transcription factor FOXO1 (forkhead box protein 1), which plays an important role in the regulation of gluconeogenesis [103].

Under fasting conditions, FOXO1 is dephosphorylated and moves to the nucleus, where it activates the transcription of PEPCK-C and G6Pase. This induces hepatic glucose production due to increased gluconeogenesis. Under feeding conditions, increased secretion of pancreatic insulin leads to the activation of PI3K/AKT signaling, which results in FOXO1 phosphorylation. Phosphorylated FOXO1 is translocated to the cytoplasm, which prevents transcriptional activation of gluconeogenic genes [103]. Similar to CREB, activation of PEPCK-C and G6Pase by FOXO1 is mediated by PGC1α transcriptional coactivator [104].

Another class of molecules important for gluconeogenesis regulation are transcriptional cofactors. Transcriptional cofactors form complexes with transcription factors to either activate or inhibit transcription of target genes [102]. PGC1α is one of the crucial cofactors involved in cell energy metabolism. PGC1α expression is significantly increased in the liver during long fasting. PGC1α promotes glucogenic genes expression predominantly via interacting with FOXO1, GR and HNF4α transcription factors [105]. Transcriptional coactivator CRTC2 is expressed in liver and

its activity and cellular localization are determined by its phosphorylation. During fasting CRTC2 is dephosphorylated by a number of serine/threonine phosphatases. Dephosphorylated CRTC2 is translocated to the nucleus, where it promotes expression of glucogenic genes *via* interaction with CREB. Additionally, CRTC2 dephosphorylation triggers H3K9Ac, which facilitates CRTC2 localization at PGC1α, PEPCK-C and G6Pase promoters. During feeding phosphorylated CRTC2 is retained in cytoplasm by 14-3-3 protein [106,107]. Pancreatic hormones, such as insulin and glucagon play a crucial role in hepatic gluconeogenesis regulation. Depending on the level of these hormones in the blood, which changes under fasting or feeding conditions, expression of gluconeogenetic genes is either activated or inhibited. Insulin is a peptide hormone secreted by β cells of the pancreatic islets. Insulin participates in the regulation of glucose transport, lipid synthesis, gluconeogenesis and glycogen synthesis *via* the PI3K/AKT signaling pathway [108]. Under feeding conditions, the level of glucose in the blood becomes higher, which stimulates insulin production by pancreatic beta cells. Secreted insulin binds to the insulin receptor (InsR) on the cell surface of target organ. This interaction simulates InsR kinase activation and recruitment of insulin receptor substrates (IRS), which results in PI3K activation. PI3K starts a cascade of reactions, resulting in AKT (protein kinase B) activation by its phosphorylation and localization at plasma membrane. Active AKT stimulates glucose utilization through inhibitory phosphorylation of FOXO1 and CRTC2, which leads to their retention in cytoplasm, thus, preventing activation of genes involved in gluconeogenesis.

Glucagon is insulin antagonist. It is also a peptide hormone, but secreted by pancreatic alpha cells. Fasting conditions cause increased glucagon production and its release from pancreas. Glucagon binds to G protein-coupled glucagon receptor (GCPR) on hepatocytes membrane, which results in CREB phosphorylation and activation. Activated CREB recognizes CRE in promoter regions of target genes, including PEPCK-C and G6Pase, which leads to induction of gluconeogenesis [102].

2.2.10 Role of lncRNAs in glucose metabolism under physiological conditions

Pancreas plays a central role in glucose metabolism by maintaining normal glucose level in the blood and lncRNAs are involved in important processes that occur in pancreatic β-cells, including their normal development. LncRNAs expression in pancreas is tissue-specific, associated with clusters of open chromatin and participate mainly in transcriptional regulation [109]. LncRNA H19 controls β-cells expansion via let-7 miRNA and activation of Akt signaling pathway. H19 inhibition results in decreased β-cells expansion in newborns, while its re-expression increases β-cells proliferation in adults [110]. Recently identified β-cell long intergenic RNA 1 (βlinc1) also plays an important role in proper functioning of pancreas. βlinc1 regulates a number of islet-specific transcription factors located in its genomic neighborhood, which contribute to the correct functioning of endocrine cells. βlinc1 deletion causes defects in islets development and disrupt glucose metabolism (**Figure 16**) [111].

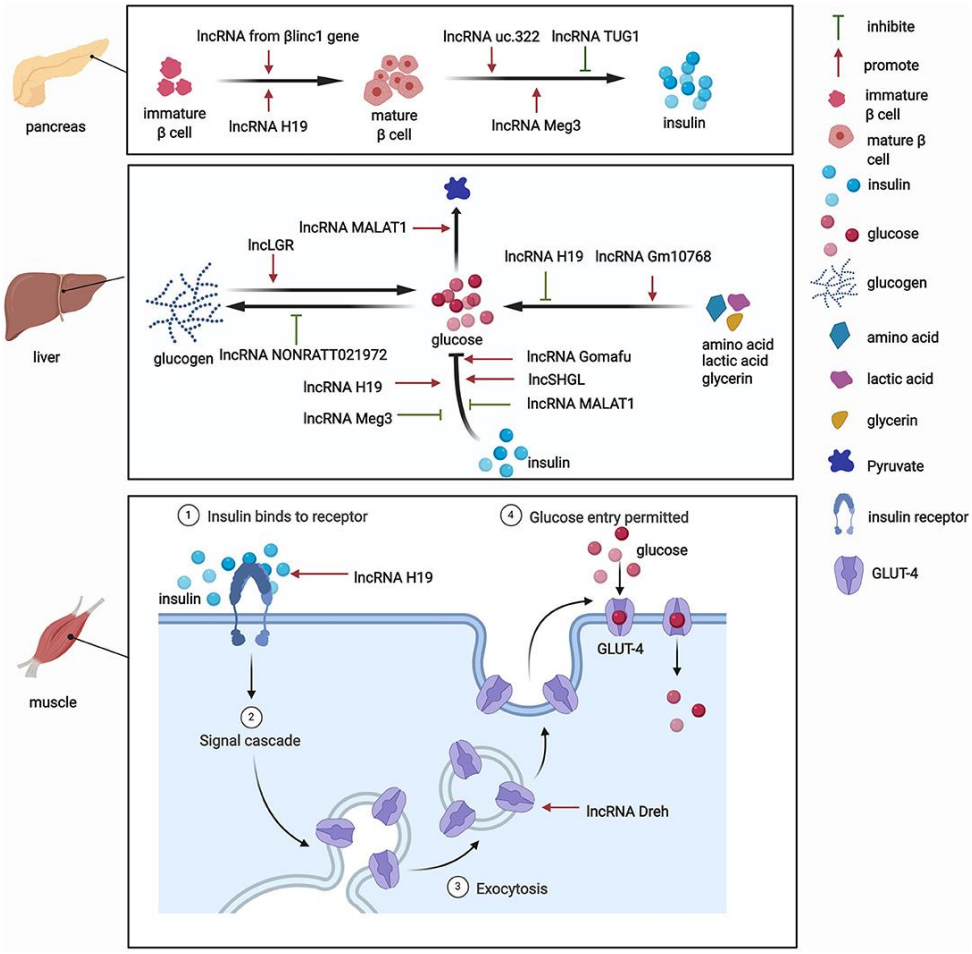

Figure 16. *The regulatory role of lncRNA in glucose metabolism under physiological conditions. Adapted from* [112].

Besides the regulation of proper pancreas development, lncRNAs can participate in control of insulin biogenesis and secretion, which directly influence glucose metabolism. For example, lncRNA Meg3 regulates insulin secretion via influence the activity of several transcription factors: Rad21, Smc3 and Sin3α. Meg3 directly binds to methyltransferase EZH2, which promotes H3K27 methylation, including in the region of the promotors of these transcription factors, resulting in their inhibition. Downregulation of Rad21, Smc3 and Sin3α leads to upregulation of MafA transcription factor and

increase in insulin synthesis [113]. Ultraconserved 322 (uc.322) lncRNA is highly expressed in pancreatic tissue. Uc.322 upregulation leads to overexpression of two insulin transcription factors PDX1 (pancreatic and duodenal homeobox1) and FoxO1, thus, promoting insulin secretion. Whereas uc.322 knockdown has an opposite effect on insulin synthesis [114]. LncRNA TUG1 is more abundant in pancreatic tissue compared with other organs and its expression levels depend on glucose. Downregulation of TUG1 leads to increased apoptosis and decreased insulin secretion on β-cells (**Figure 16)** [115].

LncRNAs are also required for normal glucose metabolism in the liver. During fasting conditions, downregulation of hepatic glucokinase (GCK) promotes the transition towards gluconeogenesis. Liver GCK repressor lncRNA (lncLGR) transcriptionally regulate GCK gene *via* binding to heterogenous nuclear ribonucleoprotein L (hnRNPL). lncLGR facilitates hnRNPL recruitment to GCK promoter and suppresses GCK transcription. Thus, lncLGR activation occurs during fasting, suppresses GCK expression and decrease glycogen storage. Meanwhile lncLGR knockdown increases GCK expression even during fasting [116]. Additionally, lncRNAs participate in glucose homeostasis regulation in adipose tissue and skeletal muscles (**Figure 16**) [112].

2.2.11 Role of lncRNAs in glucose metabolism under pathological conditions

Under pathological conditions, such as cancer or diabetes changes in glucose metabolism occur, and lncRNAs can mediate these changes. Most frequently aberrant activation of certain lncRNA in cancer leads to glycolysis upregulation, thus, promoting tumor cells proliferation and migration [112].

2.2.11.1 LncRNAs participate in glucose uptake

Glucose transporters (GLUTs) belong to a family of membrane proteins, which transport extracellular glucose into cells, thus, playing an important role in glucose metabolism. Among 13 members of GLUT family, 4 proteins GLUT1, GLUT2, GLUT3 and GLUT4 are mainly participate in glucose metabolism. As mentioned above, GLUT2 is a main glucose transporter in hepatocytes and GLUT1 regulates basal glucose uptake in different tissues and organs. GLUT3 is mainly distributed in nervous tissue and GLUT4 in adipocytes and skeletal muscles. Dysregulation of GLUTs is related to many diseases, particularly to metabolism of malignant tumor cells. Most frequently upregulation of GLUTs favors tumor cells requirements in higher energy metabolism rate [74]. NRB2 is a glucose starvation induced lncRNA. NRB2 binds to AMPK and regulates its activity during glucose starvation. A potential drug for cancer treatment phenformin induces NBR2 expression, while NBR2 downregulation increases cancer cell death induced by phenformin. Interestingly, knockout of NRB2 does not affect AMPK activity induced by phenformin, but it decreases the expression of GLUT1 and glucose uptake. These data indicate that NRB2-GLUT1 axis can serve as an adaptive response in cancer cells to survive in response to penformin treatment [117]. Colorectal neoplasia differentially expressed (CRNDE) lncRNA is activated in colorectal cancer and regulates genes expression via epigenetic changes. CRNDE contains a highly conserved intronic sequence termed gVC-In4. Knockout of gVC-In4 results in reduction of lactic acid production due to decrease in aerobic glycolysis or conversion of pyruvate to acetyl-CoA and downregulation of GLUT4 expression. (**Figure 17**) [117,118]. LncRNA HAND2-

AS1 deficiency leads to GLUT1 and GLUT3 upregulation, which promotes glucose uptake in osteosarcoma [119]. LncRNA lnc-p23154 induces both glycolysis and glucose uptake causing overexpression of GLUT1 transporter in oral squamous cell carcinoma. Lnc-p23154 binds to miR-378a-3p promoter and inhibits its transcription. miR-378a, in turn, represses GLUT1 expression by interacting with 3'UTR. Thus, lnc-p23154 overexpression promotes metastasis and invasion of oral squamous cell carcinoma by regulating GLUT1- mediated glycolysis [120]. LncRNA-NEF expression is decreased in non-small-cell lung cancer (NSCLC) compared to healthy lung tissue. Normally LncRNA-NEF targets GLUT1 and downregulates its expression, resulting in cell proliferation inhibition [121]. HOTAIR lncRNA promotes glycolysis in hepatocellular carcinoma cells by upregulation of GLUT1 glucose transporter *via* activating mammalian target of rapamycin (mTOR) signaling [122]. In gastric cancer lncRNA MACC1-AS promotes glucose uptake and glycolysis by increasing the distribution of GLUT1 in the vicinity of cell membrane [123].

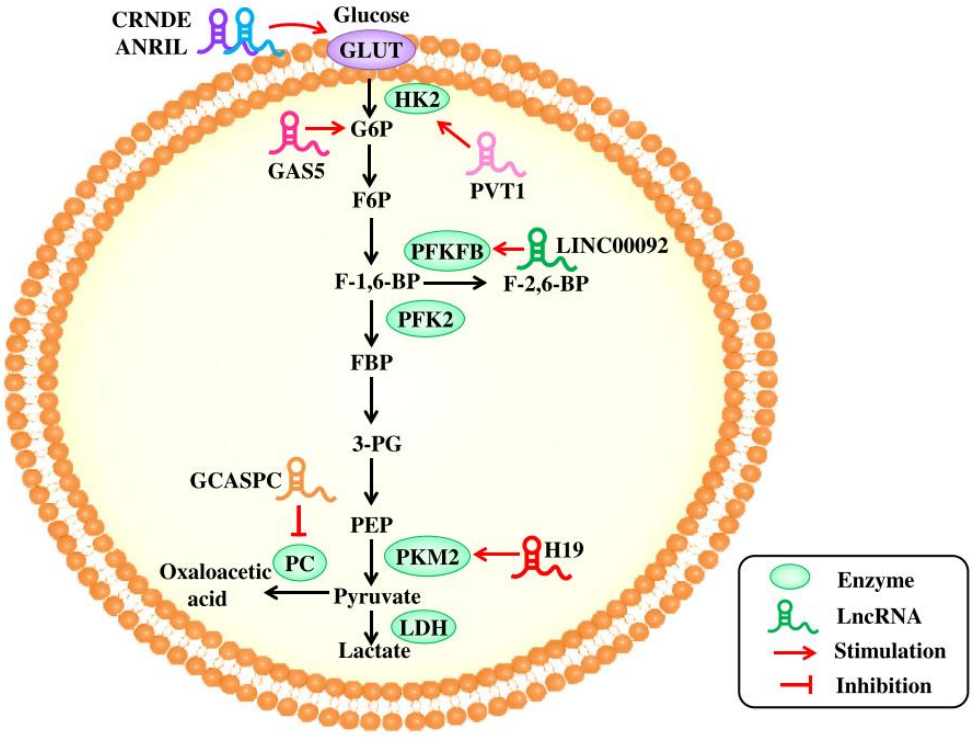

Figure 17. *LncRNAs regulate glycolysis in cancer. Adapted from* [124].

2.2.11.2 lncRNAs regulate glycolysis and oxidative phosphorylation via metabolic enzymes

Most frequently lncRNAs direct tumor cells towards mitochondrial oxidative phosphorylation and aerobic glycolysis *via* the regulation of metabolic enzymes participating in these pathways (**Figure 17, 18**). For example, in hepatocellular carcinoma lncRNA Ftx increase glycolysis by upregulating the expression of PFK and LDH via PPARγ pathway activation. Withal Ftx downregulates several key enzymes of TCA – citrate synthase (CS), isocitrate dehydrogenase (IDH) and α-ketoglutarate dehudrogenase (OGDH), which also promotes glycolysis [74]. Similarly, lncRNA SNHG3 regulates energy metabolism in ovarian cancer cells through increasing the

expression of PFK, PKM, CS, IDH and OGDH [125]. LINC00470 promotes a progression of glioblastoma by the following mechanism affecting the glucose metabolism. In glioblastoma cells LINC00470 form a ternary complex with FUS and AKT, anchoring FUS in cytoplasm to upregulate AKT activity. Increase in pAKT inhibit ubiquitination of HK1, promoting glycolysis and glioblastoma progression [126]. LncRNA TUG1 regulates cell migration, invasion and glycolysis via miRNA miR-455-3p. MiR-455-3p targets 3'UTR of AMPKβ2 (adenosine monophosphate-activated protein kinase subunit beta 2) and TUG1 knockdown leads to suppression of miR-455-3p. Moreover, TUG1/miR-455-3p/ AMPKβ2 axis regulates HK2, thus, influencing cell growth, metastasis and glycolysis in hepatocellular carcinoma [127]. Expression of TUG1 is also increased in osteosarcoma cells and affects the expression of HK2. TUG1 knockdown inhibits glucose consumption, lactate production and cell viability. And silencing of HK2 weakens the effect of overexpressed TUG1 on glycolysis in osteosarcoma cells [128]. Expression of lncRNA PVT1 is also upregulated in osteosarcoma cells. PVT1 acts as a molecular sponge for miRNA miR-497, and HK2 is a direct target of miR-497. Thus, PVT1 overexpression promotes glycolysis, cell proliferation and motility of osteosarcoma cells through miR-497/HK2 pathway [129]. In addition, PVT1 is upregulated in gallbladder cancer and positively influence HK2 expression via its competitive endogenous activity on miR-143 [130]. Also, lncRNA HOTAIR interacts with miR-125 and miR-143, promoting HK2 expression in esophageal squamous cell carcinoma cells [131].

LncRNA YIYA promotes glycolysis and tumor growth in breast cancer. It regulates CDK6-dependent phosphorylation of PFKFB3 in cell, which results in glucose 6-phosphate conversion to fructose-2,6-bisphosphate/fructose-1,6-bisphosphate [132]. LncRNA FEZF1-AS1 is upregulated in colorectal cancer and promotes cancer cells proliferation and metastasis. FEZF1-AS1 binds to PKM2 and improves its stability by reducing ubiquitination-mediated degradation, which results in increased levels of both cytoplasmic and nuclear PKM2. Cytoplasmic PKM2 enhances glycolysis and lactate production, and nuclear PKM2 activates STAT3 signaling [133]. In contrast to FEZF1-AS1 lncRNA LINC01554 promotes the ubiquitin-mediated degradation of PKM2 and inhibits Akt/mTOR signaling pathway, which leads to reduction of aerobic glycolysis. But in hepatocellular carcinoma LINC01554 is significantly downregulated [134].

LDHA pays an important role in cancer initiation and maintenance, its overexpression promotes tumor cell malignant transformation and growth [74]. LncRNA CRYBG3 directly interacts with LDHA and increases glucose uptake and lactate production. In lung cancer cells the positive correlation between the expression levels of GRYBG3 and LDHA is observed. And CRYBG3 knockdown inhibits tumor cells proliferation [135]. Another lncRNA CASC8 (cancer susceptibility candidate 8) is downregulated in bladder cancer, while its overexpression has a suppressive effect on bladder cancer cell proliferation. CASC8 binds to fibroblast growth factor receptor (FGFR1), this interaction suppresses LDHA phosphorylation, which impairs pyruvate conversion to lactate and decrease glycolysis [136].

In ovarian cancer upregulation of LINC00092 causes inhibition of glycolytic enzyme PFKBF2. PFKFB2 downregulation promotes metastasis due to glycolysis upregulation [137]. Growth arrest-specific 5 (GAS5) lncRNA downregulates the expression of gluconeogenetic genes G6Pase and PEPCK via interaction with the DNA binding domain of adrenocorticotropic hormone receptor [138]. Pyruvate carboxylase is important for cancer cell proliferation and metabolism. LncRNA GCASPC is significantly downregulated in gallbladder cancer. Ma et al. showed that GCASPC directly binds to pyruvate carboxylase, causing its destabilization and downregulation, which inhibits gallbladder cancer cells proliferation [139].

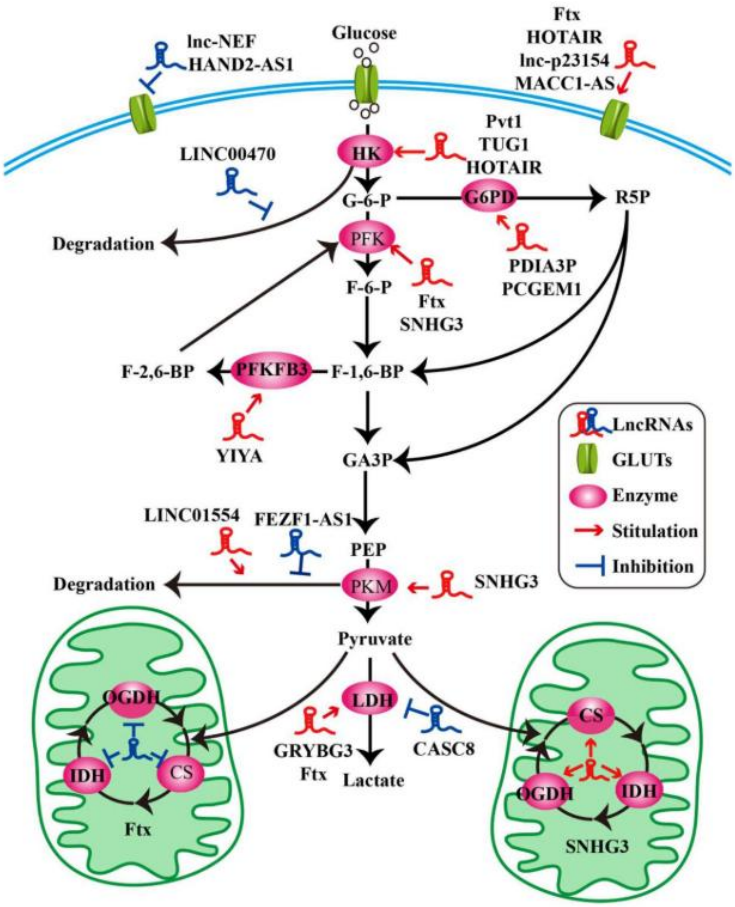

Figure 18. *LncRNAs regulate pathways of glucose metabolism. Adapted from* [74].

2.2.11.4. LncRNA regulates glucose metabolism by affecting HIF signaling pathway

In cancer cells the rates of glucose uptake and lactate production are dramatically increased even in the presence of oxygen and normally functioning mitochondria. This phenomenon is called Warburg effect [140]. Nuclear transcription factor HIF-1α serves for cancer cells adaptation to hypoxic environments and its activation tenders to Warburg effect by different mechanisms. HIF-1α may increase cell glucose uptake by GLUTs upregulation or it can activate expression of other glycolytic enzymes and to inhibit oxidative phosphorylation [124]. PVHL (von Hippel-Lindau tumor suppressor protein) is a component of ubiquitin ligase, which binds to HIF-1α protein and leads it to ubiquitinated degradation in proteasome. A hypoxia-responsive lncRNA lincRNA-p21 competes with HIF-1α for binding with pVHL, thus, preventing HIF-1α from degradation. Summing up, lincRNA-p21 promotes hypoxia-induced glycolysis by rescuing HIF-1α from decay. Moreover, there is a positive feedback loop: under hypoxic conditions HIF-1α induces lincRNA-p21 expression (**Figure 19**) [141]. Similarly to lincRNA-p21, MALAT1 may enhance arsenite-induced glycolysis in human hepatic epithelial cells by increasing HIF-1α dissociation from the complex with VHL [142]. LncRNA-LET in contrary is downregulated in several cancer types, while its overexpression results in HIF-1α destabilization and inactivation [143]. Another lncRNA LINK-A facilitates the recruitment of breast tumor kinase (BRK) to the EGFR-GPNMB complex, which results in BRK activation. HIF-1α phosphorylation by BRK leads to HIF-1α stabilization. Thus,

LINK-A promotes progression of triple negative breast cancer tumor via metabolic reprogramming by HIF-1α activation [144]. Hypoxia-responsive long intergenic non-coding RNA ROR (linc-ROR) targets miR-145, thus, regulating HIF-1α, VEGFR, TGF-β and PDK1 (**Figure 19**) [145].

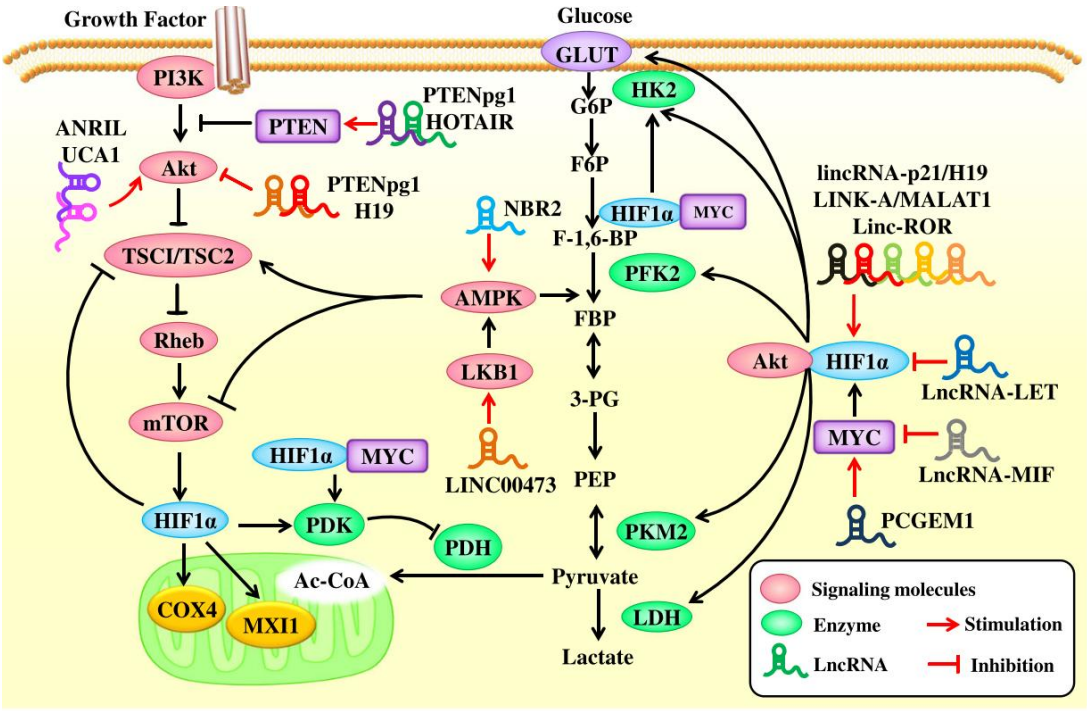

Figure 19. *Role of lncRNA-mediated HIF, PI3K/AKT/mTOR and LKB1-AMPK pathways in glucose metabolism in tumor cells. Adapted from* [124].

2.2.11.5 LncRNA regulates glucose metabolism by affecting PI3K/AKT/mTOR signaling pathway

PI3K/AKT pathway not only participates in response to insulin stimuli, but also can regulate glucose metabolism in insulin-free tissues. AKT plays a key role in choice between glycolysis or oxidative phosphorylation as a main pathway for ATP production

in the cell. AKT regulates glycolysis *via* several mechanisms: it increases the expression of glycolytic enzymes, such as HK2 and PKM2 and inhibits oxidative phosphorylation in mitochondria; it upregulates GLUTs expression; it activates HIF-1a *via* mTORC1 [146]. PTEN is a tumor suppressor that negatively regulates AKT pathway. PTEN pseudogene (PTENpg1) regulates PTEN expression by protecting its mRNA from the interaction with miRNA. Thus, PTENpg1 activity results in tumor growth inhibition via inhibition of AKT signaling (**Figure 19**) [147]. As opposite to PTENpg1, overexpression of lncRNA HOTAIR is associated with increased PTEN methylation in human tongue squamous cell carcinoma, leading to changes in glucose metabolism *via* AKT pathway [148]. LncRNA ANRIL activates mTOR signaling and enhances AKT phosphorylation, which results in GLUT1 upregulation and increased glucose uptake in nasopharyngeal carcinoma [149]. The H19 lncRNA is significantly downregulated in muscles of type-2 diabetes patients and insulin resistant rodents. H19 sponges let-7 miRNA and its downregulation leads to increased bioavailability of let-7, causing degradation of let-7 targets and impaired insulin/PI3K/AKT signaling. Moreover, H19 expression is regulated by PI3K/AKT-dependent phosphorylation of miRNA processing factor KSRP (**Figure 19**) [150].

2.2.11.6 LncRNA regulates glucose metabolism by affecting LKB1-AMPK signaling pathway

AMP activated protein kinase (AMPK) is an important cellular energy sensor, that is required for glucose metabolism. During energy deficiency, upregulated AMPK triggers activation of TSC2 complex *via* its phosphorylation, this protects cell from apoptosis [151]. Serine/threonine kinase LKB1 (liver kinase B1) acts as a tumor

suppressor and regulates cell energy metabolism and growth *via* mTOR pathway. LKB1 inhibition enhances cellular glucose uptake and its utilization mediated by HIF-1a, which leads to proliferation of tumor cells [152]. LINC00473 is a most induced lncRNA in human primary NSCLC samples with inactivated LKB1. LINC00473 activation promoted survival and growth in these cells. LKB1 inactivation together with CREB/CRTC (CREB-regulated transcription coactivator) activation induced LINC00473 expression. LINC00473 interacts with a component of the cAMP signaling pathway – NONO protein, and facilitates CRTC/CREB-mediated transcription [153]. Under energy stress, lncRNA NBR2 (neighbor of BRCA1 gene 2) is induced by LKB1-AMPK signaling pathway. At the same conditions NBR2 binds to AMPK, promoting its kinase activity and glucose catabolism. NRB2 silencing attenuates AMPK phosphorylation and mTORC1 inactivation (**Figure 19**) [154].

2.2.11.7 LncRNA regulates glucose metabolism by affecting Wnt signaling

Wnt pathway activation results in the inhibition of mitochondrial respiration because of inactivation of cytochrome c oxidase and glycolysis enhancing due to activation of pyruvate carboxylase. Moreover, epithelial-mesenchymal transition (EMT) may contribute to glucose metabolism and mitochondrial respiration regulation by Wnt pathway [155]. In metastatic colorectal cancer lncRNA-CTD903 acts as a tumor suppressor. By inhibition of Wnt/β-catenin signaling lncRNA-CTD903 represses cancer cell invasion and migration [156]. In breast cancer cells lncRNA UCA1 modulates EMT and its inhibition increases the expression of GSK-3β and impairs cells mesenchymal properties. While overexpression of UCA1 enhances breast cancer cells invasiveness *via*

Wnt/β-catenin signaling pathway (**Figure 20**) [157]. These examples show, how lncRNAs may indirectly alter glucose metabolism by affecting EMT *via* Wnt pathway [124].

2.2.11.8 LncRNA regulates glucose metabolism by affecting STAT signaling pathway

LncRNA NRCP induces glycolysis in ovarian cancer cells, thus, promoting tumor growth and cells proliferation. NRCP facilitates STAT1 interaction with RNA polymerase II that enhances expression of STAT1 downstream target genes, including glycolytic enzyme glucose-6-phosphate isomerase [158]. Another lncRNA UCA1, already described above, also promotes glycolysis in bladder cancer cells. UCA1 activates STAT3 and inhibits microRNA143 activity, which results in mTOR-mediated activation of HK2 (**Figure 20**) [159].

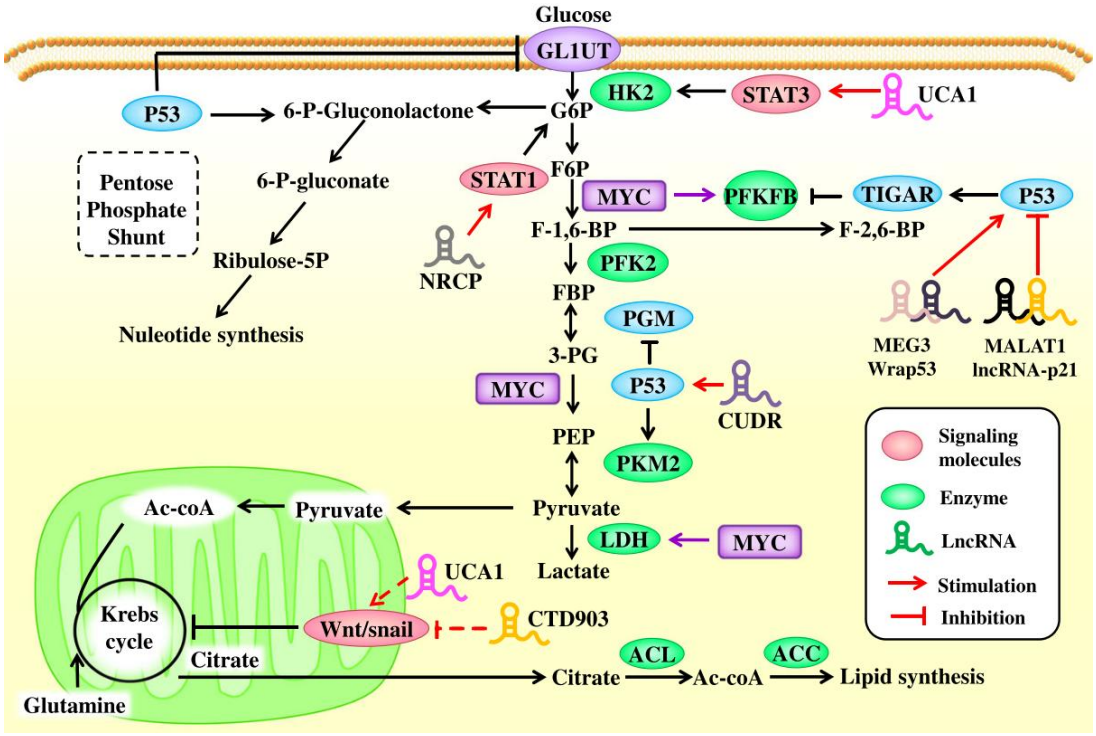

Figure 20. *Role of lncRNA–mediated Wnt/Snail, STAT and p53 pathways in glucose metabolism in tumor cells. Adapted from* [124].

2.2.11.9 P53 signaling pathway

P53 protein participates in multiple routes of glucose metabolism regulation. P53 can inhibit GLUT1 and GLUT4 expression, as a transcriptional factor it can modulate expression of many metabolism-related enzymes. P53 downregulation may cause hyperactivation of glycolysis and mitochondrial respiratory damage. Meanwhile, aberrant activation of p53 stimulates the ubiquitination of PGM (phosphoglycerate mutase), disturbing the last step of glycolysis – the conversion of fructose-1,6-bisphosphate to pyruvate [124]. A double mutation in p53 (N340Q/L344R) causes complex formation between p53 and lncRNA CUDR. This complex interacts with PKM2 promoter, increasing PKM2 phosphorylation and activity, thus, facilitating the progression of

hepatocellular carcinoma (HCC) [160]. Different lncRNAs participate in the regulation of p53 expression directly or indirectly. LncRNA MEG3 overexpression, for example, causes upregulation of p53 protein and activation of the expression of p53 target genes. A natural antisense transcript of p53 (Wrap53) regulates the level of p53 mRNA [124]. LncRNA p21 – a downstream transcript of p53 – can inhibit the p53 transcription and induce apoptosis by binding to hnRNP-K [161]. MALAT1 lncRNA, which is highly expressed in different cancer types, is also involved in p53 regulation. Depletion of MALAT1 in normal human fibroblasts causes activation of p53 and its downstream target genes, which results in cell cycle defects [162]. LncRNA ROR is inhibited by p53 and at the same time can inhibit p53 (**Figure 20**). Thus, lncRNAs participate in regulation of glucose metabolism *via* regulating p53 [124].

2.2.11.10 LncRNA regulates glucose metabolism by affecting cMyc oncogene

c-Myc is an oncogene, which aberrant activation promotes tumor growth and cancer cell proliferation. In cooperation with HIF-1α c-Myc induces HK2 and PDK1 expression, which promotes glycolysis and downregulates mitochondrial respiration [163]. Under normal oxygen conditions, c-Myc regulates multiple glycolytic genes and promotes glucose metabolism. Already described above, lncRNA PCGEM1 influences at transcriptional level different metabolic processes, such as glucose metabolism, PPP, nucleic acid and fatty acid biosynthesis. Mechanistically PCGEM1 interacts with c-Myc and promoters of target genes, this binding promotes chromatin recruitment of c-Myc and increases its transcriptional activity [164]. LncRNA-MIF interacts with miR-586,

disturbing its binding to E3 ubiquitin ligase Fbxw7, which regulates c-Myc stability. Thus, lncRNA-MIF expression reduces c-Myc protein level [165].

Human lncRNA DEANR1 (definitive endoderm-associated lncRNA1) or linc00261 also contributes to glycolysis regulation *via* c-Myc pathway. Zhai et al. found that in pancreatic cancer cells DEANR1 overexpression caused reduction of extracellular acidification rate (ECAR) and oxygen consumption rate (OCR), lower glucose consumption and lactate production. This data indicates that DEANR1 could reduce glycolysis in pancreatic cancer cells, thus, suppressing tumor growth. There are two described mechanisms of glycolysis regulation by DEANR1. First, DEANR1 sponges miR-222-3p, which leads to HIPK2-mediated activation of ERK/c-Myc pathway. Second, DEANR1 sequesters IGF2BP1 (Insulin like growth factor binding protein 1), decreasing c-Myc mRNA stability and reducing its expression [8].

2.3 LncRNA DEANR1/linc00261 and its function

Human lncRNA DEANR1/linc00261 is located on chromosome 20 downstream FOXA2 (forkhead box protein A2) transcription factor gene. DEANR1 has been reported to be involved in many cellular processes and its dysregulation was observed in different cancer types. For example, DEANR1 downregulates breast cancer cells proliferation and migration [166], inhibits epithelial-mesenchymal transition (EMT), thus, reducing the invasiveness of tumor cells in breast cancer [15]. In non-small cell lung cancer (NSCLC) and pancreatic cancer DEANR1 inhibits tumor growth through the inhibition of cell proliferation and induction of apoptosis [13,167], while for patients with endometrial carcinoma DEANR1 serves as a potential prognostic biomarker [168]. Literature analysis

on DEANR1 shows that in most cases DEANR1 is significantly downregulated in different cancers compared to the corresponding normal tissues and plays the role of a tumor suppressor [12].

Summary of all known mechanisms of DEANR1 action is presented in **Table 1**.

Table 1. *Mechanisms of DEANR1 action in different tissues*

Mechanism	**Tissue**	**Reference**
Enhances NME1 mRNA Stability	Breast cancer	[15]
Acts as a molecular sponge for microRNA-654-5p, which targets SOC3 and regulates the activity of NF-κB	Kidney	[169]
Recruits GATA6 to DKK3 promoter, binds to GATA6	Prostate cancer	[8]
Binds to GATA6, which upregulates its activity at the promoter of ITIH5	Pancreatic cancer	[170]
Acts as a molecular sponge for miR-550a-3p, thus regulating SDPR	Breast	[166]
Interacts with p300/CBP, which prevents the attraction of p300/CBP to the c-Myc promoter, resulting in the repression of c-Myc transcription	Pancreatic cancer	[171]
Binds to SMAD2/3 and attracts it to the promoter of FOXA2, thus, activating FOXA2 transcription	Definite endoderm	[22]
Activates FOXA2 transcription *via* binding to SMAD3 and recruiting it to FOXA2 promoter	Hepatocellular carcinoma	[7]
Acts as a molecular sponge for miR-552-5p and regulates FOXO3 and β-catenin/TCF4 pathway	Pancreatic cancer	[172]
Acts as a molecular sponge for miR-558, thus, regulates TIMP4.	Human trophoblasts	[173]
Acts as a molecular sponge for miR-182, miR-183, miR-153, miR-27a, and miR-96, thus, regulates Foxo1	Endometrial carcinoma	[168]
Acts as a molecular sponge for miR-1269a, thus, regulates Foxo1	Lung cancer	[9]
Acts as a molecular sponge for miR-522-3p, regulates SFRP2	NSCLC, Hepatocellular carcinoma	[13], [174]
Acts as a molecular sponge for miR-522-3p, promoting DIRAS1 expression	Esophageal carcinoma	[175]
Acts as a molecular sponge for miR-522-3p, regulates TNRC6A	Myocardial infarction, cardiomyocytes	[176]
Acts as a molecular sponge for miR-132-3p to regulate	Endometriosis	[11]

BCL2L11 expression		
Acts as a molecular sponge for miR-23a-3p	Pancreatic cancer	[167]
Acts as a molecular sponge for miR-324-3p, regulates Wnt pathway	Colon cancer	[177]
Acts as a molecular sponge for miR-222-3p, regulate HIPK2/ERK/c-myc axis. Binds to IGF2BP1	Pancreatic cancer	[10]
Acts as a molecular sponge for miR-545-3p to upregulate MT1M expression	Esophageal squamous cell carcinoma	[178]
Acts as a molecular sponge for miR-620, regulates PTEN axis	Osteosarcoma	[179]
Acts as a molecular sponge for miR-23b-3p, regulates NRF2	Embryo-derived cardiomyocytes	[180]
Binds to FOXP3 and upregulates SCP2	Pancreatic cancer	[181]

2.3.1 DEANR1 expression and function in hepatocellular carcinoma

Hepatocellular carcinoma (HCC) is the sixth most common cancer worldwide and the fourth leading cause of cancer-related death globally [182]. Multiple lncRNA are functionally significant in the liver and are closely associated with HCC tumorgenesis [183]. Here we would like to highlight a role of lncRNA DEANR1 in HCC. Zhang et al. showed that DEANR1 expression level was significantly reduced in HCC in comparison with adjacent normal tissues. The upregulation of DEANR1 in HCC cells resulted in suppression of cell proliferation, EMT and invasiveness *in vitro*. Moreover, DEANR1 levels in HCC correlated with tumor size, stage and patient survival time [184]. Sun et al. demonstrated the role of DEANR1 as an independent prognostic marker in HCC: low expression of DEANR1 negatively correlated with patients' survival time [185]. It was also observed that overexpression of DEANR1 led to the suppression of liver cancer cells migration, invasiveness and formation of lung metastatic lesions [7], meanwhile DEANR1 downregulation resulted in significant induction of cell motility [186].

Summing up the described data, DEANR1 plays a role of tumor suppressor in HCC and may serve as a prognostic marker for HCC patients.

Several mechanisms of DEANR1 action in HCC have been shown. Zhao et al. found that DEANR1 and its upstream neighbor gene FOXA2 were positively correlated in HCC. DEANR1 transcriptionally upregulates FOXA2 expression by recruiting transcription factor SMAD3 to its promoter. Additionally, a histone methyltransferase EZH2 suppresses DEANR1 transcription *via* modulating H3K27Me3 modification in HCC [7]. Ma et al. showed that in HCC cell line MHCC-97H overexpressed DEANR1 upregulated SFRP2 *via* sponging miR-522-3p, which led to a decrease in cell proliferation and invasion. Zhang et al. demonstrated that overexpression of DEANR1 led to significant downregulation of Notch1 and Hes-1 (crucial components of Notch signaling pathway) expression in HCC cell lines, resulting in suppression of HCC cell invasion and proliferation [184].

2.3.2 DEANR1 activates FOXA2 expression in definite endoderm

Jiang et al. identified DEANR1 as a differentially (100-fold increase) expressed lncRNA in a definite endoderm (DE), which expression increased together with progression of endoderm differentiation. Further investigations showed that expression of FOXA2, which is physically closed to DEANR1 in its genomic location, positively correlates with DEANR1 expression. Moreover, DEANR1 or FOXA2 knockdown resulted in similar downstream changes and defects in endoderm differentiation. Defects caused by knockdown of DEANR1 were recovered by FOXA2 expression, suggesting that FOXA2 is a main mediator of DEANR1 function in definite endoderm. RNA and

chromatin immunoprecipitation experiments results suggested that DEANR1 interacts with SMAD2/3 transcription factor and facilitates its recruitment to FOXA2 promoter to activate FOXA2 transcription. (**Figure 21**) [187]

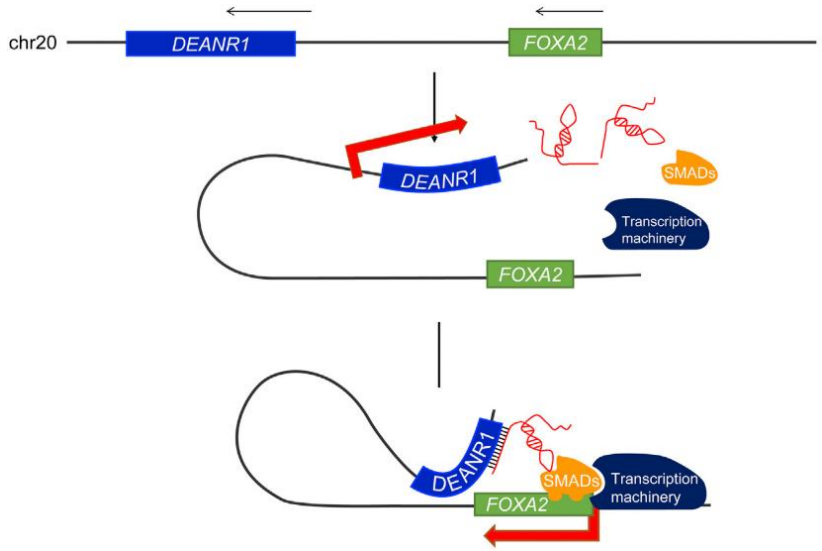

***Figure 21**. Proposed mechanism of DEANR1 action in definite endoderm. Adapted from* [187].

2.3.3 DEANR1 binds to GATA6 and suppresses prostate and pancreatic cancer tumorigenesis

DEANR1 expression is significantly reduced in prostate cancer compared to normal prostate tissue, meanwhile its overexpression resulted in decreased proliferation, migration and invasion of tumor cells. RNA immunoprecipitation (RIP) analysis identified GATA6 (GATA binding protein 6) transcriptional factor as a protein partner of DEANR1 in prostate cancer cells. DEANR1 binding to GATA6 promotes transcriptional activation of DKK3 (Dickkopf WNT signaling pathway inhibitor 3) gene by GATA6 transcription factor. DKK3 expression results in pancreatic cancer cells phenotype

observed after DEANR1 overexpression. Thus, DEANR1 suppresses prostate cancer tumorigenesis *via* GATA6/DKK3 axis [8].

Another study by Zou et al. confirmed that DEANR1 expression is downregulated in pancreatic cancer cells and pancreatic cancer stem cells together with ITIH5 (Inter-Alpha-Trypsin Inhibitor Heavy Chain 5) expression level. At the same time, upregulation of DEANR1 and ITIH5 in these cells led to the suppression of stem cell markers expression, cell proliferation, self-renewal ability and cell invasion. Dual-luciferase reporter gene, ChIP and RIP assays revealed that DEANR1 directly binds to GATA6, leading to its recruitment and increased activity at ITIH5 promoter [170].

2.3.4 DEANR1 regulates c-Myc via p300/CBP binding in pancreatic cancer

DEANR1 expression is significantly downregulated in pancreatic cancer tissue. Moreover, its expression positively correlates with the prognosis of patients with pancreatic cancer. Liu et al. found that overexpression of DEANR1 decreased pancreatic cancer cells proliferation, migration and metastasis both *in vitro* and *in vivo*. This phenotype was mediated by epigenetic regulation of c-Myc expression by DEANR1. DEANR1 binding with bromo domain of p300/CBP prevents p300/CBP recruitment to promoter region of c-Myc and diminishes H3K27Ac level, thus, repressing c-Myc transcription. Additionally, the methylation level of DEANR1 promoter was increased in pancreatic cancer tissue compared to normal tissue. While targeted demethylation of DEANR1 promoter suppressed pancreatic cancer progression [171].

2.3.5 DEANR1 interacts with NME1 mRNA and increases its stability in breast cancer

As in other cancer types described above, expression of lncRNA DEANR1 is significantly downregulated in breast cancer tissue compared to normal tissue. DEANR1 knockdown promoted proliferation and migration in breast cancer cells, while its DEANR1 overexpression inhibited both processes. Guo et al. found that DEANR1 inhibits the EMT in breast cancer. Further studies indicated that DEANR1 regulated EMT *via* binding to metastasis suppressor NME1 (Nucleoside diphosphate kinase A) mRNA. This interaction increases NME1 mRNA stability and half-life. NME1 overexpression resulted in the inhibition of breast cancer cells proliferation and EMT caused by DEANR1 knockdown. And silencing of NME1 disturbed tumor suppression caused by DEANR1 activity. Thus, DEANR1 prevents breast cancer tumorigenesis *via* EMT inhibition by increasing NME1 mRNA stability [15].

2.3.6 DEANR1 upregulates SCP2 and inhibits angiogenesis and cell cycle progression of pancreatic cancer cells

Zou et al. described one more mechanism of DEANR1 function in pancreatic cancer. They performed RNA pull-down, RIP, dual-luciferase reporter gene and ChIP assays to confirm that DEANR1 directly binds to FOXP3 (forkhead box P3) protein, which in turn can interact with SCP2 (sterol carrier protein-2). DEANR1 overexpression in pancreatic cancer cells resulted in significant increase in SCP2 expression and decrease in FOXP3 expression. At the same time, ChIP assay revealed reduced SCP2 enrichment in FOXP3 after DEANR1 overexpression. Thus, DEANR1 upregulates SCP2 by

preventing its repression by FOXP3. This results in the inhibition of angiogenesis and cell cycle progression of pancreatic cancer cells [181].

2.3.7 DEANR1 acts as a molecular sponge for multiple miRNAs

Multiple studies revealed that DEANR1 influence on various signaling pathways and cellular processes is mediated by miRNAs. DEANR1 acts as a molecular sponge for different miRNAs, thus, preventing their target mRNAs from degradation.

Chen at al. showed that in pancreatic cancer cells, where DEANR1 expression is significantly decreased and associated with poor patients' outcomes, DEANR1 directly interacts with miR-522-5p and reduces its expression. Forkhead box O3 (FOXO3) is a target of miR-552-5p. In pancreatic cancer FOXO3 inhibits EMT via inhibition of Wnt signaling pathway, thus, arresting the metastasis development. Overexpression of DEANR1 increases FOXO3 expression, resulting in Wnt pathway inhibition, decreased proliferation and invasion of pancreatic cancer cells. Meanwhile, miR-552-5p overexpression neutralizes the effect from DEANR1 overexpression, leading to FOXO3 degradation [172]. Wang et al. found that in pancreatic cancer cells DEANR1 also sponges miR-23-3p. High expression of miR23-3p in pancreatic cancer indicated low survival probability. And by targeting and decreasing miR23-3p DEANR1 represses cell viability, invasion and enhances apoptosis [167].

In lung cancer tissues expression of DEANR1 is also significantly downregulated and associated with more advance tumor stage. At the same time, DEANR1 overexpression in lung cancer suppressed metastasis development and tumor growth. Guo et al. showed that DEANR1 binds to miR-1269a, thus, preventing FOXO1 mRNA

degradation by miR-1269a and decreasing lung cancer progression [9]. In NSCLC cells DEANR1 directly interacts with miR-522-3p, which binds to 3'UTR of SFRP2 (Secreted Frizzled related protein 2) mRNA. SFRP2 is a suppressor of Wnt signaling pathway. Thus, DEANR1 inhibits NSCLC cells progression by sponging miR-522-3p and inhibiting Wnt signaling due to SFRP2 activity [13].

Downregulation of DEANR1 in endometrial carcinoma results in increased cell proliferation, invasion and migration. Fang et al. discovered, that the effect of DEANR1 in endometrial carcinoma is mediated by FOXO1 activity. DEANR1 sponges several miRNAs, including miR-182, miR-183, miR-153, miR-27a, and miR-96. All 5 miRNAs can target FOXO1. Overexpression of DEANR1 in endometrial carcinoma led to increase in FOXO1 protein level, suppressing cell proliferation, invasion and migration [168]. DEANR1 expression is also significantly decreased in endometriosis tissue, where DEANR1 acts as a molecular sponge for miR-132-3p to regulate BCL2L11 (Bcl-2-like protein 11) expression. BCL2L11 upregulation due to DEANR1 overexpression suppresses proliferation and invasion of endometriosis cells [11].

Li et al. observed that patients with sepsis had decreased level of DEANR1 in their serum samples compared to healthy controls. The same was found in a mouse model of sepsis induced by treatment with lipopolysaccharide (LPS). DEANR1 overexpression in LPS model suppressed the apoptosis, reduced inflammation and improved cell viability. The described underlying mechanism is following: DEANR1 sponges miR-654-5p, preventing its binding to suppressor of cytokine signaling 3 (SOCS3), which, in turn, inhibits NF-κB (nuclear factor-κB) activity [169].

In breast cancer cells DEANR1 interacts with miR-550a-3p, thus, increasing SDPR (serum deprivation response) expression. SDPR activity suppresses breast cancer cell viability, metastasis development and invasion [166].

DEANR1 reduction in colon cancer cells also leads to increase in cell proliferation, viability, migration, invasion and downregulation of apoptosis. Yan et al. showed that DEANR1 binds to miR-324-3p, which expression is significantly upregulated in colon cancer. miR-324-3p sequestering by DEANR1 results in WNT signaling pathway inactivation [177].

DEANR1 expression is downregulated in both esophageal squamous cell carcinoma (ESCC) and cisplatin-resistant ESCC. Wang et al. described that DEANR1 overexpression in ESCC led to the inhibition of cell proliferation and cisplatin resistance and to the promotion of cell apoptosis. This tumor suppressor effect of DEANR1 is explained by its sponging of miR-545-3p, which results in upregulation of MT1M (Metallothionein 1M) gene [178]. Additionally, Yang et al. showed that in esophageal carcinoma DEANR1 binds to miR-552-3p and sequesters it from inhibition of DIRAS1 (DIRAS Family GTPase 1). Thus, overexpression of DEANR1 and DIRAS1 promoted cell apoptosis and resulted in tumor growth suppression and reduced radioresistance of esophageal carcinoma [175]. Interestingly, that similar mechanism, involving DEANR1 sequestering of miR-552-3p, was observed by Jiang et al. during studying of DEANR1 function in cardiomyocytes after myocardial infarction. TNRC6A (Trinucleotide Repeat Containing Adaptor 6A) protein participates in the induction of myocardial infarction, and its action can be reversed by the overexpression of miR-522-3p. Jiang et al. described

that knockout of DEANR1 in cardiomyocytes increases cell viability and inhibits cell apoptosis. Summing up, elevated expression of DEANR1 in cardiomyocytes suppresses miR-522-3p, leading to upregulation of TNRC6A. This study indicates that DEANR1 may serve as a potential therapeutic target for myocardial infarction treatment [176].

Han et al. described the functional significance of DEANR1 in osteosarcoma (OS). Apatinib has the ability to inhibit OS cells proliferation and migration. Han et al. found upregulation of DEANR1 in OS after apatinib treatment. Luciferase reporter and RIP assays revealed that DEANR1 acted as a competitive endogenous RNA (ceRNA) to sponge miR-620, which in turn upregulated PTEN (phosphatase and tensin homolog) expression, resulting in downregulation of cell proliferation and migration *in vitro* as well as the tumorigenesis *in vivo* [179].

Zhang et al. investigated the role of DEANR1 in hypoxia/reoxygenation – induced cardiomyocyte apoptosis. Initially DEANR1 is downregulated in myocardial tissues, while its overexpression improves cardiac function and reduces myocardium apoptosis. DEANR1 acts as a sponge for miR-23b-3p and positively regulates NRF2 (nuclear factor erythroid 2-related factor) expression in cardiomyocytes [180].

Cheng et al. observed that DEANR1 expression was upregulated in placental tissues of pre-eclampsia women compared to healthy pregnant women. DEANR1 interacts with miR-558, preventing the degradation of its target mRNA – TIMP4 (TIMP metallopeptidase inhibitor 4). DEANR1 overexpression causes cell apoptosis and cell cycle arrest in G0/G1 phase, resulting in suppression of trophoblast invasion and migration via targeting miR-558/TIMP4 axis [173].

2.3.8 DEANR1 was predicted to form DNA-RNA triplexes

Kuo et al. developed a new computational method for triplexes detection. This method is called Triplex Domain Finder (TDF) and allows to statistically characterize DNA targets and DNA-binding domains. They applied TDF to lncRNAs involved in cardiac differentiation to analyze their potential to form triplexes with DNA. Their study revealed DEANR1 as a top-ranked lncRNA with triplex formation ability to regulate differentially expressed genes during cardiac differentiation [188]. This prediction indicates, that besides experimentally described mechanisms of DEANR1 action, it also has a potential to participate in transcriptional regulation of target genes *via* direct binding to DNA.

2.4 LL35/Falcor – a possible functional analogue of DEANR1 in mice

Human lncRNA DEANR1 is located downstream FOXA2 transcription factor gene [187]. In the mouse genome, a similar locus downstream FOXA2 shares lncRNA LL35/Falcor (Foxa2-adjacent long noncoding RNA), NCBI official symbol – 9030622O22Rik [5,17]. LL35 is raised from genomic region of 103kb in length downstream from 3' terminus of FOXA2 gene on chromosome 2. It was shown, that LL35 forms a separate transcriptional locus with no intersection with FOXA2 transcriptional frame (**Figure 22**). The promoter region, transcriptional start site and first exon of LL35 have strong conservation across all primates and placental mammals, the conservation extends to Xenopus tropicalis, zebrafish and tetraodons but not lampreys [5]. The rest LL35 sequence is poor conservative between mouse and human DEANR1, showing only 16% of similarity (calculated by DEANR1), while upstream FOXA2 gene

shows 72% similarity between species and its ortholog was found even in *Drosophila* [189].

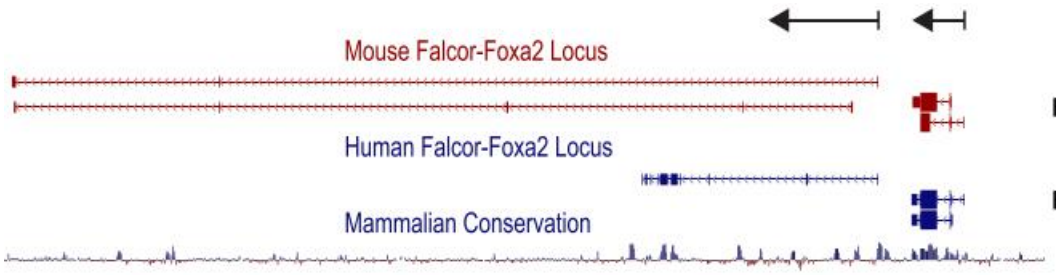

Figure 22. *LL35 (Falcor) genomic location and conservation. Adapted from* [5].

Swarr et al. showed that LL35 is predominantly expressed in the neural tube and endoderm-derived organs, such as lung, liver, intestine and pancreas. The highest level of both LL35 and FOXA2 expression in adult mice were observed in the airway epithelium, where LL35 has predominantly nuclear localization. Authors showed that LL35 knockout resulted in 25-30% loss of FOXA2 expression (**Figure 23A**). And LL35 promoter analysis together with ChIP-seq data and FOXA2 overexpression experiment suggested an existence of a feedback loop, where LL35 positively regulates FOXA2 expression and FOXA2 by direct binding to LL35 promoter inhibits its expression. Further investigation of mice with LL35 knockout revealed that LL35 depletion may cause loss of epithelial integrity at homeostasis and poor reaction to injury in epithelial cells. Finally, Swarr et al. suggested that LL35-FOXA2 regulatory feedback loop is required inhibit cell migration and to maintain cell-substrate adhesion (**Figure 23B**). Loss of LL35-FOXA2 feedback loop results in disrupted airway epithelial barrier integrity, peribronchial inflammation and impaired epithelial regeneration after injury in the lung *in vivo* [5].

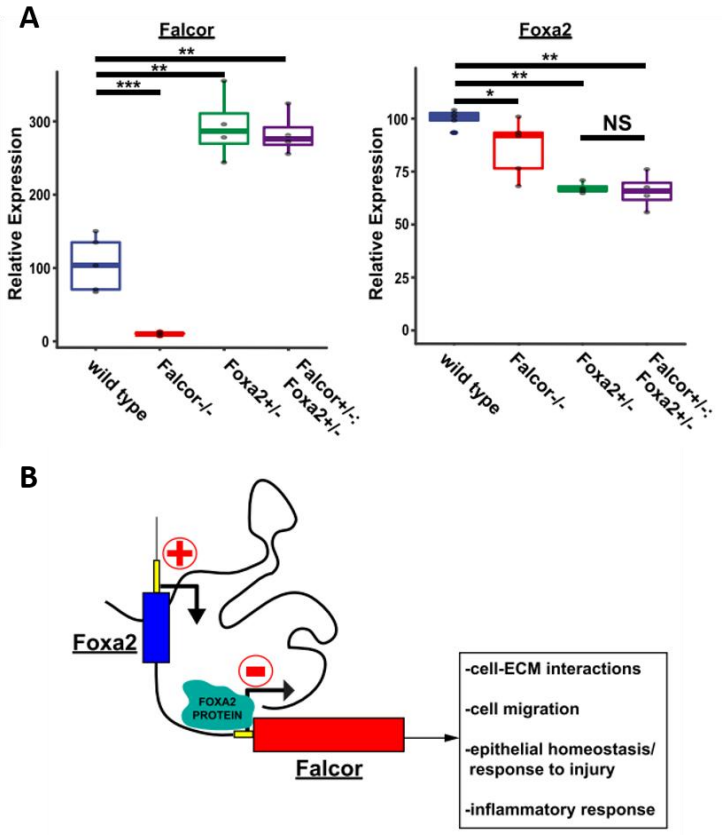

Figure 23. *(**A**) Expression of LL35 (Falcor) and Foxa2 in Falcor−/−, Foxa2+/−, and Falcor+/−;Foxa2+/− mice. Loss of Falcor−/− results in 25%–30% decrease in Foxa2 expression, whereas haploinsuffi ciency for Foxa2 leads to a marked increase in Falcor expression.*
*(**B**) Model for Falcor regulation of Foxa2 in lungs. Adapted from* [5].

Previous studies of our research group confirmed that LL35 is predominantly expressed in murine lungs and liver (**Figure 24**).

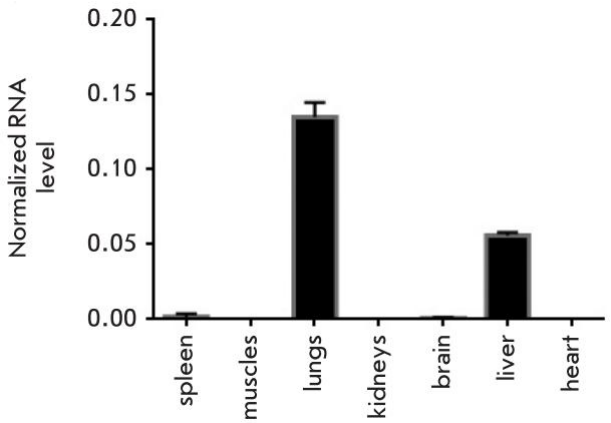

Figure 24. *LL35 expression in different murine organs. Adapted from* [17].

Sergeeva et al. showed that in AML12 (mouse hepatocytes) cell line LL35 is mainly located in nucleus (80% versus 20% in cytoplasm). A 70% decrease in LL35 expression level was observed in mouse liver two weeks after induction of fibrosis, followed by partial LL35 expression restoration after several weeks. LL35 knockdown with a combination of antisense oligos in AML12 resulted in only 20% reduction of FOXA2 mRNA expression and 30% reduction in its protein level [17]. Obtained data suggests that FOXA2 regulation can be not the main function of LL35 in murine hepatocytes and its role and mechanism of action is needed to be further investigated. Moreover, it is important to investigate whether LL35 is a functional analogue of DEANR1 in the liver, because the study of murine analogue of DEANR1 is advantageous in terms of available methods for *in vivo* experiments.

Chapter III. Materials and Methods

3.1 Murine cell culture and transfection

Experiments were performed using a normal hepatocytes cell line AML12 (alpha mouse liver 12) (ATCC®CRL-2254, VA, USA). AML12 cell line was derived from normal hepatocytes from 3-month-old mouse (CD1 strain, line MT42) transgenic for human TGF alpha. Cells were cultured in DMEM/F12 medium (Gibco, Waltham, MA, USA), 10% FBS (Gibco), 1 % penicillin and 1 % streptomycin (10,000 U/mL, Gibco) at 37 °C and under 5 % CO2. Additionally, hepatoma hepa-1c1c7 (ATCC®CRL- 2026, VA, USA) and hepa1-6 (ATCC®CRL- 1830, VA, USA) cell lines were used to estimate LL35 expression level in liver pathology. Both cell lines were also cultured in DMEM/F12 medium (Gibco), 10 % FBS (Gibco), 1 % penicillin and 1 % streptomycin (10,000 U/mL, Gibco) at 37 °C and under 5 % CO2. Cells were transfected with antisense oligonucleotides (ASOs) using Lipofectamine RNAiMAX (Invitrogen, Waltham, MA, USA) according to the manufacturer's protocol. Cells were analyzed 48 hours after transfection. For insulin stimulation experiment AML12 cells were cultured for 2 hours in reduced serum Opti-MEM media (Gibco) and then treated with 100 nM insulin solution (Paneco, Moscow, Russia).

3.2 Analysis of exon inclusion frequencies

We performed an exon inclusion frequencies analysis based on the RNA sequencing data for murine liver previously produced in our laboratory. SAJR [190] software was used for the calculation of exon inclusion frequencies. The detailed protocol

is described in Mazin et al [190]. First, SAJR splits gene into segments based on gene annotation. Obtained segments are intervals between neighboring consecutive splicing sites. Second, based on reads location relative to the segment, the number of inclusion and exclusion are calculated for each read for further segment inclusion frequency analysis.

3.3 Rapid amplification of cDNA ends (RACE)

RACE experiment was performed with Evrogen Mint RACE cDNA amplification set (SKS03). During RACE experiment, MMLV-based reverse transcriptase synthesizes cDNA from RNAs matrix with the help of oligo-dT adapter primer. Briefly, 3'-primer for the reverse transcription reaction contains oligo(dT) region, which anneals to the polyA tail of RNA during the synthesis of the first strand of cDNA. Moreover, at the end of the first strand synthesis reverse transcriptase adds several dC at the 5'-end of cDNA, which interacts with oligo(dG) region in PlugOligo, which is further included into 5'-end of cDNA. PCR amplification is used for further synthesis of double-stranded cDNA.

First-strand or ds cDNA is used for Step-Out PCR with gene-specific primer and specially designed Step-Out primer mix, consisting of 3' part specific to adapter and 5' part, which can't anneal to adapter. This diminishes background amplification. Evrogen Mint RACE cDNA amplification was used to determine both 3' and 5' end of the transcript.

3.4 Antisense oligonucleotides (ASOs)

A mix of 5 ASOs for effective knockdown of LL35 was developed earlier in our laboratory [17]. First, 14 ASOs complementary to LL35 exons were synthesized. For the improvement of ASO binding to target RNA and its exonucleolytic stability together with high RNase H catalytic activity, ASOs were synthesized as gapmers (phosphorothioate 2'-deoxynucleotides in central gap and 2′-OMe phosphorothioate nucleotides at the flanking regions). Second, developed ASOs were tested alone and in different combinations to reach the best knockdown efficacy. Finally, a mix of 5 ASOs (**Supplementary Table S1**) with a concentration of 20 nM of each was used, which made it possible to achieve more than 75% reduction in LL35 RNA level. As a control in our experiments we used ASO targeted the Firefly Luciferase gene (Luc). For targeted delivery to the mouse liver, we synthesized inhouse 3'-GalNAc-conjugated ASO [191] with the same core sequences as described above (**Supplementary Table S2**).

3.5 Animal care and treatments

Balb/c mice for this study were purchased from "Stolbovaya" Scientific Center of Biomedical Technologies of the Federal Medical and Biological Agency. Study protocols were approved by the Bioethics Committee of the Institute of Developmental Biology, all animals received human care according to the National Institute of Health guidelines. Mice were maintained at 22 °C using a 12 h light to 12 h dark cycle and fed ad libitum with regular rodent chow. Hepatocellular carcinoma was induced using plasmids encoding human ΔN90-β-catenin, human MET, and Sleeping Beauty transposase as described in [192]. Partial hepatectomy was performed as described in [193].

For the depletion of LL35 in the liver a mix of ASO was diluted in sterile saline and injected intravenously via the tail vein at the following total ASO doses: 25 mg/kg, 50 mg/kg, 100 mg/kg 150 mg/kg and 200 mg/kg (three mice per group). Mice were sacrificed at day 2 and 5 after ASOs injection and serum and liver samples were collected for analysis. Serum was collected by cardiac puncture, followed by centrifugation at 1700×g for 20 min. Serum biochemical analysis was performed in Paster Laboratories (Moscow, Russia). Liver samples were snap-frozen for further RNA-seq, RT-qPCR and LC-MS-based analysis. Mice treatment and blood collection were performed by Tatiana Abakumova (Center for Molecular and Cellular Biology, Skolkovo Institute of Science and Technology).

3.6 Insulin tolerance test

Mice were fasted overnight. Soluble human insulin (Paneco) at 1 U/kg was administered by intraperitoneal injection. Glucose was monitored by tail bleeding at 0, 15, 30, 45 and 60 min using a glucometer. Mice were sacrificed after the last glucose measurement.

3.7 Histological analysis

Freshly collected liver samples were dehydrated and embedded into paraffin in the Tissue TEK VIP 5 Jr (Sakura, Tokyo, Japan). Eight-micrometer-thick sections were subjected to hematoxylin and eosin (Abcam, Cambridge, UK), Oil Red O (Sigma-Aldrich, St. Louis, MO, USA) and Ki-67 (12202, Cell Signaling, Danvers, MA, USA) staining.

For hematoxylin and eosin staining liver sections were deparaffinized and hydrated in distilled water and then covered with Hematoxylin, Mayer's (Lillie's Modification) for 5 min. After several steps of washing with water, slides were incubated with Bluing Reagent for 10-15 sec. After washing, slides were dipped in 96 % ethanol and then fully covered with Eosin Y Solution (Modified Alcoholic) for 2-3 min. After rinsing and dehydrating with 96 % ethanol, slides were mounted in synthetic resins and analyzed with light microscope.

For Oil Red O staining we used sections fixed in formalin. First, we rinsed slides with 60 % isopropanol, then stained with Oil Red O working solution (recipe is described in section "3.17 Lipid staining with Oil Red O for AML12") for 15 min at room temperature. After one more rinse in 60 % isopropanol and distilled water, slides were mounted in mounting medium and analyzed with light microscope.

Before Ki-67 staining sections were rinsed with distilled water three times for 5 min each and then incubated in 3% hydrogen peroxide for 10 min. Then sections were again washed two times with water for 5 min each and then washed in wash buffer for 5 min. Sections were incubated in blocking solution for 1 h at room temperature and then at 4 °C overnight with primary antibodies for Ki-67. After 3 steps of washing, sections were incubated with secondary antibodies for 1 h at room temperature and washed again. Then we stained cell nuclei with DAPI (Invitrogen) and after washing off the DAPI imaging was performed by Nikon A1+MP confocal imaging system (Nikon, Japan) by Pavel Melnikov (Serbsky National Medical Research Center for Psychiatry and Narcology).

3.8 RNA isolation and RT-qPCR

Total RNA was isolated from cells or liver tissue using TRIzol (Thermo Fisher Scientific, Waltham, MA, USA), followed by precipitation with isopropanol, according to the manufacturer's instructions. Liver tissue samples were homogenized in TRIzol using the Precellys® homogenizer. 0.5–1 μg of total RNA was further treated with DNase I (Thermo Fisher Scientific) and supplied with RiboLock RNase Inhibitor (40 U/μL) to the final concentration 0.4 U/μL. cDNA was generated using a Maxima First Strand cDNA Synthesis Kit (Thermo Fisher Scientific) according to manufacturer's protocol. RNA levels were assessed by qPCR using qPCRmix-HS LowROX Kit (Evrogen, Moscow, Russia), containing a fluorescent dye SYBR green I, which intercalates between DNA bases of double-stranded DNA, causing energy release, in the Cycler CFX96 Touch Real-Time PCR detection system (Bio-Rad Laboratories, CA, USA). The relative RNA levels of interest were calculated based on delta Ct or delta delta Ct analysis via normalization to the level of the mouse housekeeping genes GAPDH (glyceraldehyde 3-phosphate dehydrogenase) or ACTB (β actin) and to the average value of the control group where needed. RT-qPCR and primer design for accessing the expression levels of miRNA was done as described by Kramer, 2011 [194]. RT-qPCR was performed using specific primers listed in **Supplementary Table S3**.

3.9 Western Blotting

Cell protein extracts were prepared from LL35 KD and control cell samples using RIPA Lysis and Extraction Buffer (ThermoFisher Scientific) and supplied with 1× Halt™ Protease Inhibitor Cocktail (ThermoFisher Scientific) according to manufacturer's

protocol. Liver samples were homogenized using the Precellys® homogenizer and protein extracts were prepared using RIPA Lysis and Extraction Buffer (ThermoFisher Scientific) supplied with 1× Halt™ Protease Inhibitor Cocktail (ThermoFisher Scientific), 0.05% Triton X-100 (Helicon, Moscow, Russia), 1 mM dithiothreitol (DTT) (Helicon), 0.2 mM phenylmethylsulfonylfluoride (PMSF) (Sigma-Aldrich). To measure the total protein concentration in the prepared lysates we used Pierce™ BCA protein assay kit (ThermoFisher Scientific) or Pierce™ Coomassie Plus (Bradford) Assay Kit (ThermoFisher Scientific). 20–60 μg of total protein samples were run on 10 % SDS–polyacrylamide gels (PAGE) and transferred to PVDF membranes (Bio-Rad Laboratories Inc.). Transfer was performed by Mini Trans-Blot®Cell and Criterion™ Blotter (Bio-Rad Laboratories Inc.) at standard protocol (80 V, 40 min). Membrane was further incubated with primary antibody for β-actin (MA1-140, Thermo Fisher Scientific, 1:5000 dilution), GAPDH (2118, Cell Signaling, 1:3000), IκBα (9242, Cell Signaling, 1:1000), p105/p50 (NF-κB) (13586, Cell Signaling, 1:1000), AKT1 (2938, Cell Signaling, Danvers, 1:1500), pAKT1(4060, Cell Signaling, 1:1500), Jagged1 (2620T, Cell Signaling, 1:1000), Pck1/PEPCK (ab70358, Abcam, 1:1000) overnight at 4 °C or for 1 h at room temperature after membrane blocking in TBS/Tween with 5% bovine serum albumin (Sigma-Aldrich) at 4 °C overnight. For protein bands' visualization we used the appropriate HRP-linked secondary antibodies and Clarity™ Western ECL Blotting Substrates (Bio-Rad Laboratories Inc.). Western blot images were quantified with ImageJ software according to its standard protocol [195].

3.10 Cell Viability Assay

To estimate cell viability, we cultured AML12 cells in 48 well plate, ~22 × 10^3 cells per well, and transfected with LL35 ASOs mix or control Luc ASO (final concentration 20 nM of each ASO, four replicates per condition) using Lipofectamine RNAiMAX (Invitrogen) according to the manufacturer's protocol. Cell viability was measured at 24, 48, and 72 hours after initial transfection and 3 h incubation at 37 °C with CellTiter 96®Aqueous One Solution Cell Proliferation Assay (MTS) (Promega, Madison, WI, USA) according to manufacturer's protocol. The measurement of the fluorescent signal at 490 nm was performed by Varioscan Microplate reader (Thermo Fisher Scientific). The obtained data were presented on a plot of optical density (O.D.) versus number of days, showing mean ± SD. Assessment of the significance of the difference in viability between cells with LL35 knockdown and control cells was performed using the multiple t-test.

3.11 Wound-Healing and Migration Assay

AML12 cells transfected with LL35 ASOs or control Luc ASO using Lipofectamine RNAiMAX (Invitrogen) were cultured in 6 well plates. When the cell confluence reached 70–80 %, we did several scratches on the cell surface monolayer using pipette tip. To measure the wound-healing we photographed scratches 2 and 3 days after their introduction. For each condition we used 6 replicas. The calculation of total wounding area was made by ImageJ software [195].

3.12 Cell Cycle Analysis with Flow Cytometry

AML12 cells were cultured in 6 well plates in triplicates, ~3 × 10^5 cells per well, and transfected with LL35 ASO mix or control Luc ASO (final concentration 20 nM of each ASO) using Lipofectamine RNAiMAX (Invitrogen). On the day 2 after transfection cells were collected, washed twice with 1× PBS and fixed over-night at 4 °C with 2 mL of 70 % ethanol. After fixation cells were washed with 1× PBS and then re-suspend in 0.5 mL of 1× PBS with 5 μg/ml RNase A and 30 μg/ml PI (propidium iodide). Cell cycle measurement was performed by Flow Cytometer Bio-Rad ZE5 (Bio-Rad Laboratories Inc.) by Dr. Olga Sergeeva (Center for Molecular and Cellular Biology, Skolkovo Institute of Science and Technology). To analyse the flow cytometry results we used FlowJo™ v10.8 Software (BD Life Sciences, NJ, USA).

3.13 RNA-seq Data Processing and Analysis

For AML12 cells transcriptome analysis, we used ~1,2 × 10^6 cells per sample after 48 hours of ASO-mediated LL35 knockdown or control Luc knockdown; 4 replicates per experiment were used. For liver transcriptome analysis we collected samples 5 days after LL35 ASOs or Luc ASO injection; 3 mice per experiment were used. Total RNA from cells and liver samples was isolated using a TRIzol (Thermo Fisher Scientific), followed by precipitation with isopropanol, according to the manufacturer's protocol. As a starting quantity for library preparation, we used four micrograms of total RNA. First, we performed rRNA depletion using a NEBNext rRNA Depletion Kit (NEB E6310L, New England Biolabs, Ipswich, MA, USA) according to the manufacturer's protocol with the following changes. Before the depletion we fragmented the total RNA

to ~200 nt-long RNA fragments by incubation at 95 °C for 5.5 min in 100 mM Tris (pH 8.0) and 2 mM MgCl2. After the fragmentation RNA was purified by 96 % ethanol precipitation with a 1/10 volume of 3 M sodium acetate. One microgram of fragmented and purified RNA was used for rRNA depletion reaction by NEBNext rRNA Depletion Kit (NEB E6310L, New England Biolabs). The second purification of RNA after rRNA depletion step was again performed by 96 % ethanol precipitation with a 1/10 volume of 3 M sodium acetate (instead of purification using magnetic beads as described in manufacturer's instructions). Then we measured RNA concentration using a NanoDrop™ OneC Spectrophotometer (Thermo Fisher Scientific), and 300 ng of purified RNA were used for further preparation of sequencing library. We obtained libraries using NEBNext Ultra II Directional RNA Library Prep Kit for Illumina (NEB 7760, New England Biolabs), according to the manufacturer's protocol. For the purification of newly synthesized double-stranded cDNA we used AMPure XP magnetic beads (A63881, Beckman Coulter, Brea, CA, USA). To evaluate library quality, we used a Bioanalyzer2100 (Agilent Technologies, Santa Clara, CA, USA). Libraries were sequenced by HiSeq4000 (Illumina, San Diego, USA) instrument in a single-read mode (performed by Maria Logacheva at Skoltech Genomics Core Facility). bcl2fastq2 software (Illumina) was used for conversion to fastq format.

RNA-seq reads were aligned to mouse genome using STAR v2.5.3a with default settings, except –quantMode GeneCounts, Genome annotations were obtained from Ensembl. We used R package DESeq2 for gene counts processing and RLE method for further normalization. Differential expression analysis was performed using DESeq2

package based on the Wald test. Genes were considered as differentially expressed if they passed the following thresholds: FDR < 0.1 and |log2foldChange| > 0.8. For differentially expressed genes we performed functional enrichment analysis with PANTHER [196] using BP/MF/CC ontology and Reactome pathways as annotation set. Differential expression analysis for AML12 cells was performed by Ilia Kurochkin (Center for Molecular and Cellular Biology, Skolkovo Institute of Science and Technology) and for liver tissue by Ksenia Deinichenko (Institute of Biomedical Chemistry).

3.14 LC-MS-based proteomics

Cells were cultivated in 6 well plate and collected at the second day after LL35 knockdown, washed twice with 1× PBS and processed for further LC/MS analysis. Protocol for reduction, alkylation and digestion of the proteins in solution were optimized from Kulak et al. [197] with several modifications. In short, sodium deoxycholate (SDC) lysis, reduction and alkylation buffer 100 mM Tris-HCl, 1 % (w/v) SDC, 10 mM TCEP and 20 mM 2-chloroacetamide (pH 8.5) were added to a cell sample. First, we heated each sample for 10 min at 95 °C, second, we added in 1:100 (w/w) ratio the equal volume of trypsin solution in 100 mM Tris-HCl (pH 8.5) and samples have been subjected to overnight digestion at 37 °C. Then 1 % trifluoroacetic acid (TFA) was used for peptides acidification for SDB-RPS binding, and 20 µg of sample was loaded on three 14-gauge StageTip plugs. The StageTips were centrifuged at 400 g after adding the same volume of ethyl acetate. Then the StageTips were washed with a 100 µl of 1 % TFA/ethyl acetate mixture and 100 µl of 0.2 % TFA. For the elution of peptides 50 µl of elution solution

(50 % acetonitrile, 45 % water and 5 % ammonia) were used. The collected material was stored at -80 °C after vacuum drying.

Peptides were dissolved in 2 % acetonitrile/ 0.1 % TFA solution and sonicated for 2 min in ultrasonic water bath. Then samples were placed in a home-made trap column 20 × 0.1 mm with Inertsil ODS3 3 μm sorbent (GL Sciences, Tokyo, Japan), in the loading buffer contained 2 % ACN, 98 % H2O, 0.1 % TFA at 10 μl/min flow and separated in a home-packed [198] fused-silica column 300 × 0.1 mm packed with Reprosil PUR C18AQ 1.9 (Dr. Maisch, Ammerbuch-Entringen, Germany) at RT into an emitter prepared with P2000 Laser Puller (Sutter, Atlanta, GA, USA). Ultimate 3000 Nano LC System (Thermo Fisher Scientific) coupled to the Q Exactive Plus Orbitrap mass spectrometer (Thermo Fisher Scientific) via a nanoelectrospray source (Thermo Fisher Scientific) was used for reverse-phase chromatography. After loading the peptides in a loading solution contained 98 % 0.1 % (v/v) formic acid and 2 % (v/v) acetonitrile they were eluted with a linear gradient as follows: 3–35 % solution B (0.1 % (v/v) formic acid, 80 % (v/v) acetonitrile) for 105 min; 35-55 % B for 18 min, 55-99 % B for 0.1 min, 99 % B during 10 min, 99-2 %B for 0.1 min at a flow rate of 500 nl/min. The preequilibration of the column with solution A (0.1 % (v/v) formic acid, 2 % (v/v) acetonitrile) for 10 min was performed after each gradient. We used the following MS1 parameters: 70K resolution, 350-2000 scan range, 30 msec maximum injection time, AGC target – 3 × 106. For ions isolation 1.4 m/z window, preferred peptide match and isotope exclusion were used. MS2 fragmentation was performed in HCD mode at 17.5K

resolution with HCD collision energy 29 % and 80msec maximum injection time, AGC target – 1 × 105. Settings for charge exclusion: unassigned, 1, >7.

We used MaxQuant [199] and Perseus [200] for raw spectra processing, search was conducted against Mus musculus Uniprot Tremble database (version from 03.2018). For MaxQuant search the default parameters included Trypsin/p protease specificity with maximum 2 missed cleavages. Met oxidation, protein N-term acetylation and Asn/Gln deamidation were used as variable modifications, while Carbamidomethyl Cys were used as a fixed modification with maximum 5 modifications per peptide; PSM and protein FDR were applied as 1%. All runs were processed in Perseus. Proteins with maxLFQ values in at least 3 out of 6 LC-MS runs were chosen for further analysis. Missing values for selected proteins were imputed from normal distribution with 1.8 intensity distribution center downshift and 0.3 intensity distribution sigma width. Statistically significantly changed proteins after LL35 knockdown were selected based on two-sample t-test with permutation-based FDR 5 %. LC-MS for proteomics was done by Rustam Ziganshin (Shemyakin-Ovchinnikov Institute of Bioorganic Chemistry).

3.15 Seahorse Extracellular Flux Analysis

To measure the respiration activity of AML12 cells we used a Seahorse XF96 Extracellular Flux Analyzer (Agilent, CA, USA). Cells were seeded at the density of ~12×10^3 cells per well in a XF96 plate, the next day cells were transfected with LL35 or Luc ASOs. The Glycolysis Stress Test and Mito Stress Test were performed at the second day after transfection according to manufacturer's protocol. Briefly, during Mito Stress

Test cells are sequentially treated with 1μM oligomycin, 1μM FCCP and 1μM rotenone/antimycin A and oxygen consumption rate (OCR) is measured during 80 min. In Glycolysis Stress Test cells are subjected to the treatment with 10 mM glucose, 1 μM oligomycin and 50 mM 2-DG (2-Deoxyglucose) and extracellular acidification rate (ECAR) is measured during 80 min. All Seahorse XF96 measurements were normalized to the protein contents in each well, measured by Pierce™ BCA protein assay kit (ThermoFisher Scientific). The relative levels of glycolysis, glycolytic capacity, and glycolytic reserve were calculated based on ECAR data obtained in the Glycolysis Stress Test using Seahorse Wave software for XF analyzers. Non-mitochonrial consumption, basal respiration, maximum respiration, proton leak, ATP production and spare respiratory capacity were calculated based on OCR data obtained during Mito Stress Test.

3.16 Mitochondria staining with TMRE and Mito Green FM

For mitochondria staining AML12 cells were cultivated on poly-L-lysine-coated microscopy glasses. We used three glasses per condition and performed TMRE (tetramethylrhodamine, ethyl ester) (Thermo Fisher Scientific) and MitoTracker Green FM (Thermo Fisher Scientific) staining on live adherent cells on the day 2 after LL35 knockdown. For TMRE staining AML12 cells were incubated with 200–400 nM TMRE solution for 15-30 min and then washed twice with PBS / 0.2 % BSA. For cells staining with MitoTracker Green we prepared a 25–500 nM working solution in serum-free medium and covered glasses with this solution for 15–45 min. Stained cells analysis was immediately performed by Nikon A1+MP confocal imaging system (Nikon) by Pavel Melnikov (Serbsky National Medical Research Center for Psychiatry and Narcology).

3.17 Lipid staining with Oil Red O for AML12

AML12 cells were cultivated on 35 mm confocal dishes (VWR International, Rad-nor, PA, USA) and Oil Red O (Sigma-Aldrich) staining was performed 48 hours after ASO-mediated LL35 knockdown or control Luc knockdown. Briefly, Oil Red O powder was dissolved in 100 % isopropanol to get a 30 % solution. Then 3 parts of 30 % Oil Red O solution were added to 2 parts of water, mixed and filtered to get a working solution. Cells were washed twice with 1× PBS and fixed for 30 min in 4 % formaldehyde. After two washes with water and 5 min incubation in 60 % isopropanol cells were stained with Oil Red O working solution for 20 min followed by staining of cell nuclei with DAPI (Invitrogen). After washing off the DAPI cell imaging was performed by Nikon A1+MP confocal imaging system (Nikon) by Pavel Melnikov (Serbsky National Medical Research Center for Psychiatry and Narcology). Mean lipid droplet diameter and signal intensity of Oil Red O were calculated using ImageJ software [195].

3.18 Cell lines and liver tissue extraction protocol for lipids and metabolites analysis

AML12 cells were plated into 150 mm cell culture dish (1 dish per biological replica, 3 replicas per condition). At day 2 after transfection with ASOs mix (20 nM each) for LL35 or Luc using Lipofectamine RNAiMAX (Invitrogen), cells were collected and washed with PBS solution twice, supernatant was discarded and cell pellets were frozen at −80 °C until extraction. On extraction day, cells were thawed on ice for several minutes and randomized. For liver samples (3 samples per group), 10–15 mg liver tissue

pieces were dissected from the frozen tissue samples on dry ice, weighed, randomized and transferred to cooled 2 mL Precellys tubes with 6 zirconium oxide beads (Bertin Technologies, Montigny-le-Bretonneux, France). Extraction blank samples were inserted in the end of main batch, consisting of an empty tube without cell or tissue sample. The extraction buffer (methanol/ methyl-t-butyl ether (MTBE) (1/3, v/v)) with spiked lipid standards (0.5 µg/ml): triacylglycerol TAG(15:0/18:1-d7/15:0) (791648C, Avanti Lipids), diacylglycerol DAG(15:0/18:1-d7) (791647C, Avanti Lipids), ceramide Cer(d18:1-d7/15:0) (860681, Avanti Lipids), lyso phosphocholine LPC(18:1-d7) (791643C, Avanti Lipids), phosphoglycerol PG(15:0/18:1-d7) (791640C, Avanti Lipids), phosphocholine PC(15:0/18:1-d7) (791637C, Avanti Lipids), phosphoethanolamine PE(15:0/18:1-d7) (791638C, Avanti Lipids) was added. Additionally, for liver samples SM (791649, Avanti Lipids), PS (791639, Avanti Lipids), Chol (700041, Avanti Lipids) were added to extraction buffer. In case of cell culture samples after vigorous vortexing for 1 min, mixture was sonicated (35-kHz frequency) in ice-cold bath (Bandelin Sonorex Super RK 100 H, BANDELIN electronic GmbH & Co. KG) for 10 minutes, vortexed for 10 min and sonication repeated for 10 min. After addition of 0.5 mL of extraction buffer to liver tissue samples, homogenization of the tissue pieces was performed on a Precellys Evolution Tissue Homogenizer with dry ice-filled Cryolys cooling system (Bertin Technologies). Then another 0.5 mL of extraction buffer was added and homogenates were sonicated for 10 min in an ice-cooled sonication bath (Bandelin Sonorex Super RK 100 H, BANDELIN electronic GmbH & Co. KG) and incubated for 40 min at 4 °C on an orbital shaker, sonication was repeated for 10 min.

Phase separation was induced by adding 700 µL of water/methanol (3/1, v/v) mixture with the following standards (6.7 µg/ml): L-Glutamic acid-13C5 (604860, Sigma-Aldrich), methionine-methyl-13C, d3 (299154, Sigma-Aldrich), GMP-15N5 (662674, Sigma-Aldrich). Extract was vortexed for 15 min at 4 °C, then centrifuged for 10 min at 18000×g, at 4 °C. A total of 540 µL (for cells) or 300 µL (for liver) of the upper layer, containing most of the lipids, was collected to an Eppendorf tube. 900 µL (for cells) or 1000 µL (for liver) of polar lower phase was collected in a separate Eppendorf tube. Solvents were evaporated under reduced pressure at 30 °C in the Speed Vac concentrator (mode V-HV, Eppendorf Concentrator plus Complete System, Hamburg, Germany). Dried samples were stored in -80 °C until mass spectrometry analysis. Pellets were reconstituted in 200 µL of acetonitrile/isopropanol (7/3 (v/v)) or in 100 µL of 20 % acetonitrile in water for lipids and polar metabolites analysis, respectively. After brief rigorous vortexing, samples were shaken for 10 min at 4 °C, sonicated (35-kHz frequency) in an ice-cooled sonication bath for 10 min, and centrifuged 10 min at 18000×g at 4 °C. Extracts were diluted prior lipidome analysis as follows: 1:10 and 1:5 (1:50 and 1:3 for liver samples) with acetonitrile:isopropanol (7:3 (v:v)) for positive and negative mode, respectively. Extracts were diluted prior to metabolome analysis as follows: 1:10 and 1:3 (1:5 and 1:2 for liver samples) with 20 % acetonitrile in water for positive and negative mode, respectively. For quality control of samples, equal volumes of each diluted sample were additionally collected in a pool sample. Samples preparation from frozen cells and liver tissue for LC-MS was performed by Elena Stekolshchikova and Nikolay Anikanov

(Center for Neurobiology and Brain Restoration, Skolkovo Institute of Science and Technology).

3.19 Liquid chromatography/mass spectrometry analysis of lipidome

Liquid chromatography/mass spectrometry system consisted of Waters Acquity I-Class UPLC system (Waters, Manchester, UK) and Q Exactive orbitrap mass spectrometer (Thermo Fisher Scientific) equipped with a heated electro-spray ionization (HESI) probe was used for lipids and metabolites data acquisition from AML12 cells and liver tissue samples. We did a lipid separation at 60 °C on a reverse phase ACQUITY UPLC BEH C8 Column (2.1×100 mm, 1.7 μm, Waters co., Milford, MA, USA) equipped with Vanguard pre-column at flow rate of 0.4 mL/min. The resulting mobile phases consisted of water with 10 mM ammonium acetate, 0.1 % formic acid (Buffer A), and a mixture of acetonitrile and isopropanol (7:3) with 10 mM ammonium acetate, 0.1 % formic acid (Buffer B). For negative polarity of detection acetic acid was used instead of formic acid as mobile phase additive in the same concentration. The gradient elution was used for separation with the following profile: 1 min 55 % B, 3 min linear gradient from 55 to 80 % B, 8 min linear gradient from 80 to 85 % B, 3 min linear gradient from 85 to 100 % B. The column was repeatedly equilibrated with 55 % B for 4.5 min after washing for 4.5 min with 100 % B. The volume for injection – 3 μL. Mass spectra were acquired in positive mode with a mass range of m/z 120–1500 (positive mode) and 200-2300 (negative mode) at a mass resolving power of 140,000 Full Width Half Maximum (FWHM) (m/z 200). The mass spectrometer was operated with following parameters for full scan and data dependent acquisition (DDA) modes: ion transfer tube temperature,

320 °C; vaporizer temperature, 350 °C; spray voltage, 4.5 kV; S-lens RF level, 60; AGC target value, 5E5, sheath gas (N2) flow rate, 45 arbitrary units (a.u.); auxiliary gas (N2) flow rate, 20 a.u.; sweep gas (N2) flow rate, 4 a.u. Data was acquired on the profile mode. External mass axis calibration (Pierce positive and negative calibration solutions, Thermo Fisher Scientific) without the use of the specific lock masses was employed. DDA Top-10-acquisition mode was used for pooled samples to access fragmentation patterns of lipids and confirm lipid classes. Operating parameters were established as follows: resolution 17500 at m/z 200, AGC: 2e4, IT: 100 ms, mass isolation window: 1.2 Da, retention time window width: expected time ± 1 minute, stepped normalized collision energy: 15, 20, 25 %, dynamic exclusion 12 s, inclusion: on, customize tolerances: 10 ppm. The spectra were recorded in the profile mode. The same procedure was repeated with inclusion lists to confirm putative lipid annotations. LC-MS for lipidome analysis was performed by Elena Stekolshchikova and Nikolay Anikanov (Center for Neurobiology and Brain Restoration, Skolkovo Institute of Science and Technology).

3.20 Liquid chromatography/mass spectrometry analysis of metabolome

Liquid chromatography/mass spectrometry system consisted of Waters Acquity I-Class UPLC system (Waters) and Q Exactive orbitrap mass spectrometer (Thermo Fisher Scientific) equipped with a heated electro-spray ionization (HESI) probe was used for lipids and metabolites data acquisition from AML12 cells and liver tissue samples. We did a polar metabolites separation at 40 °C on a ZIC-HILIC Column (2.1×100 mm, 3.5 μm, SeQuant, Merck, Germany) equipped with pre-column at a flow rate of 0.4 mL/min. The resulting mobile phases consisted of water/acetonitrile mixture (95/5, v/v) with 20

mM ammonium acetate, 0.2 % acetic acid (Buffer A), and a mixture of acetonitrile/water (95/5, v/v) with 20 mM ammonium acetate, 0.2 % acetic acid (Buffer B). The gradient elution was used for separation with the following profile: 0-1.5 min 0 % B, 4.5 min linear gradient from 0 to 15 % B, 7 min linear gradient from 15 to 45 % B, and 5 min linear gradient from 45 to 100 % B. The column was repeatedly equilibrated with 0 % B for 5 min after washing for 2 min with 100 % B. The volume for injection – 3 μL. Mass spectra were acquired with a mass range of m/z 60–1000 at a mass resolving power of 140,000 Full Width Half Maximum (FWHM) (m/z 200) for both polarities. The mass spectrometer was operated with following parameters: ion transfer tube temperature, 320 °C; vaporizer temperature, 350 °C; spray voltage, 4.5 kV; S-lens RF level, 60; AGC target value, 5e5, sheath gas (N2) flow rate, 45 arbitrary units (a.u.); auxiliary gas (N2) flow rate, 20 a.u.; sweep gas (N2) flow rate, 4 a.u. Data was acquired on the profile mode. External mass axis calibration (Pierce positive and negative calibration solutions, Thermo Fisher Scientific) without the use of the specific lock masses was employed. DDA-acquisition Top-10 mode was used for pooled samples to access fragmentation patterns of polar metabolites. Operating parameters were established as follows: resolution 17500 at m/z 200, AGC: 2e4, IT: 100 ms, mass isolation window: 1.2 Da, retention time window width: expected time ± 1 minute, stepped normalized collision energy: 15, 35, 55 %, dynamic exclusion 12 s, inclusion: on, customize tolerances: 10 ppm. The spectra were recorded in the profile mode. LC-MS for metabolome analysis was performed by Elena Stekolshchikova and Nikolay Anikanov (Center for Neurobiology and Brain Restoration, Skolkovo Institute of Science and Technology).

3.21 Post-acquisition processing and statistical analysis of lipidome and metabolome data

Vendor-format files (.raw) were imported to Progenesis software (version 2.3, Non-linear Dynamics, Newcastle, UK), then features were automatically extracted, aligned and deconvoluted with default software settings and following adducts: M+H, M+NH4, M+Na, M+K, M+H-H2O, M+H-2H2O, M+2Na, M+H+Na, M+2H+Na for positive polarity and M-H, M+FA-H, M+AA-H, M-H2O-H for the negative one. All quality control samples were used for alignment references. Alignment quality was more than 92 % for all biological and technical samples and more than 85 % for extraction blanks. Data (rt-m/z matrix) was exported to .csv format, then subsequent normalizations and data analysis were carried out in R environment (v.4.1.2). Features having any missing values across all samples or with retention time more than 20 min were removed from the down-stream analysis. Features with coefficient of variation (CV) > 0.25 across the pooled quality control (QC) samples were filtered out. Lipid features from all the samples were normalized by the median abundances of internal standards and features from liver samples were also normalized by sample weight. The resulting abundances were log2-transformed. Features with mean abundance in samples < mean abundance in blank samples + 2 (in log2-scale) were removed from the analysis.

Putative annotation of lipids and metabolites species was performed based on exact mass (ppm error < 5) and isotope distribution similarity against LipidMaps [201] and Human Metabolome Database [202] databases. Non-annotated features were excluded from downstream analysis. Putatively annotated features were checked for presents of

lipid-class specific adducts. After-wards, significantly enriched lipids were used to create an inclusion list for DDA-mode analysis. LipoStar [203] software was employed for confirmation of lipid classes based on accurate m/z values of precursors (within 5 ppm error) and fragmentation data (within 15 ppm error). All spectra were manually cured afterwards. To visualize variation in lipid and metabolite content across samples, we performed principal component analysis (PCA). To assess the effect of the LL35 knockdown on the abundance of different lipid classes, we applied fast gene set enrichment analysis (fgsea) [204] with lipid classes in place of gene sets. To rank lipid features for this procedure, we used log2 fold changes (logFC). We subsequently performed confirmation of features from lipid classes for which significant alteration (fgsea FDR< 5 %) was observed. Only lipid features with MS2-confirmed annotations were used for further fgsea recalculation. After that, fgsea was performed again and only lipid classes with FDR< 10 % both before and after confirmation were considered to be significantly influenced by LL35 knockdown. Lipid classes with FDR<5% in cell culture before confirmation included 711 features. 447 of them were filtered out, being unable to reproduce during confirmation and annotations of 174 were corrected or specified. In mice, after the confirmation, annotation of 128 out of 232 features from significant classes was changed or specified, while 57 features had to be removed. The alterations in the abundance of metabolites were as well determined using fgsea. In this case it was performed on pathways from KEGG [205] and on a subset of 99 SMPDB [206] metabolite sets used by MetaboAnalyst [207], ranking features by their logFC. To identify the metabolites responsible for differences between samples we also used sparse

PCA [208] as implemented in R package mixOmics [209] and pairwise Welch t-test with unequal variance assumption and Benjamini-Hochberg (BH) correction for multiple testing. Data analysis and visualization was done by Daniil Bobrovskiy (Faculty of Bioengineering and Bioinformatics, Lomonosov Moscow State University) under the supervision of Ekaterina Khrameeva (Center for Molecular and Cellular Biology, Skolkovo Institute of Science and Technology).

3.22 Lipid Peroxidation Imaging

To analyze changes in lipid peroxidation we used the Click-iT® Lipid Peroxidation Imaging Kit (Thermo Fisher Scientific) according to manufacturer protocol. AML12 cells were pated in 2 mm cell culture dishes suitable for confocal microscopy. Lipid peroxidation was analyzed on the second day after transfection with ASOs for LL35 or control. To detect protein modifications in fixed cells derived by lipid peroxidation the kit uses copper-catalyzed click chemistry and the linoleamide alkyne (LAA) reagent. Lipid peroxidation induces the oxidation of LAA with further formation of hydroperoxides, which after further processing are involved in proteins modification. Click-iT® chemistry detects alkyne-containing modified proteins. Briefly, cells were incubated with 50 μM Click-iT® LAA solution for 2 hours, 100 μM cumene hydroperoxide was used as a positive control. After incubation cells were washed three times with 1× PBS and then fixed and permeabilized. Click-iT® reaction cocktail was prepared according to manufacturer's instruction and was added to the cells, completely covering them, for 30 min. After washing off the Click-iT cell nuclei were stained with DAPI (Invitrogen) and imaging was performed by Nikon A1+MP confocal microscope

(Nikon) by Pavel Melnikov (Serbsky National Medical Research Center for Psychiatry and Narcology).

3.23 RNA immunoprecipitation (RIP)

AML12 cells were cultured on 10 cm^2 tissue culture plates, 2 plates were used per condition (~16 × 10^6 cells). Cells were trypsinized and incubate on ice for 5 min. Then cells were harvested by centrifugation for 2 min at 100 × g at room temperature, and the cell pellet was resuspended in 2 mL ice-cold 1 × PBS. 143 µl of 37% formaldehyde were added to cell pellet and after 10 min of incubation at room temperature formaldehyde was blocked by 685 µl of 2 M glycine for 5 min. Cells were harvested by centrifugation for 2 min at 100 × g at room temperature. The supernatant was decanted and the cell pellet was transferred to ice. Cells were twice washed with 5 mL of ice-cold 1 × PBS and harvested 2 min at 100 × g at 4 °C. After the last wash we added 1 mL of IP lysis buffer (50 mM Hepes (pH 7.5), 0.4 M NaCl, 1 mM EDTA, 1 mM DTT, 0.5 % TritonX-100, 10 % Glycerol), 20 µl of 0.1 M phenylmethylsulfonyl fluoride (PMSF), 20 µl of complete protease inhibitor (50x) and 5 µl RNase inhibitor (40 U/µl) to each cell sample. Cells were sonicated on ice 10 times (10 sec on, 10 sec off, Amplitude 15 %) until the lysate was clear. The lysates were centrifuged for 5 min at 14,000 × g at room temperature, 50 µl of the supernatant were kept as an INPUT control (used for qPCR analysis).

30 µl of Protein G Magnetic Beads (New England Biolabs) were incubated overnight at 4 °C (on a rotating wheel) with specific antibody (amount as described in manufacturer's) and 400 µl of IP lysis buffer, 1 % BSA. The following antibodies were used for RIP: PGC1α (1:100, AB3242, Merck, Rahway, NJ, USA), STAT3 (1:200,

9139S, Cell Signaling), pSTAT3 (1:100, 9145S, Cell Signaling), PKM1 (1:200, NBP2-14833, Novus Biologicals, Centennial, CO, USA), CTNNB1 (1:100, 9562, Cell Signaling), SIRT1 (10 µg, S5447, Sigma-Aldrich), IGF2BP2 (10 µg, PA5-29869, Thermo Fisher Scientific); RECQ (1:100, PA5-27100, Invitrogen) and human IgG (10 µg) were used as controls. On the next day total cell lysates were added to the beads and incubated overnight at 4 °C on a rotating wheel beads. On the next day samples were washed 5 times with 900 µl of IP lysis buffer. After the last wash the supernatant was removed and 100 µl of RIP buffer (50 mM Hepes (pH 7.5), 0.1 M NaCl, 5 mM EDTA, 10 mM DTT, 0.5% TritonX-100, 10% Glycerol, 1% SDS with 1 µl of RNase inhibitor) was added to the beads. Samples and INPUT controls were then incubated for 1 h at 70 °C to reverse the cross-link. Beads were collected using magnetic rack and 100 µl of supernatant was saved for RNA extraction with Trizol reagent (Thermo Fisher Scientific) according to the manufacturer's instruction. Further steps, including RT-qPCR for LL35, were performed as described in the paragraph 3.8 of this Chapter.

3.24 RNA pull-down assay

LL35 sequence obtained by RACE PCR was cloned to pcDNA3.1 vector by restriction enzyme digest cloning approach [210]. T7 transcription of LL35 from the vector was performed using TranscriptAid T7 High Yield Transcription Kit (Thermo Fisher Scientific) according to the manufacturer's instruction for High Yield *in vitro* Transcription. Newly synthesized transcript was purified by phenol/chloroform extraction. For transcript desthiobiotinylation we used a Pierce™ RNA 3' End Desthiobiotinylation Kit (Thermo Fisher Scientific) according to the manufacturer's protocol with further

phenol/chloroform extraction RNA purification. RNA pull-down was performed using Pierce™ Magnetic RNA-Protein Pull-Down Kit (Thermo Fisher Scientific). Briefly, AML12 cells were cultured in T-175 flasks. Cells were trypsinized, washed twice with 1×PBS and collected by centrifugation at 200 × g, 5 min. 10^7 cells were used for each replica. Total cell lysates were prepared using IP lysis buffer (Thermo Fisher Scientific) according to the manufacturer's protocol. For the binding of labeled RNA transcript to streptavidin magnetic beads we used 100 pmol of desthiobiotinylatited LL35 transcript and 50 µl of beads as described in manufacturer's protocol. For protein binding we used 30 µl of prepared lysate with concentration higher than 2 mg/ml. At the end of the protocol after two washes and elution of RNA-protein complexes, protein mixture was run on the SDS-PAGE. Then we performed a silver staining as follows: gel was fixed in 20 % ethanol, 10 % acetic acid for 2 hours, washed 5 times for 15 min in H_2O, incubated with thiosulfate (0,3 g/L), washed 3 times for 1 min in H_2O, stained with silver nitrate (1 g/L AgNO3, 1 mL/L formalin) for 15 min, washed 3 times with H_2O for 30 sec, incubated with developer (40 g/L Na_2CO_3, 20mL of 0,3g/L thiosulfate per 100 mL of total solution, 1 mL/L formalin) until clear bands and stopped with 10 % acetic acid. Then lanes of different weights with visible proteins enrichment compared to the negative control were cut and proceeded to LC-MS analysis of gel pieces similar as LC-MS for proteome (section 3.14 of this chapter).

3.25 Statistical analysis

All diagrams presented here are based on at least three independent experiments. Statistical processing of obtained data was performed using the GraphPad Prism soft-

ware (version 8.0.1) (Graphpad Holdings, LLC, CA, USA) with a multiple t-tests. The data were considered statistically significant at p-value < 0.05. Venn diagram was built using Venny 2.1 software [211].

Chapter IV. Results

This work was performed by the author at Dr. Timofei Zatsepin's laboratory, at Center for Molecular and Cellular Biology, Skolkovo Institute of Science and Technology. The author performed all molecular biology experiments, data analysis and visualization described in this chapter, except the following. LC-MS for proteomics was done by Dr. Rustam Ziganshin (Shemyakin-Ovchinnikov Institute of Bioorganic Chemistry), LC-MS for lipidomics and metabolimics was performed by Elena Stekolshchikova and Nikolay Anikanov (Center for Neurobiology and Brain Restoration, Skolkovo Institute of Science and Technology), Dr. Tatiana Abakumova (Center for Molecular and Cellular Biology, Skolkovo Institute of Science and Technology) performed mice treatment and blood collection, Dr. Pavel Melnikov (Serbsky National Medical Research Center for Psychiatry and Narcology) did confocal microscopy analysis. RNA-seq data processing to obtain a list of differentially expressed genes was performed by Dr. Ilia Kurochkin (Center for Molecular and Cellular Biology, Skolkovo Institute of Science and Technology) and Ksenia Deinichenko (Institute of Biomedical Chemistry). Lipidome and Metabolome data analysis and visualization was done by Daniil Bobrovskiy (Faculty of Bioengineering and Bioinformatics, Lomonosov Moscow State University) under the supervision of Dr. Ekaterina Khrameeva (Center for Molecular and Cellular Biology, Skolkovo Institute of Science and Technology). RNA-sequencing was performed by Dr. Maria Logacheva at Skoltech Genomics Core Facility. Dr. Olga Sergeeva (Center for Molecular and Cellular Biology, Skolkovo Institute of

Science and Technology) participated in the design of the experimental work and flow cytometry analysis of the cell cycle.

4.1 LL35 expression in murine hepatocytes and liver

Previously in our laboratory we demonstrated prevalent expression of LL35 lncRNA gene (9020622O22Rik) in murine liver, lungs and spleen [17]. To further assess the role and functional significance of LL35 in the physiology of hepatocytes we compared its RNA expression level in normal murine hepatocyte cell line (AML12) and two hepatoma cell lines (Hepa1-6 and Hepa-1c1c7) by RT-qPCR. Obtained data revealed that LL35 RNA level in both hepatoma cell lines are hardly detected and more than 200 times lower compared with LL35 amount in normal hepatocytes AML12 (**Figure 25A**).

Downregulation of LL35 in hepatoma cells prompted us to check LL35 RNA levels in the murine model of hepatocellular carcinoma (HCC). We used plasmids encoding human ΔN90-β-catenin, human MET, and Sleeping Beauty transposase to induce HCC in mice. This murine HCC model is the closest one to human HCC among others [192]. The obtained results showed that LL35 RNA expression in HCC model is more than two times lower compared with normal liver samples (**Figure 25B**).

Alterations in LL35 RNA expression under proliferative conditions, such as HCC, and evidence, that many lncRNAs change their levels during liver regeneration [212] urged us to measure LL35 expression level in the murine liver after partial hepatectomy [193]. RT-qPCR data revealed LL35 RNA downregulation in 2 h after surgery followed by the increase of LL35 expression level during the liver regeneration (**Figure 25C**).

Moreover, previously our research group has found that LL35 is ~70 % downregulated in mouse liver in two weeks after induction of fibrosis with carbon tetra-chloride [17]. Taking data above together, one can consider that LL35 lncRNA is functionally significant in normal murine liver and may be a probable biomarker in different liver diseases.

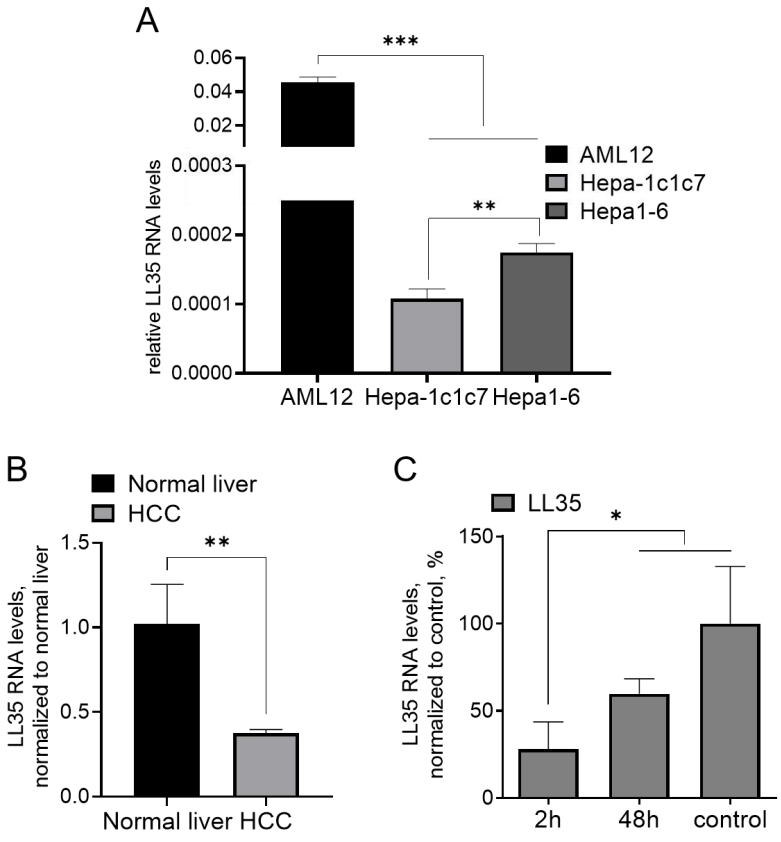

Figure 25*. Evaluation of LL35 RNA expression in hepatocyte cell lines and murine liver.* ***(A)*** *Hepatocyte cell lines.* ***(B)*** *Normal and HCC murine liver.* ***(C)*** *Partial hepatectomy murine model. ACTB – reference gene in RT-qPCR. Results show mean ± SD. * $p < 0.05$, ** $p < 0.01$ and *** $p < 0.001$.*

4.2 LL35 transcripts in murine liver and AML12 cell line

LL35 was initially annotated as RIKEN cDNA 9030622O22 gene (NCBI Gene Symbol: 9030622O22, Ensembl ID: ENSMUSG00000086141.8). According to current NCBI annotation release 109 [213] LL35 has 42 transcripts, while in Ensembl release 106 [214] there are only 3 annotated transcripts of LL35. Bioinformatic analysis of RNA sequencing data for murine liver samples disclosed that only 10 exons of LL35 are expressed in normal mouse liver. These 10 exons fit into two LL35 transcripts annotated by NCBI: XR_866812.3 and XR_866829.3 (**Figure 26**). For LL35 PCR analysis in hepatocytes we further designed multiple primers specific for these 2 transcripts and located in different exons. Using various combinations of designed PCR primers, we successfully verified that AML12 cells contain a region from exon 4 to exon 6 of XR_866812.3 and XR_866829.3 transcripts. We used this region as a starting point for RACE PCR (rapid amplification of cDNA ends) experiment, in which we identified a new LL35 transcript in AML12 cells. The found that the transcript is 1193 nt long and does not have a 100 % identity with any of the annotated transcripts in the databases. The closest annotated sequence for the obtained by RACE PCR LL35 transcript is XR_866813.3 isoform from NCBI, which is 148 nt longer at 5'- end and 279 nt longer at 3'- end (**Figure 26**). Thus, AML12 cells contain at least one LL35 transcript 1193 nt long and we found it using RACE method followed by additional confirmation using Sanger sequencing (**Supplementary Figure S1**).

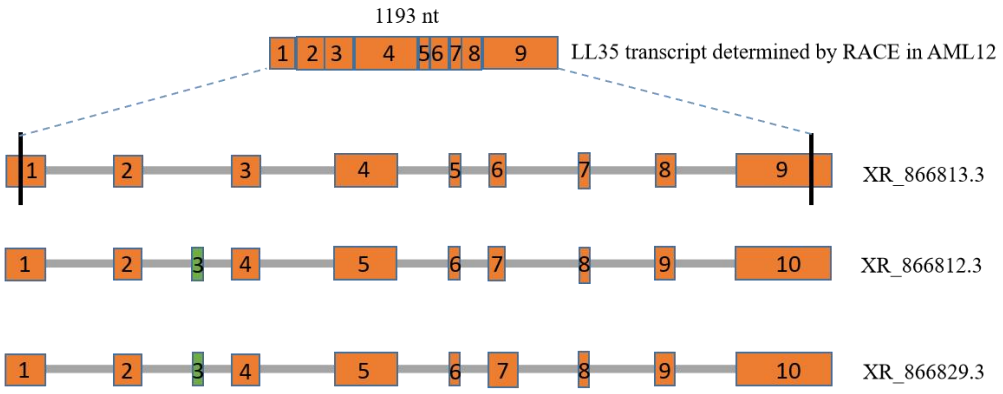

Figure 26. *Schematic representation of LL35 transcripts found by RACE experiment in AML12 cells and by exons expression analysis of RNA-seq data of murine liver. Upper transcript was identified by RACE PCR in AML12 cells. XR_866813.3 is the closest transcript from NCBI database to one identified by RACE, XR_866812.3 and XR_866829.3 are transcripts that contain 10 LL35 exons identified by RNA-seq data for nurine liver. Orange box – exon present in all LL35 transcripts described here, green box – exon present only in those LL35 transcripts that match RNA-seq data for murine liver, and absent in transcript determined by RACE PCR.*

4.3. LL35 downregulation using antisense oligonucleotides in vitro and in vivo

To study the function of LL35 lncRNA *in vitro* and *in vivo* we performed its knockdown using antisense oligonucleotide (ASO) technology. We have chosen ASO instead of RNA interference (siRNA) technique, because LL35 is predominantly located in the nucleus [17], where RNA interference is not efficient while ASO can downregulate RNA transcripts both in nucleus and cytoplasm. An effective mix of 5 different ASOs (**Supplementary Table S1**) specific to various regions of LL35 lncRNA, was designed based on predicted LL35 structure with Vienna RNA software and localization of target exons [17]. As a control for knockdown experiments, we used ASO specific to Firefly luciferase mRNA (Luc) in 100 nM concentration. Using a described above ASOs mix

with 20 nM final concentration of each ASO we managed to achieve 85 % knockdown of LL35 in AML12 cells on the day 2 after transfection (**Figure 27A**).

For LL35 downregulation *in vivo* we synthesized five ASOs (**Figure 27B**) (**Supplementary Table S2**) with the same core sequences as ASOs for *in vitro* studies, but 3'- GalNAc-conjugated for improved targeted delivery to the liver after intravenous or subcutaneous injection [191]. To choose the best conditions for knockdown *in vivo* we tested several concentrations of GalNAc-ASO conjugates for LL35 and two time points: day 2 and day 5. GalNAc-ASO conjugate for Luc in appropriate concentrations was used as a control. We injected GalNAc-ASO conjugates in murine tail vein at different concentrations: 25 mg/kg, 50 mg/kg, 100 mg/kg, 150 mg/kg and 200 mg/kg in total for 5 oligos and analyzed the efficacy of LL35 RNA inhibition at days 2 and 5 by RT-qPCR. At day 2 after single injection we observed only ~63 % decrease in LL35 expression level in comparison with control Luc GalNAc-ASO (**Figure 27C**). Meanwhile, on the day 5 the knockdown efficacy of LL35 in mice that received 150 mg/kg and 200 mg/kg doses reached 81 % and 84 %, respectively (**Figure 27D**). After analyzing RT-qPCR data, we decided to choose a day 5 time point and ASOs mix concentration of 150 mg/kg in total for further experiments (**Figure 27E**).

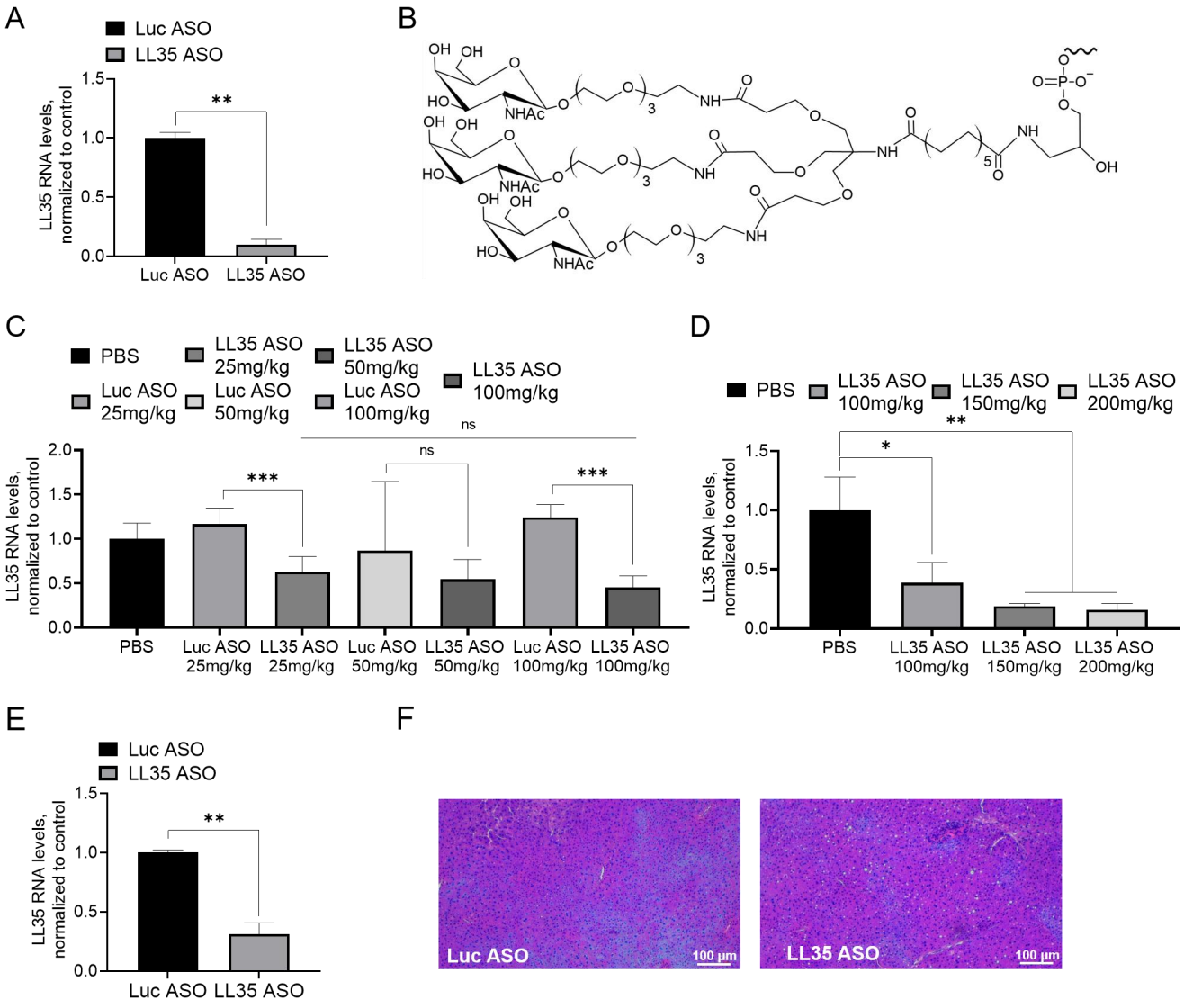

Figure 27. *ASO-mediated LL35 knockdown (KD) in vitro and in vivo. (**A**). LL35 knockdown on the 2nd day after AML12 cells treatment with 20nM mix of 5 ASOs specific to LL35 (LL35 ASO), Luc ASO – control. (**B**). Schematic structure of GalNAc-ASO conjugates used for LL35 depletion in vivo. (**C**). LL35 knockdown on the day 2 of mice injection with different concentrations of GalNAc-ASO conjugates (LL35 ASO), Luc ASO, PBS - control. (**D**). LL35 knockdown on the day 5 of mice injection with different concentrations of GalNAc-ASO conjugates (LL35 ASO), PBS - control. Normalization on ACTB gene. (**E**). LL35 KD in the liver at day 5 after injection of GalNac-ASO conjugates (LL35 ASO). Luc ASO – control. Normalization on ACTB gene. (**F**). Hematoxylin-eosin (H&E) staining of liver samples after LL35 depletion (LL35 ASO). Three biological replicas per condition were used in each experiment; results show*

*mean ± SD. n.s.—not significant, * $p < 0.05$, ** $p < 0.01$ and *** $p < 0.001$, p-value was obtained using multiple t-test in GraphPad Prism.*

To assess the physiological conditions of mice and pathological changes in the liver, which could be caused by the administration of GalNAc-ASO conjugates for LL35 depletion, we conducted a morphological study of murine liver and biochemical blood analysis. Hematoxylin and eosin staining of liver samples did not reveal any changes after LL35 inhibition in comparison with control samples (**Figure 27F**). Also we did not observe any signs of liver damage or inflammation, such as neutrophil or lymphocyte infiltration or focal necrosis. Moreover, the animal blood analysis demonstrated that levels of key factors, such as ALT, AST, ALP and others, remained unchanged (**Figure 28**). Also, we didn't observe significant changes in weight or differences in the behavior of the mice between LL35 knockdown and control groups. Taking together, our data demonstrates that administration of GalNAc-ASO was well tolerated.

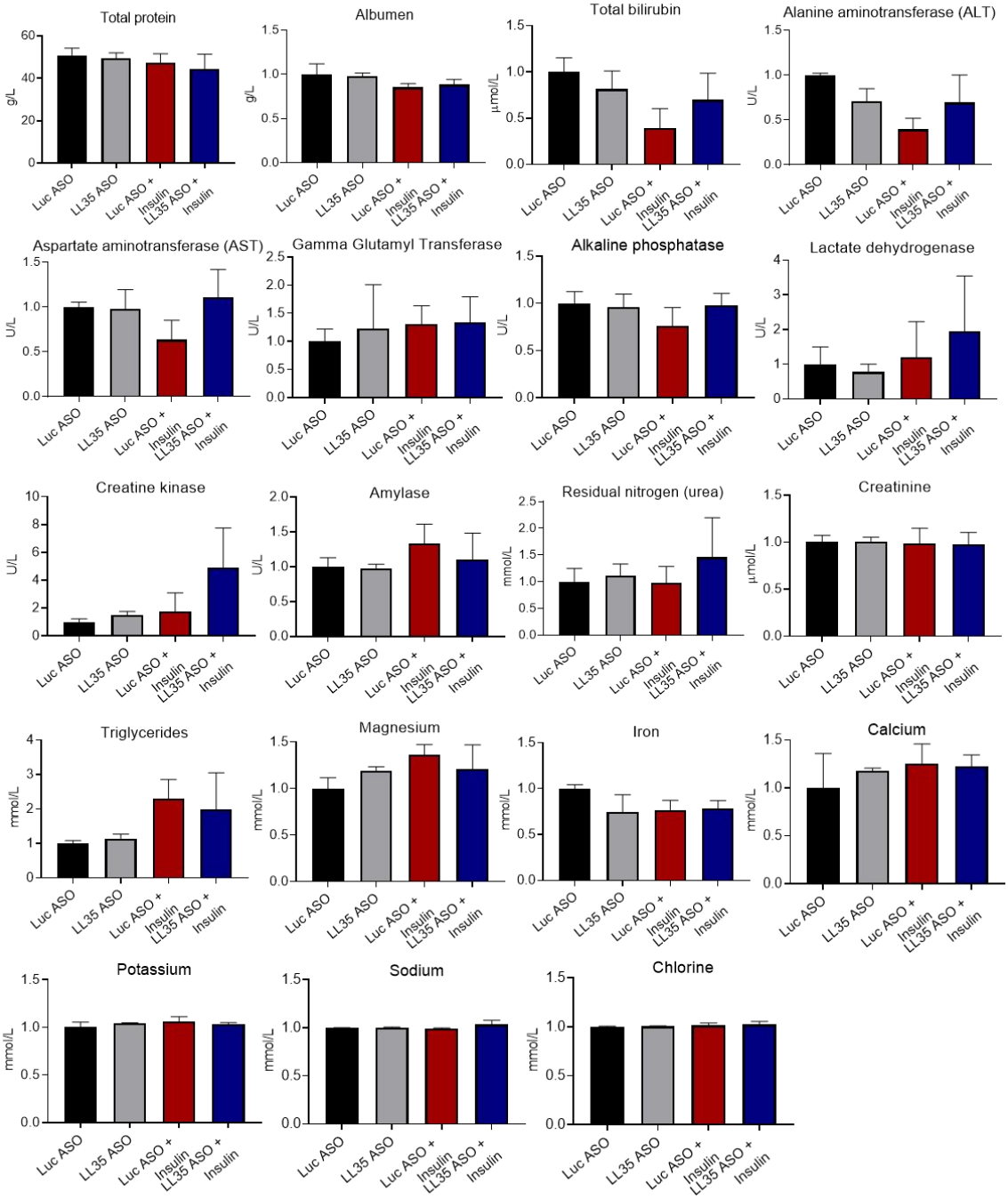

Figure 28. *Biochemical markers analyzed in animal blood on the 5th day after LL35 depletion by injection of GalNAc-ASO conjugates (LL35 ASO), Luc ASO - control. Luc ASO + Insulin and LL35 ASO + Insulin indicates groups of animals which were treated with 1U/kg insulin 1 hour before blood sampling for analysis.*

4.4 Analysis of gene and protein expression after LL35 knockdown in vitro and in vivo

To understand which biological processes and functions are affected by LL35 in the cell, we analyzed changes in mRNA profiles of AML12 cells on the day 2 and in the murine liver on the day 5 after LL35 knockdown by deep RNA sequencing. Volcano plots for AML12 cells and murine liver of RNA-seq data were shown in **Supplementary Figure S2A and S2B**, respectively. We calculated differential mRNA expression and based on obtained data we defined a following cut-off for differentially expressed genes: |log2foldchange| > 0.8, adjusted p-value < 0.1. Thereby we found significant changes in expression of 796 genes *in vitro* and 170 genes *in vivo* after LL35 depletion in comparison with Luc control. It is interesting to note that only 5 differentially expressed genes were common between *in vitro* and *in vivo* sets (**Figure 29A**), which could be explained by more complex intercellular interactions in murine liver compared with cell lines. Among 796 differentially expressed genes in AML12 cells 273 genes were downregulated and 523 were upregulated, meanwhile in liver tissue 107 genes showed significant downregulation and 63 upregulation.

For differentially expressed genes we performed the PANTHER Reactome pathway analysis [196] to study the processes affected by LL35 depletion. We observed, that in AML12 cells the most enriched pathways (p-value < 0.05) are related to cell cycle, development, rRNA processing and lipid metabolism (particularly, glycerophospholipid biosynthesis, complex I biogenesis, metabolism of steroids) (**Figure 29B**). Pathway enrichment analysis results for liver samples partially correlate with changes *in vitro:*

among significant pathways (p-value < 0.05) we observed metabolism, glutathione conjugation, biological oxidations and sulfur amino acid metabolism (**Figure 29C**). At the same time, we did not find alterations in pathways related to cell cycle after LL35 knockdown *in vivo,* which could be explained by the slow turnover of hepatocytes [215], and observed enrichment in stress-related pathways, such as HSF1-dependent transactivation and regulation of HSF1-mediated heat shock response.

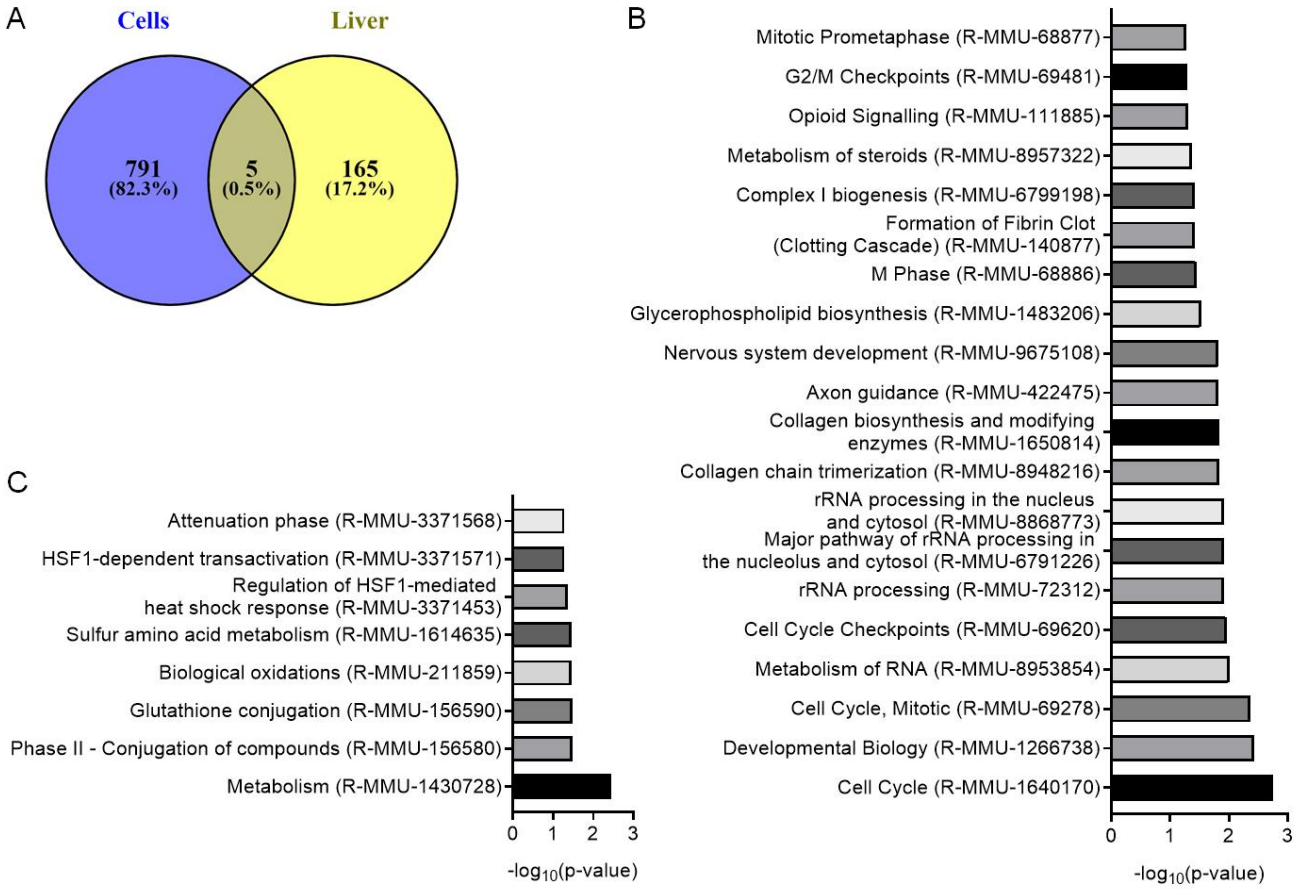

Figure 29. *Results of transcriptome analysis of AML12 cells and murine liver after LL35 depletion. (**A**). Venn diagram for differentially expressed genes after LL35 knockdown in AML12 cells in comparison with murine liver. Top representative pathways with p-value<0.05 obtained by PANTHER Reactome analysis of differentially expressed genes after LL35 depletion in (**B**). AML12 cells; (**C**). murine liver.*

For the additional investigation of transcriptomic changes after LL35 knockdown in AML12 cells and murine liver we conducted a gene ontology analysis for differentially expressed genes by three gene attributes: molecular function (MF) (**Supplementary Figure S3A, S3B**), cellular component (CC) (**Supplementary Figure S3C, S3D**) and biological process (BP) (**Supplementary Figure S3E, S3F**). Enriched data showed similar effects of LL35 knockdown *in vitro* and *in vivo* in the reaction to endogenous stimulus, signaling receptor activity and signal transduction. For *in vivo* data we again observed changes in multiple metabolic processes. Interesting difference was found in the analysis of the cellular components changes: for liver tissue we saw an abundance of changes in nuclear compartments, while for AML12 cells – in the compartments associated with intracellular contacts.

Then we performed RT-qPCR analysis of the genes related to cell cycle regulation, lipid biosynthesis and metabolism to confirm the transcriptomic data for LL35 depleted AML12 cells and murine liver (**Figure 30**). RT-qPCR analysis confirmed changes in expression of genes of interest, thus, showing the correlation between RT-qPCR and RNA-seq data and verifying the results of the PANTHER enrichment analysis.

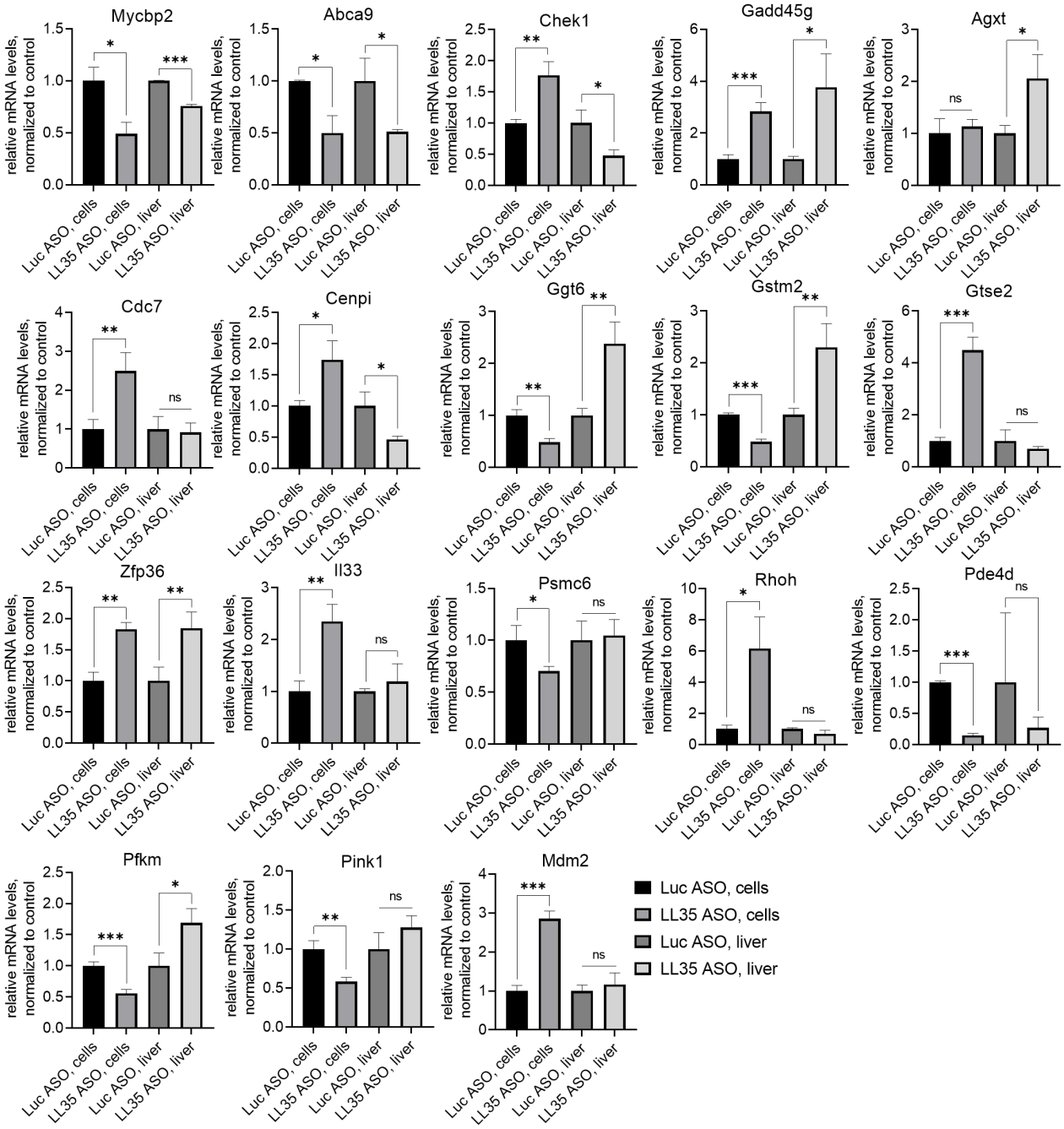

Figure 30. *Validation of transcriptome data by RT-qPCR, normalization on ACTB gene. Three biological replicas per condition were used in each experiment; results show mean ± SD. n.s.—not significant, * $p < 0.05$, ** $p < 0.01$ and *** $p < 0.001$, p-value was obtained using multiple t-test in GraphPad Prism.*

In addition, we took RNA-seq data for LL35 knockout in murine lungs tissue, previously published by Swarr et al. [5], and performed PANTHER Reactome pathways analysis using the same parameters as we did for our data. Among enriched pathways in lung tissue (**Figure 31A**) we would like to highlight metabolism of amino acids and derivatives, cell cycle, extracellular matrix organization, which correlates with observed changes in AML12 cells.

For AML12 cells we also conducted a LC-MS-proteomic analysis at day 2 after LL35 inhibition. Totally, expression levels of 232 proteins were changed significantly (cutoff 2) after LL35 knockdown in comparison with Luc control. 102 proteins were upregulated, while 130 appeared to be downregulated. PANTHER Reactome pathways analysis showed abundance in following pathways: signaling transduction, proteins modification, translation and phospholipid metabolism (**Figure 31B**). Obtained proteomic data correlate with transcriptomic data for AML12 cells.

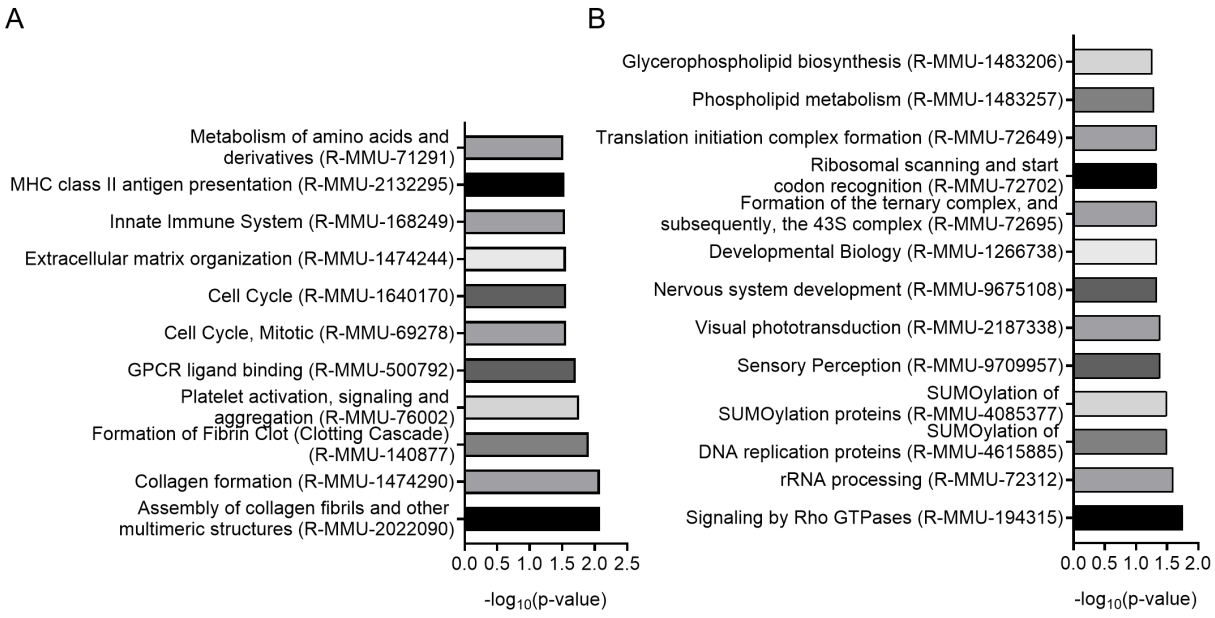

Figure 31. *(**A**). Top representative pathways obtained by PANTHER Reactome analysis of differentially expressed genes (|log2FC|>0.8, adjusted p-value <0.1) in lung epithelium isolated from null LL35 mice* [5]. *(**B**). Top representative pathways obtained by PANTHER Reactome analysis for significantly changed proteins after LL35 depletion in AML12 cells.*

4.5 LL35 knockdown causes changes in hepatocytes lipidome and metabolome both in vitro and in vivo

Transcriptomic and proteomic data for LL35 depletion revealed enrichment in pathways associated with cellular metabolism and lipid biosynthesis, so we performed a high-throughput LC-MS-based lipidome and metabolome analysis of LL35 depleted AML12 cells and murine liver on the day 2 and day 5, respectively.

We revealed abundances for 6429 polar metabolite and 3074 lipid features from the cell culture samples and 3135 polar metabolite and 1681 lipid features from the liver tissue samples. Among them only 294 polar metabolite and 1111 lipid features from the AML12 cells and 382 polar metabolite and 661 lipid features from murine liver were putatively annotated. We performed the principal component analysis (PCA) of the lipid and metabolite data for visualization of samples variation. According to PCA AML12 cells samples showed clear separation between the LL35 knockdown and control groups (**Figure 32A**).

We performed a group-based analysis to evaluate the significance of LL35 downregulation at the level of individual lipid classes and found that a number of classes affected by LL35 knockdown both in cell culture and in liver tissue. All the features from these lipid classes were then subject to additional MS2 confirmation and only lipid classes with fgsea FDR < 10 % both before and after confirmation were considered to be

significantly dependent on LL35 knockdown. This approach revealed that the abundance of plasmanyl-/plasmenylphosphatidylcholines (O-PC/P-PC) decreased in both AML12 cells and liver tissue (**Figure 32B, 32C**). Furthermore, the abundance of phosphatidylethanolamines (PE) and hexosylceramides (HexCer) increased only in cell culture (**Figure 32B**), while diradylglycerols (DG), ceramides (Cer;O2) and lysophosphatidylcholines (LPC) showed significant increase solely in murine liver (**Figure 32C).** To establish the relationship between lipidomic changes and specific genes, we checked mRNA levels of crucial enzymes involved in lipid metabolism after LL35 knockdown *in vitro* and *in vivo* by RT-qPCR and found dysregulation of the following: Pcyt1b, Chpt1, Cept1, Pisd, Etnk1 and Etnk2 (participate in PC and PE biosynthesis), Lpcat1 and Lpcat3 (LPC synthesis), Pla2g4a (DG synthesis), Smpd1 and Asah1 (ceramides production). (**Figure 32D**).

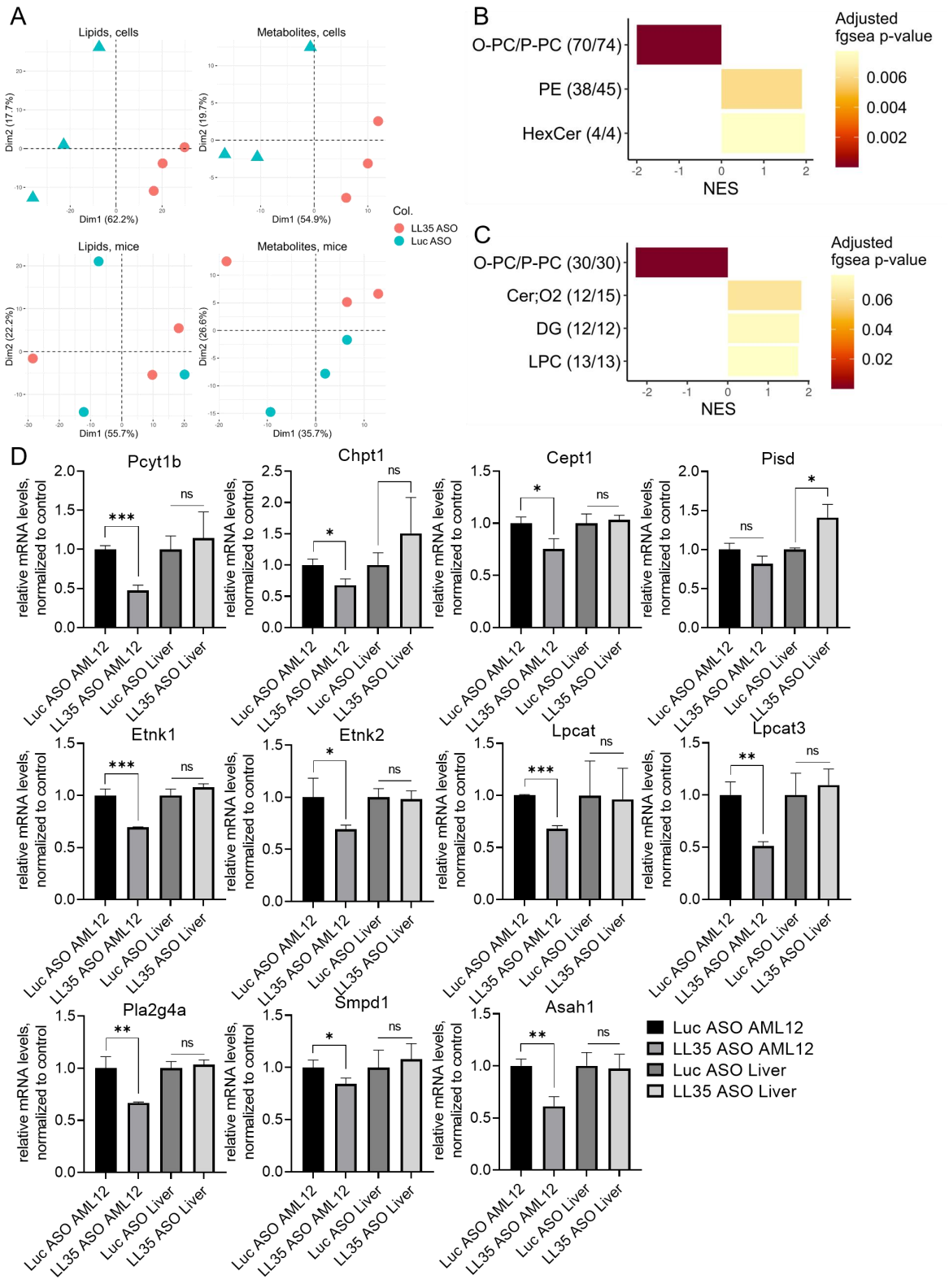
A
Lipids, cells
Metabolites, cells
Lipids, mice
Metabolites, mice
Dim1 (62.2%)
Dim2 (17.7%)
Dim1 (54.9%)
Dim2 (19.7%)
Dim1 (55.7%)
Dim2 (22.2%)
Dim1 (35.7%)
Dim2 (26.6%)
Col.
LL35 ASO
Luc ASO
B
O-PC/P-PC (70/74)
PE (38/45)
HexCer (4/4)
NES
Adjusted fgsea p-value
0.006
0.004
0.002
C
O-PC/P-PC (30/30)
Cer;O2 (12/15)
DG (12/12)
LPC (13/13)
NES
Adjusted fgsea p-value
0.06
0.04
0.02
D
Pcyt1b
Chpt1
Cept1
Pisd
Etnk1
Etnk2
Lpcat
Lpcat3
Pla2g4a
Smpd1
Asah1
relative mRNA levels, normalized to control
Luc ASO AML12
LL35 ASO AML12
Luc ASO Liver
LL35 ASO Liver
ns

Figure 32. *Lipidome and metabolome analysis of AML12 cells and murine liver after LL35 depletion. (**A**). PCA score plots for AML12 cells and liver samples, LL35 ASO – LL35 KD, Luc ASO – control. Significantly changed lipid classes after LL35 depletion in (**B**). AML12 cells; (**C**). murine liver. Numbers in brackets: the number of confirmed features and the total number of features. (**D**). RT-qPCR analysis of RNA expression levels of the key genes participated in synthesis and break-down of significantly changed lipids classes after LL35 knockdown (LL35 ASO) and control (Luc ASO), normalization on ACTB gene. NES – normalized enrichment score. Three biological replicas per condition were used in each experiment; results show mean ± SD. n.s.—not significant, * $p < 0.05$, ** $p < 0.01$ and *** $p < 0.001$, p-value was obtained using multiple t-test in GraphPad Prism.*

The effect of LL35 knockdown on polar metabolite features could not be measured by pairwise tests, since the statistical effects were too low to define a proper FDR threshold for metabolites associated with treatment. However, we identified significant effects of LL35 depletion on the polar metabolites using group-based analysis. While no pathways were enriched in case of liver tissue samples, 5 KEGG pathways were affected by the knockdown in cell culture: purine metabolism, aminoacyl-tRNA biosynthesis, central carbon metabolism in cancer, glutathione metabolism and phenylalanine, tyrosine and tryptophan biosynthesis (fgsea FDR<5%) (**Figure 33A)**. Significant difference in purine metabolism between knockdown and Luc control cells was supported by the enrichment analysis on a subset of 99 SMPDB metabolic sets suggested by MetaboAnalyst (fgsea FDR<5%).

The fact that purine metabolism in cell culture seems to be affected by LL35 knockdown is also supported by sparse PCA. Using this method, we selected 30 features for the first principal component, along which the samples were divided into knockdown and control groups. Out of these 30 features, 10 turned out to be involved in purine metabolism (MetaboAnalyst Over Representation Analysis, FDR=0.024). We could not

apply sparse PCA to liver samples analysis, since the knockdown and control groups were harder to distinguish even on normal PCA.

Afterwards we performed an Oil Red O staining to visualize and measure the lipid droplets formation in cells, where neutral triglycerides and lipids could be accumulated [216]. At day 2 after LL35 knockdown in AML12 cells we observed an increase in lipids droplets size (mean diametr for LL35 ASO = 2.9 ±0.7 μm, mean for Luc ASO = 1.6 ±0.6 μm) and accumulation (mean fluorescent intensity for LL35 ASO = 0.41 ±0.1 RFI, mean for Luc ASO = 0,3 ±0.08 RFI) in comparison with control cells (**Figure 33B**). Meanwhile there were no significant difference in lipid droplets between liver samples with LL35 depletion and control liver samples (**Figure 33C**). Obtained micrograph for *in vitro* data correlates with lipidomic analysis. Probably to observe phenotype changes *in vivo* we need to perform longer knockdown of LL35. On the other hand, prolonged knockdown *in vivo* can lead to the multiple secondary effects.

Finally, we used a Click-iT® Lipid Peroxidation Imaging Kit to check if LL35 depletion causes changes in lipid peroxidation in AML12 cells. We found that depletion of LL35 results in significant increase of lipid peroxidation *in vitro* (**Figure 33D, 33E**).

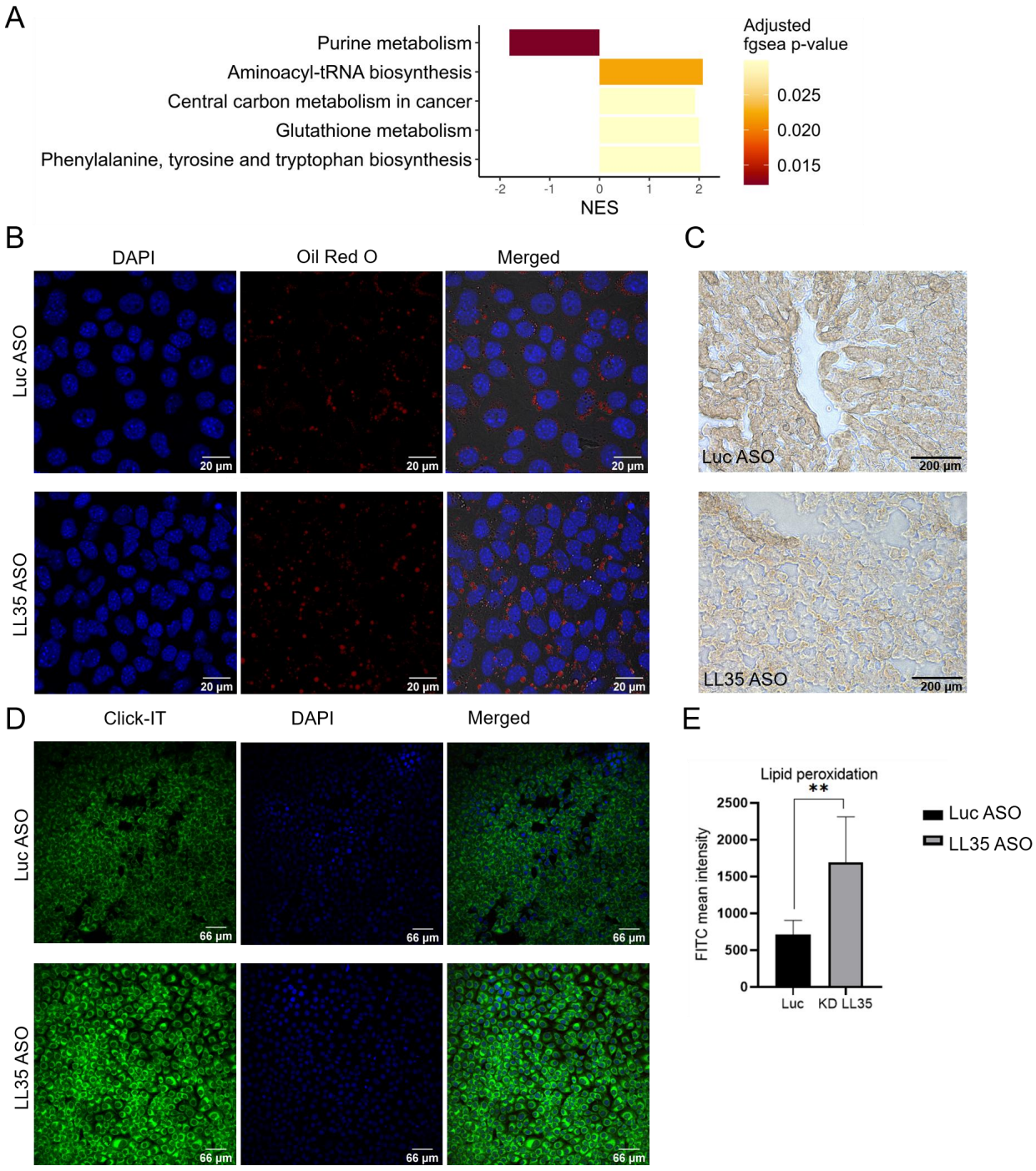

Figure 33. *(**A**). KEGG pathways analysis of the metabolites, which are significantly influenced by LL35 knockdown in AML12 cells. NES – normalized enrichment score. Lipid droplets staining with Oil Red O after LL35 depletion (LL35 ASO) (**B**). in AML12 cells (nucleus were stained with DAPI); (**C**). in murine liver. Control – Luc ASO. (**D**). LL35 knockdown upregulates lipid peroxidation. Data obtained from Click-*

*iT® Lipid Peroxidation Imaging Kit with (**E**). further analysis by confocal microscopy. KD LL35 – cells transfected with ASOs for LL35, Luc – control cells transfected with ASO to luciferase. Three biological replicas per condition were used in each experiment; results show mean ± SD. n.s.—not significant, * $p < 0.05$, ** $p < 0.01$ and *** $p < 0.001$, p-value was obtained using multiple t-test in GraphPad Prism.*

4.6 Knockdown of LL35 lncRNA interferes with glucose metabolism in normal hepatocytes in vitro and in vivo

Lipid metabolism is tightly associated with glucose metabolism, in particular, through *de novo* synthesis of fatty acids and glycerol [217]. Moreover, several years ago it was discovered, that DEANR1 – a functional human analog of LL35, is involved in the regulation of pancreatic cancer glycolysis and proliferation and also induces cell cycle arrest and apoptosis [10]. Based on this knowledge we decided to check glucose metabolism after LL35 depletion in AML12 cells.

Mitochondrial oxidative phosphorylation and glycolysis are the main sources of total ATP in the cell. To assess the possible involvement of LL35 in ATP synthesis we first performed a Mito Stress Test, which measures key parameters of the mitochondrial function by the direct measuring the oxygen consumption rate (OCR) of cells, at day 2 after LL35 knockdown in AML12 cells using a Seahorse analyzer. During Mito assay the following components are added to the cells media that affect the activity of the electron-transport chain, which makes it possible to assess its functionality: 1 μM oligomycin, 1 μM FCCP and 1μM rotenone/antimycin A. Measured OCR values showed no significant difference in mitochondrial respiration for AML12 cells with LL35 knockdown in comparison with Luc control, which indicates a normal electron flux through mitochondrial electron transport chain (**Figure 34A, 34B, 34C**). During glycolysis

glucose is converted to pyruvate, which, in turn, is converted to lactate with protons release into the extracellular medium. The Seahorse XF instrument measures the extracellular acidification rate (ECAR), which allows to assess the key parameters of glycolytic flux: glycolysis, glycolytic capacity, glycolytic reserve and non-glycolytic acidification. We performed a Glycolysis stress test on the day 2 after LL35 knockdown in AML12 cells, and measured ECAR values indicated that LL35 knockdown causes decrease of glycolytic flux, in particularly, the downregulation of glycolytic capacity, glycolytic reserve and non-glycolytic acidification (**Figure 34D, 24E**).

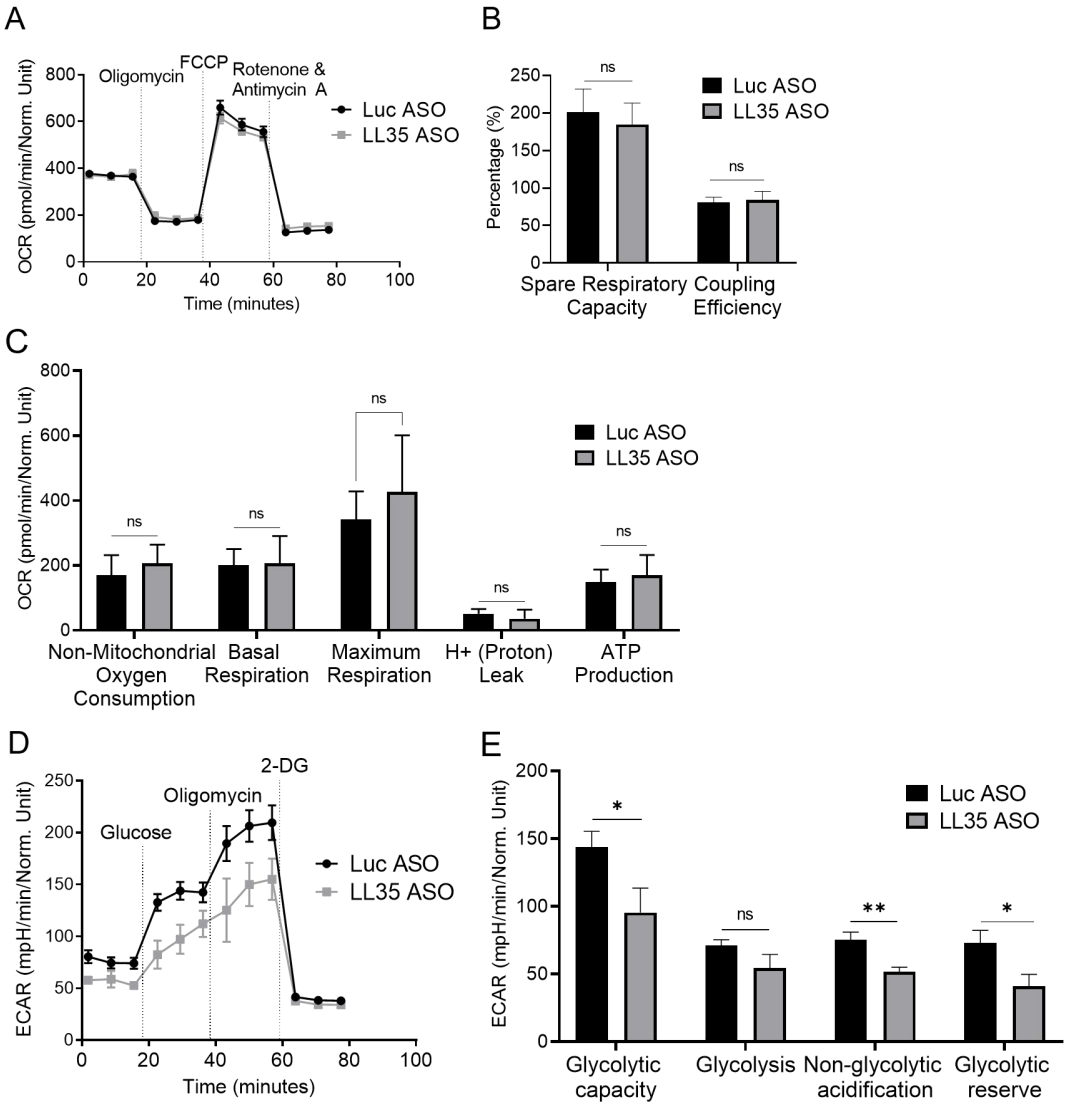

Figure 34. *Analysis of OCR and ECAR values in AML12 cells after LL35 depletion using Seahorse XF. (**A**). The average time curve for OCR after subsequent injections of 1μM oligomycin, 1μM FCCP and 1μM rotenone/antimycin A. Each data point represents an OCR value used for calculations. (**B**). Individual parameters for cell respiration in %, including spare respiratory capacity and coupling efficiency for AML12 cells after LL35 depletion (LL35 ASO) and control (Luc ASO). (**C**). Individual parameters for the cell respiration, including non-mitochondrial oxygen consumption, basal respiration, maximum respiration, proton leak, ATP production for AML12 cells after LL35 depletion (LL35 ASO) and control (Luc ASO). (**D**). An averaged time curve for ECAR after subsequent injections of 10 mM glucose, 1 μM oligomycin and 50 mM 2-DG. Each data point represents an ECAR value used for calculations. (**E**).*

*Individual parameters for the cell glycolytic function, including glycolytic capacity, glycolysis, non-glycolytic acidification and glycolytic reserve, for AML12 cells after LL35 depletion (LL35 ASO) and control (Luc ASO). Six biological replicas per condition were used in each experiment; results show mean ± SD. n.s.—not significant, * $p < 0.05$, ** $p < 0.01$ and *** $p < 0.001$, p-value was obtained using multiple t-test in GraphPad Prism.*

For additional characterization of mitochondria function after LL35 depletion, we performed mitochondria staining with TMRE and MitoTracker green FM. TMRE allows to quantify changes in the mitochondria membrane potential due to its accumulation in active mitochondria because of their relative negative charge. Meanwhile inactive or depolarized mitochondria have decreased potential and do not sequester TMRE. MitoTracker green FM localizes to mitochondria regardless of the membrane potential, allowing to estimate the total mitochondria number in the cell. Analysis of mitochondria staining with TMRE and MitoTracker using confocal microscopy showed that LL35 knockdown does not cause changes in number of active mitochondria as well as in total number of mitochondria (**Figure 35A**). Summing up the data received from Seahorse analyzer and mitochondria staining, we can conclude that LL35 does not participate in the proper functioning of mitochondria.

We found that L35 knockdown causes changes in the glucose metabolism, and to look in more detail at the changes in the mechanisms of this process, we performed analysis of multiple mRNAs and proteins after LL35 knockdown in AML12 cells. First, we checked mRNA expression of enzymes involved in main pathways of glucose metabolism, such as glycolysis, gluconeogenesis, pentose phosphate pathway, glutaminolysis, glycogen synthesis and acetyl-CoA synthesis by RT-qPCR and observed

significant alterations in some of them (**Figure 35B**). Thus, hexokinase (Hk2), lactate dehydrogenase (Ldha), enolase (Eno2), phosphofructokinase-2 (Pfkfb2), phosphofructokinase-2 (Pfkfb3), glucose transporter-1 (Glut1) showed significant upregulation of its mRNA expression on the day 2 after LL35 depletion (scheme of glycolysis and gluconeogenesis with differentially expressed genes is shown in **Supplementary Figure S4A**). Meanwhile, mRNA of the main glucose transporter in hepatocytes – Glut2 and phosphoinositide-dependent kinase-1 (Pdk1) were downregulated. Also, we checked mRNA expression of the enzymes, involved in gluconeogenesis pathway, the opposite pathway to glycolysis, which leads to glucose synthesis inside the cell. We showed that LL35 knockdown results in significant upregulation mRNA of two key gluconeogenic enzymes: G6pc and Pepck. Moreover, in the case of PEPCK, we observed a significant increase in both mRNA and protein levels (**Figure 35B, 35C**). Finally, we analyzed expression of main transcription factors, which participate in the regulation of glucose and lipid metabolism, and observed increased mRNA expression levels of Myc, Pgc1α, Egr1 and Sirt1, and decreased expression levels of FoxJ1 after LL35 knockdown (**Figure 35B**). All these data confirmed the involvement of LL35 lncRNA in the regulation of the glucose metabolism *in vitro*, but the molecular mechanism of the regulation is still under investigation.

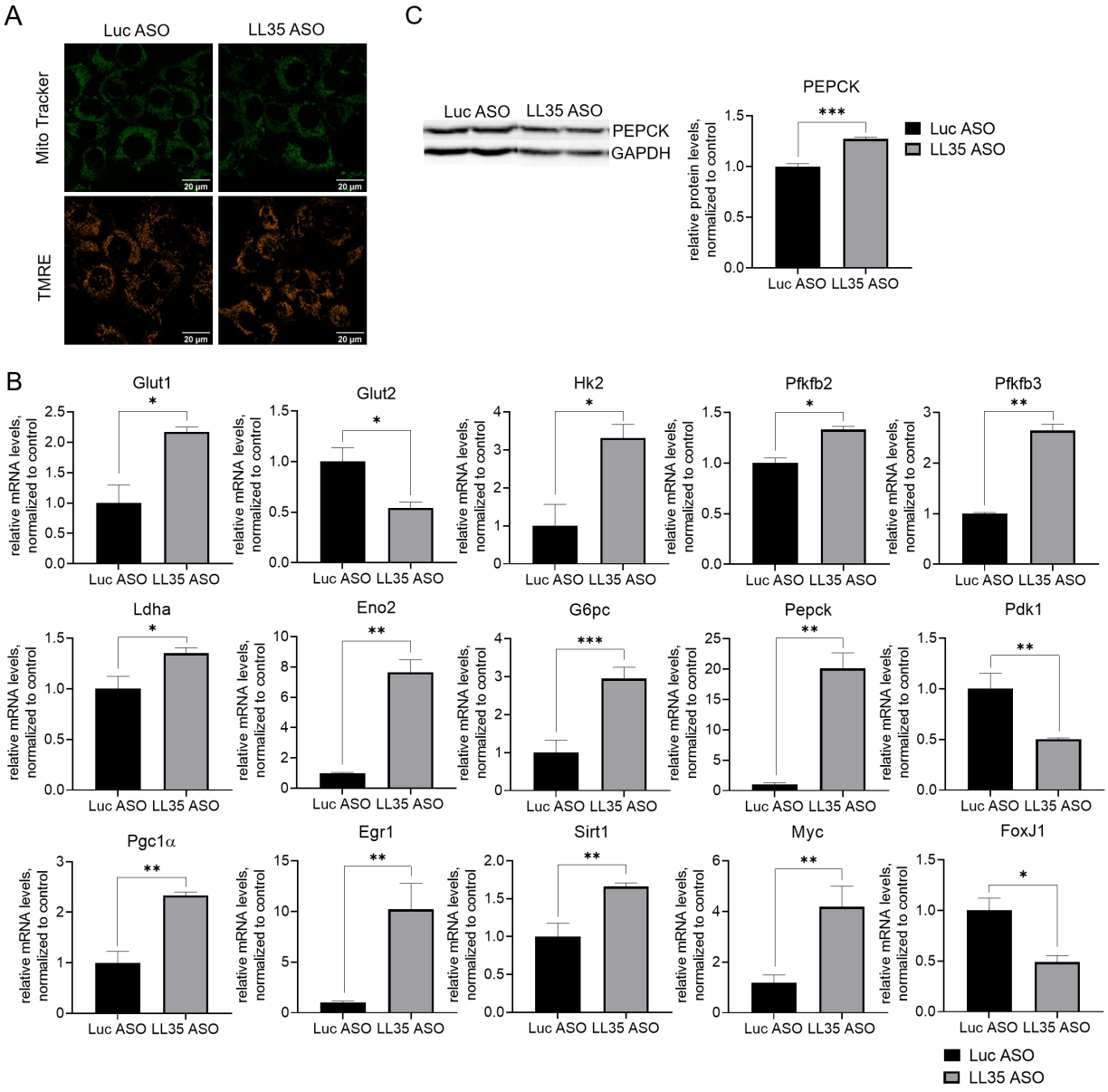

Figure 35. *Mitochondria staining and analysis of mRNA expression of genes related to glucose metabolism. (**A**). AML12 cells mitochondria staining with TMRE and Mito Tracker green after LL35 depletion and in control cells. (**B**). Evaluation of mRNA levels for key genes and transcription factors, which participate in glucose metabolism after LL35 knockdown (LL35 ASO) and control (Luc ASO) by RT-qPCR with normalization on ACTB gene. (**C**). Western blot and its quantification of PEPCK protein levels in AML12 cells after LL35 inhibition (LL35 ASO) and control (Luc ASO), quantification was performed using ImageJ. Three biological replicas per condition were used in each experiment; results show mean ±*

*SD. n.s.—not significant, * $p < 0.05$, ** $p < 0.01$ and *** $p < 0.001$, p-value was obtained using multiple t-test in GraphPad Prism.*

To investigate the involvement of LL35 lncRNA in the glucose metabolism *in vivo*, we performed insulin tolerance test. Insulin is a master regulator of glucose, lipid, and protein metabolism, and together with glucagon maintains normal glucose concentration [218]. We monitored glucose blood level in mice at day 5 after LL35 knockdown each 15 minutes during first hour after insulin injection (1 U/kg) and found that glucose blood level in mice with LL35 KD was 1,5-2 times higher than in control mice (**Figure 36A**). An injection of insulin activates glycolytic enzymes, leading to glucose digestion and rapid decrease in its level in the blood. Elevated glucose suggests that LL35 depletion results in a decreased insulin response. Analysis of the animal blood after the insulin injection demonstrated the compensation of the effects found for the LL35 depletion. LL35 depletion *in vivo* resulted in decrease of direct bilirubin, elevated levels of cholesterol, inorganic phosphorus and AST/ALT ratio (**Figure 36B**). Injection of insulin caused the absence of the differences between LL35 ASO mice and control mice. After we evaluated the effect of insulin treatment *in vivo*, we decided to look at the status of the AKT1/PI3K signaling pathway *in vitro* for additional confirmation of obtained data. Insulin leads to the activation of the phosphatidylinositol 3-kinase (PI3K)/Akt pathway by autophosphorylation of the β subunit of IR or IGF1 [219,220]. We measured pAKT1/AKT1 proteins ratio before and 1 hour after cells stimulation with 100 nM insulin. Level of AKT1 phosphorylation dramatically decreased (pAKT1/AKT1 before insulin stimuli was 3,5 times lower) after LL35 depletion in comparison to control cells, but insulin addition restored AKT1 phosphorylation (**Figure 36C, 36D**).

Deregulation of AKT1 signaling pathway in LL35 depleted cells, which participates in regulation of glycolysis and gluconeogenesis, may explain the observed changes in expression of genes related to glucose metabolism.

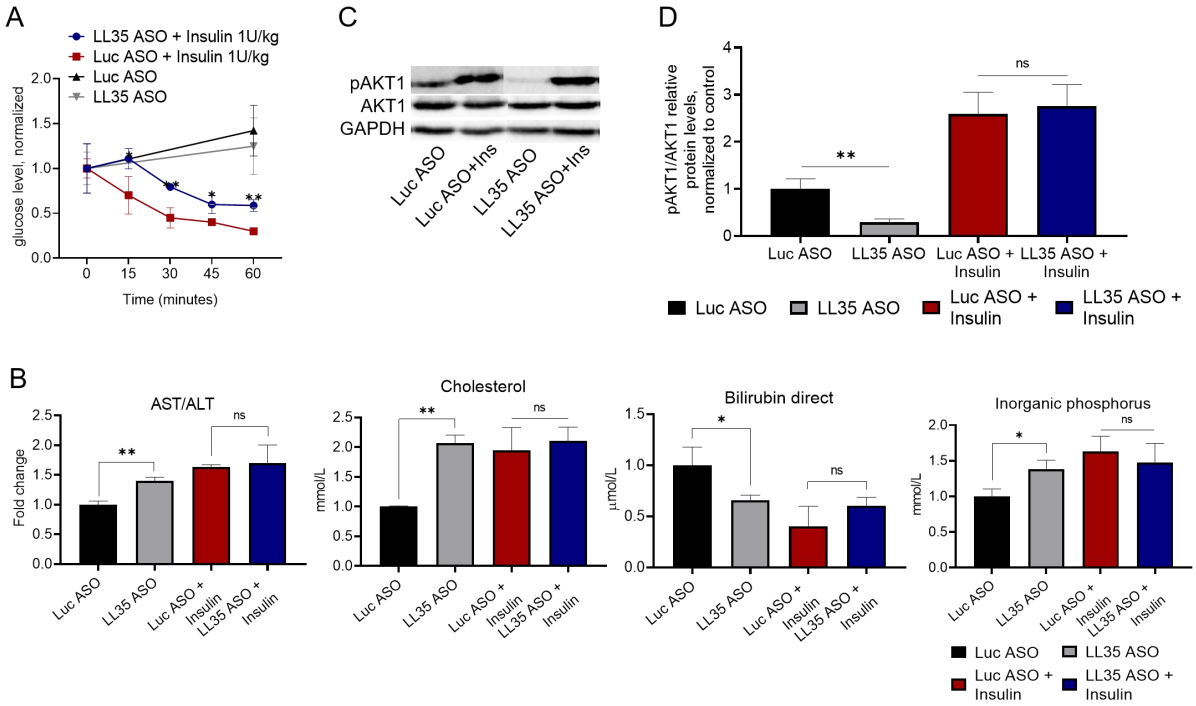

Figure 36. *The influence of insulin in mediating the effects of LL35 depletion in vitro and in vivo. (**A**). Insulin tolerance test in vi-vo. Glucose blood level in mice was measured each 15 minutes for 1 hour after insulin injection (1 U/kg). LL35 ASO – mice with depleted LL35, luc ASO – control mice. (**B**). Biochemical parameters of mice blood at day 5 after LL35 depletion (LL35 ASO) in comparison to control mice (Luc ASO). Insulin treatment compensates these differences. (**C**). Western blot of pAKT1 and AKT1 proteins in AML12 cells after LL35 knockdown (LL35 ASO) and control (Luc ASO) with 100 nM (+Ins) or without insulin treatment. (**D**). Quantification of pAKT1/AKT1 ratio for AML12 cells after LL35 knockdown and insulin treatment. Three biological replicas per condition were used in each experiment; results show mean ± SD. n.s.—not significant, * $p < 0.05$, ** $p < 0.01$ and *** $p < 0.001$, p-value was obtained using multiple t-test in GraphPad Prism.*

Finally, to find potential protein partners of LL35, which could mediate the effects of LL35 depletion on glucose and lipid metabolism, we performed RNA immunoprecipitation (RIP) analysis. RIP method allows to uncover direct interactions

between RNA and proteins. This technique is based on the usage of a specific antibody against the protein of the interest to pull down the targeted protein-RNA complexes, RNA molecules in which could be further analyzed by RT-qPCR. Based on our data for glycolysis dysregulation after LL35 knockdown and literature analysis of the main factors involved in the regulation of glucose metabolism, we picked up the following proteins for RIP: PGC1α, STAT3, pSTAT3, PKM1, CTNNB1, SIRT1, IGF2BP2. We incubated antibodies against these proteins with lysates from AML12 cells as described in Chapter III, isolated precipitated RNA and performed RT-qPCR analysis with primers specific to LL35 gene. Unfortunately, obtained data did not reveal abundancy of LL35 RNA for the selected proteins complexes (**Supplementary Figure S5A**).

Then we conducted an alternative experiment – RNA pull-down, allowing to enrich RNA Binding Proteins (RBPs) using biotinylated RNA and streptavidin magnetic beads. We performed a T7 transcription from pcDNA3.1 plasmid containing LL35 gene obtained by RACE. Desthiobiotinylated LL35 transcript was used for RNA pull-down assay, and the interacted proteins were analyzed using LC-MS. Among the enriched proteins only hnRNPA2B1 (Heterogeneous Nuclear Ribonucleoprotein A2/B1) was significant (**Supplementary Table S4**). Thus, based on RNA pull-down assay hnRNPA2B1 is a potential partner for LL35, but specificity of this interaction should be further confirmed.

Human lncRNA DEANR1 is involved in glycolysis regulation in pancreatic cancer *via* sponging miR-222-3p [8]. We decided to check the expression levels of miR-222-3p and miR-23a-3p (participates in gluconeogenesis regulation [221]) after LL35

knockdown in AML12 cells to test the hypothesis of glycolysis regulation by LL35 *via* sequestering miRNAs. Our RT-qPCR data did not show upregulation of studied miRNAs after LL35 depletion (**Supplementary Figure S5B**), suggesting that LL35 unlikely participates in their sponging.

4.7 LL35 is required for proper hepatocytes survival and migration

Glucose and lipid metabolism plays a central role in the cell biogenesis and its normal functioning is essential for cell life and proliferation. To study the influence of LL35 on the survival of hepatocytes *in vitro* and for the investigation of the phenotype resulting from the changes in transcriptome and proteome analysis, we performed MTS assay for AML12 with depleted LL35 versus control Luc cells (**Figure 37A**). Starting from the day 2 after LL35 knockdown we observed decrease in cell survival in comparison to control cells. At day 3 the difference between cells with depleted LL35 and control cells reaches two times. To assess whether LL35 interferes with the cell migration ability we conducted a wound-healing assay (**Figure 37B, 37C**). On the third day we saw that wound closing rate was significantly lower in cells with LL35 knockdown compared with control, indicating that LL35 downregulation impairs cell migration ability.

Further, we performed a cell cycle analysis using flow cytometry and PI staining (**Figure 37D**). Obtained data revealed that LL35 knockdown leads to the cell cycle stagnation in S phase (13% of cells with LL35 knockdown versus 9% of control cells), which may result in decreased cell viability. E-cadherin protein participates in the formation of adherent junctions to bind cells with each other, which is directly related to

the ability to migrate. We checked its mRNA expression level and found, that LL35 depletion results in downregulation of E-cadherin mRNA (**Figure 37E**). Moreover, 74 genes related to cell junction (**Figure S3E**) showed differential expression in transcriptome data of AML12 cells after LL35 downregulation. Also, we performed a Ki-67 staining of liver tissue samples to check if LL35 depletion interfere with hepatocytes proliferation *in vivo.* We observed no difference in proliferation rate between samples with LL35 knockdown and control Luc samples (**Figure 37F**). Obtained data may suggest that 5 days after LL35 inhibition may be too short time period to see phenotypic changes in the murine liver.

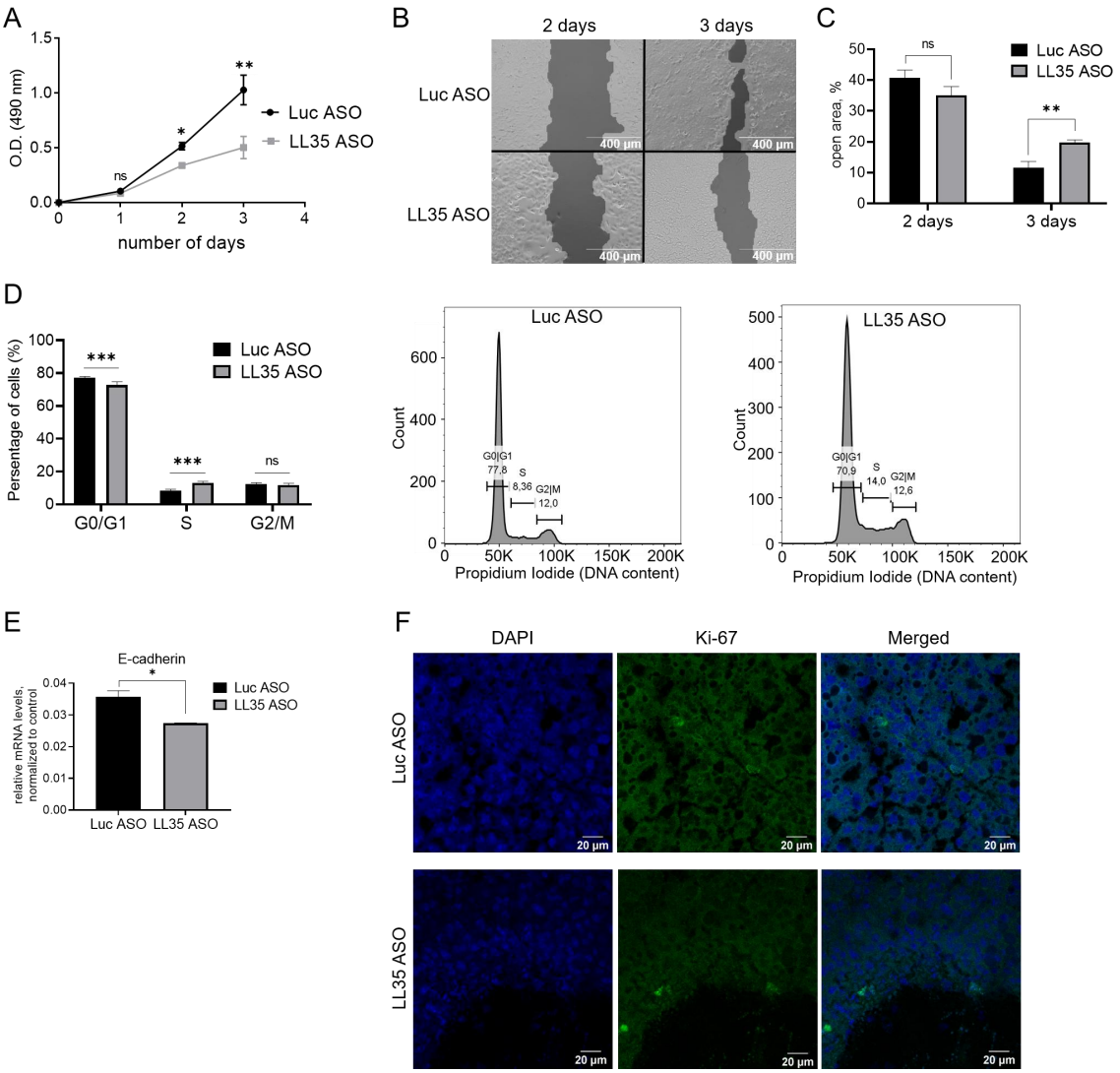

Figure 37*. Study of hepatocyte survival and migration after LL35 depletion (LL35 ASO) in comparison with control cells (Luc ASO).* ***(A)****. MTS assay for AML12 cells after LL35 knockdown compared with Luc control.* ***(B)****. Wound-healing assay for AML12 cells after LL35 knockdown and control.* ***(C)****. Quantification of wound-healing assay with imageJ software.* ***(D)****. Cell cycle analysis of the cells with LL35 knockdown and control cells by flow cytometry. Percentage of cells in different cell cycle phases after LL35 knockdown compared with control obtained from flow cytometry analysis after PI staining.* ***(E)****. E-cadherin mRNA expression levels after LL35 depletion in comparison with luciferase control measured by RT-qPCR.* ***(F)****. Ki-67 staining of liver tissue samples. Four biological replicas per condition were used in MTS assay and 3 replicas in other presented here experiments; results show mean ± SD. n.s.—not significant, * $p < 0.05$, ** $p < 0.01$ and *** $p < 0.001$, p-value was obtained using multiple t-test in GraphPad Prism.*

Finally, we analyzed the expression of multiple genes involved in important signaling pathways connected with cells viability and migration after LL35 depletion in AML12 cells and observed alteration in two pathways: Notch and NF-κB.

The Notch signaling pathway participates in the regulation of proper cellular proliferation, apoptosis and differentiation. Indirect immobilized of Notch ligand Jagged1 significantly reduced cell proliferation, colony forming unit ability, and the number of cells in S phase [222,223]. We demonstrated that LL35 knockdown results in significant upregulation of Jagged1 protein – one of the main ligands, which binds to Notch receptors and triggers Notch signaling (**Figure 38A**). Moreover, Notch1, Notch4 were also upregulated at mRNA level, as well as Notch signaling target genes – Hes-1 and Hey-1 (**Figure 38B**). Thus, we can conclude, that LL35 contributes in normal Notch pathway signaling, which also affected on the changes in viability and migration of hepatocytes with depleted LL35.

NF-κB pathway is one of the main controllers of transcription, cytokine production and cell survival [224]. We measured p105/p50 proteins ratio after LL35 knockdown and observed its slight increase (p-value=0.06) (**Figure 38C**). But there is an alternative way to activate NF-κB pathway, *via* stimulation of the IκB (inhibitor of κB) kinases. We evaluated the expression levels of IκBα mRNA and protein and observed their significant upregulation in two days after LL35 knockdown (**Figure 38D, 38E**), which also contributes in the regulation of the cell viability and migration.

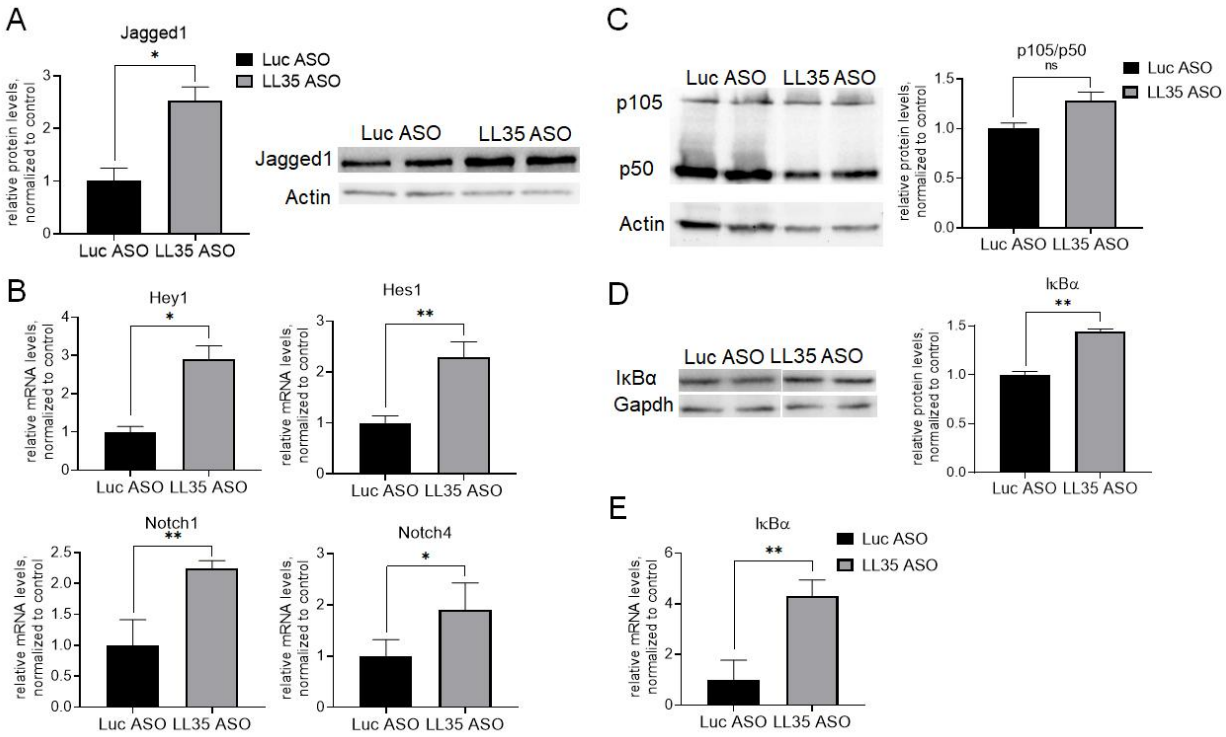

.

Figure 38. *Changes in Notch and NF-κB pathways after LL35 depletion in vitro. (**A**). Estimation of Jagged1 protein level after LL35 knockdown in vitro by western blot, normalized at ActB protein level. (**B**). RT-qPCR measurement the mRNA expression levels of major genes involved in Notch signaling pathway after LL35 knockdown (LL35 ASO) in AML12 cells and control (Luc ASO), normalization on ACTB gene. (**C**). Estimation of p105/p50 proteins ratio after LL35 knockdown in AML12 cells by western blot, normalized on ActB protein level. (**D**). Estimation of IκBa protein level after LL35 knockdown by western blot, normalization on GAPDH protein level. (**E**). RT-qPCR meas-ured expression levels of IκBa mRNA after LL35 knockdown and control. ACTB-reference gene. Three biological replicas per condition were used in each experiment; results show mean ± SD. n.s.—not significant, * $p < 0.05$, ** $p < 0.01$ and *** $p < 0.001$, p-value was obtained using multiple t-test in GraphPad Prism.*

Taking our data together, we conclude that LL35 depletion affects multiple cellular processes, such as lipid and glucose metabolism, Notch and NF-κB signaling pathways, which may result in impaired viability and migration ability of hepatocytes.

Chapter V. Discussion

LncRNAs are valuable regulators of biological processes in mammalian cells. Their function and mechanism of action may be tissue- or condition-specific, and, unfortunately, are still poorly understood. In this work we have focused on the study of murine lncRNA LL35 function in normal hepatocytes *in vitro* and *in vivo*.

LL35 was proposed to be a functional analog of human lncRNA DEANR1 in lungs [5], which functionality and mechanism of action were described predominantly in different cancer types or tissues during development [12,187]. By now, LL35 function was studied only in the lung tissue by Swarr et al. [5]. Interestingly, that authors showed that LL35 knockout did not lead to any aberrations during lung development, but caused defects in the regeneration of the airway epithelium after injury [5]. Also our research group previously reported a decreased expression of LL35 at early stages of murine liver fibrosis [17]. However, the question whether LL35 is a functional analogue of human DEANR1 in the liver remained to be under consideration. Here we found downregulation of LL35 RNA levels in HCC mouse model (**Figure 25B**), which correlates with DEANR1 expression in liver samples of patients with HCC [7,12], and its low expression in the murine model of the partial hepatectomy (**Figure 25C**). LL35 levels in several murine hepatocyte cell lines (AML12, Hepa-1c1c7, Hepa1-6) additionally proved predominant LL35 expression in normal liver cells (**Figure 25A**). Based on our data we consider that LL35 is functionally significant in normal murine liver and may be a probable biomarker in different liver diseases. Moreover, we suggest that studying of

LL35 in HCC mouse model will be helpful to uncover the molecular mechanisms of its action *in vivo* that is crucial for studying of human lncRNA DEANR1.

For *in vitro* studies we selected AML12 cell line derived from normal hepatocyte of 3-months-old mouse. The liver is one of the key metabolic organs, and it was shown that AML12 cells most accurately phenocopied *in vitro* energy metabolism of primary mouse hepatocytes [225]. To investigate LL35 functions in hepatocytes *in vitro* and *in vivo* we conducted loss-of-function study by generating ASO-mediated knockdown of LL35 lncRNA (**Figure 27A, 27E**). We previously showed that LL35 is predominantly localized in the cell nucleus (80% versus 20% in cytoplasm) [17]; therefore, we chose the ASO strategy that induces target cleavage by RNase H, since it leads to inhibition of the target both in the nucleus and in the cytoplasm [226], in contrast to the siRNA strategy, which is active only in the cytoplasm. For LL35 knockdown in liver we synthesized conjugates of ASO with N-acetylgalactosamine (GalNAc) (**Figure 27B**). GalNAc-ASO conjugates became a breakthrough approach for liver-targeted delivery in the therapeutic oligonucleotide field [227]. Single administration of GalNAc-ASO led to more than 80 % downregulation of LL35 in the murine liver without any damage confirmed by blood and morphological analysis (**Figure 27E, 27F, 28)**. This result is consistent with previously shown data that the conditional knockout of LL35 lncRNA in mice miserably interfere with normal development, including endoderma-derived organs such as lungs [5]. We got highly efficient (85% *in vitro*, 81% *in vivo*), but not 100% downregulation of LL35. Therefore, residual expression of LL35 may diminish effects of its downregulation.

Then we compared changes in gene expression caused by LL35 depletion *in vitro* and *in vivo* using RNA-seq and LC-MS-proteomics technologies. PANTHER Reactome pathway analysis of transcriptome revealed that LL35 depletion both in cells and in the liver caused changes in metabolism, glutathione conjugation, biological oxidations and sulfur amino acid metabolism (**Figure 29B, 29C**). At the same time, we found changes in the cell cycle related pathways only in AML12 cells (**Figure 29B**). This may be explained by the slow turnover of hepatocytes in the liver [215]. Despite some similarity in changed pathways, we found poor overlap between differentially expressed genes (only 5 genes were common) after LL35 depletion in AML12 cells and murine liver (**Figure 29A**). Such difference in transcriptome data between *in vitro* and *in vivo* may be explained by more complex cellular communications in the liver than in cell culture. Moreover, GalNAc-conjugates provide targeted delivery to hepatocytes only, while liver contains other cell types, such as hepatic stellate cells, Kupffer cells and liver sinusoidal endothelial cells, which were not excluded from RNA-seq analysis. Moreover, rather often RNA-seq data for cell culture and tissue have low similarities [228,229]. Small intersection between sets of differentially expressed genes highlights the importance of conducting *in vivo* studies. Despite AML12 is considered to be highly similar to primary hepatocytes [225], probably, usage of another murine hepatocyte cell line or more complex cell culture studies would give more similarities with liver transcriptome than AML12. Previously, Swarr et al. performed RNA-seq analysis for lung epithelium isolated from null LL35 mice [5]. For this data we conducted the same PANTHER Reactome pathway enrichment analysis as we did for our RNA-seq data and found

similar changes in cell cycle, cell adhesion and metabolism of amino acids pathways as we observed for AML12 cells after LL35 knockdown (**Figure 31A**).

Since transcriptome analysis revealed significant changes in the genes involved in metabolism, in order to fully characterize the role of LL35 depletion in cell metabolic processes, we conducted LC-MS-based lipidome and metabolome analysis. We found that abundance of plasmanyl-/plasmenylphosphatidylcholines (O-PC/P-PC) was decreased in both cells and murine liver while phosphatidylethanolamines (PE), hexosylceramides (HexCer) increased only in cell culture, and diradylglycerols (DG), ceramides (Cer;O2) and lysophospha-tidylcholines (LPC) showed significant increase in mice (**Figure 32B, 32C**). Metabolome analysis revealed only changes in the purine and glutathione metabolism and amino acids biosynthesis *in vitro* affected by LL35 depletion (**Figure 33A**). Also, we checked the expression of many enzymes genes involved in the metabolism of altered lipid classes, and found changes in their expression (**Figure 32D**). It is known that lipid metabolism can be regulated by lncRNAs at different levels. For example, lncRNAs LOC100506036 regulates the activity of enzyme involved in ceramide synthesis [83], ANRIL mediates PC hydrolysis, while SNHG14 participates in DG synthesis *via* sponging miR-145-5p [84]. MALAT1 regulates transcription of multiple genes associated with lipid metabolism *via* interaction with SREBP-1c transcription factor [81], and lncRNA LINK-A participates in the activation of AKT1/PI3K pathway [85]. Glucose metabolism is tightly connected with lipid metabolism. We measured an indicator of glycolysis – extracellular acidification rate (ECAR) and oxygen consumption rate (OCR) after LL35 depletion in cells. We found

that OCR level was not changed after LL35 knockdown (**Figure 34A-34C**), while ECAR level was significantly reduced, particularly indicating a decrease in glycolytic capacity and glycolytic reserve (**Figure 34D, 34E**). We found dysregulation of multiple genes involved in the main pathways of glucose metabolism, such as glycolysis, gluconeogenesis, pentose phosphate pathway, glutaminolysis, glycogen synthesis and acetyl-CoA synthesis *in vitro* (**Figure 35B**). LL35 knockdown led to significant upregulation of hexokinase 2 (**Figure 35B**), which is involved not only in glucose, but also in dietary fructose metabolism. Excess of fructose leads to elevated TAG, LDL cholesterol, apolipoprotein B, which are risk factors of cardiovascular disease, as well as it is associated with high blood pressure, nonalcoholic fatty liver disease (NAFLD) and fructose malabsorption [230]. In liver hexokinase predominantly converts glucose to glucose-6-phospate, but can also convert fructose to fructose-6-phospate to a lower degree [231]. Possibly, hexokinase upregulation after LL35 knockdown may also lead to an imbalance in fructose metabolism. We performed insulin tolerance test *in vivo* to prove relations between LL35 depletion and glycolysis and found that glucose blood level in mice with LL35 KD was 1,5-2 times higher than in control mice (**Figure 36A**), which confirms a poorer insulin response. Analysis of the animal blood after the insulin injection demonstrated the compensation of the effects found for the LL35 depletion: decrease of direct bilirubin, elevated levels of cholesterol, inorganic phosphorus and AST/ALT ratio (**Figure 36B**). For human DEANR1 Zhai et al. previously found that in pancreatic cancer cells DEANR1 overexpression reduces glycolysis, lowers glucose consumption and lactate production. They linked such phenotypic changes to two

possible mechanisms of DEANR1 action: *via* sponging miR-222-3p, which leads to HIPK2-mediated activation of ERK/c-Myc pathway and by sequestering IGF2BP1, which decrease c-Myc mRNA stability and reducing its expression [10]. Changes in c-Myc expression caused by DEANR1 correlates with our results: we showed that LL35 depletion leads to significant upregulation of c-Myc mRNA. Our data suggest that in normal hepatocytes LL35 knockdown downregulates glycolysis, while in pancreatic cancer cells DEANR1 overexpression results in the decrease of glycolysis. There are few known examples of how lncRNAs regulate glucose metabolism in normal tissues. Predominantly, they participate in proper development of pancreatic islets and insulin secretion [110,111].

20% of LL35 is localized in the cytoplasm [17], and the main mechanisms of lncRNAs action in the cytoplasm are the formation of sponges with miRNAs, the regulation of target mRNAs decay and participation in the translation and the post-translational modification of proteins. Proteome analysis after LL35 knockdown didn't reveal many changes in protein expression, especially in comparison with transcriptome analysis, and DEANR1 has been described to sponge various miRNAs [167–169], therefore, we assumed that cytoplasmic LL35 is most likely also involved in the formation of sponges (or at least in the mRNAs decay). We checked the expression levels of several miRNAs, which may participate in the regulation of glucose metabolism, after LL35 depletion and found no difference (**Supplementary Figure S5B**). Since the main fraction of LL35 is localized in the cell nucleus [17], we didn't continue with search for miRNAs, but focused in the search for a LL35 protein partner. We attempted to identify

the LL35 protein partner by RIP (RNA immunoprecipitation) analysis. RIP is a protein-centric approach, which it is performed under physiological conditions allowing to preserve native RNA-protein complexes. RIP gives opportunity to identify both directly and indirectly associated proteins with RNA and is commonly used for lncRNAs along with CHART (capture hybridization analysis of RNA targets) or pull-down assays [232]. For RIP analysis we chose proteins, involved in the glycolysis and insulin signaling, such as PGC1α, STAT3, pSTAT3, PKM1, CTNNB1, SIRT1, IGF2BP2, all selected proteins, except SIRT1, were previously described as RNA-binding proteins (RBPs) [56,233–236], and interaction with other lncRNAs were shown for STAT3 [56], PKM1 [234], IGFBP2 [236]. But unfortunately, none of these proteins turned out to be a LL35 partner (**Supplementary Figure S5A**). Then we decided to apply a RNA-centric approach and performed RNA pull-down assay in attempt to identify all proteins from AML12 cell lysate which could interact with LL35. Pull-down results revealed that hnRNPA2B1 (Heterogeneous Nuclear Ribonucleoprotein A2/B1) might interact with LL35 (**Supplementary Table S4**), but additional work is needed to reaffirm such interaction. Interestingly, that several studies describe hnRNPA2B1 as a possible binding partner for lncRNAs. For example, a lncRNA lnc-HC interacts with hnRNPA2B1 in the cell nucleus forming lncRNA-protein complex and then bind target mRNAs - Cyp7a1 and Abca1, promoting their degradation. Decreased expression of Cyp7a1 and Abca1 lead to impaired cholesterol metabolism in hepatocytes [237]. Based on these evidences we can not exclude the possibility of LL35 interaction with hnRNPA2B1 but specificity and the role of this interaction should be further investigated.

Discovered changes in transcriptome, lipidome and glycolysis raised a question about the influence of LL35 depletion on the viability and migration of hepatocytes. We found decreased cell viability and cell cycle stagnation in S phase after knockdown of LL35. Cells migration test demonstrated that LL35 downregulation in AML12 murine hepatocytes impairs cell migration ability, which was additionally proved by E-cadherin downregulation. To assess the proliferative status of hepatocytes *in vivo* after LL35 depletion we performed a Ki-67 staining of liver tissue samples and found that LL35 inhibition doesn't affect cell proliferation *in vivo*. Such phenotypic difference between AML12 cells and murine liver can again be explained by the fact that 5 day time point may be to short period for proper turnover of hepatocytes *in vivo* [215]. Studies of the human functional analog DEANR1 were mainly conducted in the cancer cells, in which overexpression of lncRNA inhibits cell proliferation and both cell invasion and migration by various ways [7–12]. Summing up, LL35 is involved in the regulation of cell viability and migration by different mechanisms both in cancer and noncancerous cells, while most molecular mechanisms are still under investigation.

Finally, we checked the status of the main signaling pathways like Notch and NF-κB pathway to explain the phenotype changes like viability and migration after LL35 depletion. Also several studies demonstrated participation of human DEANR1 in the regulation of the multiple signaling pathways such as Wnt/β-catenin signaling pathway, p38 MAPK signaling pathway, and Notch signaling pathway [15,184,238]. We found that LL35 depletion resulted in significant upregulation of Jagged1 protein – one of the main ligands, which binds to Notch receptors and triggers Notch signaling. Also we

evaluated the significant upregulation in the expression levels of IκBα mRNA and protein, which indicated the involvement LL35 in the regulation of NF-κB pathway. Thus, murine lncRNA LL35 participate in the regulation of main signaling pathways in the cells like its human analog DEANR1.

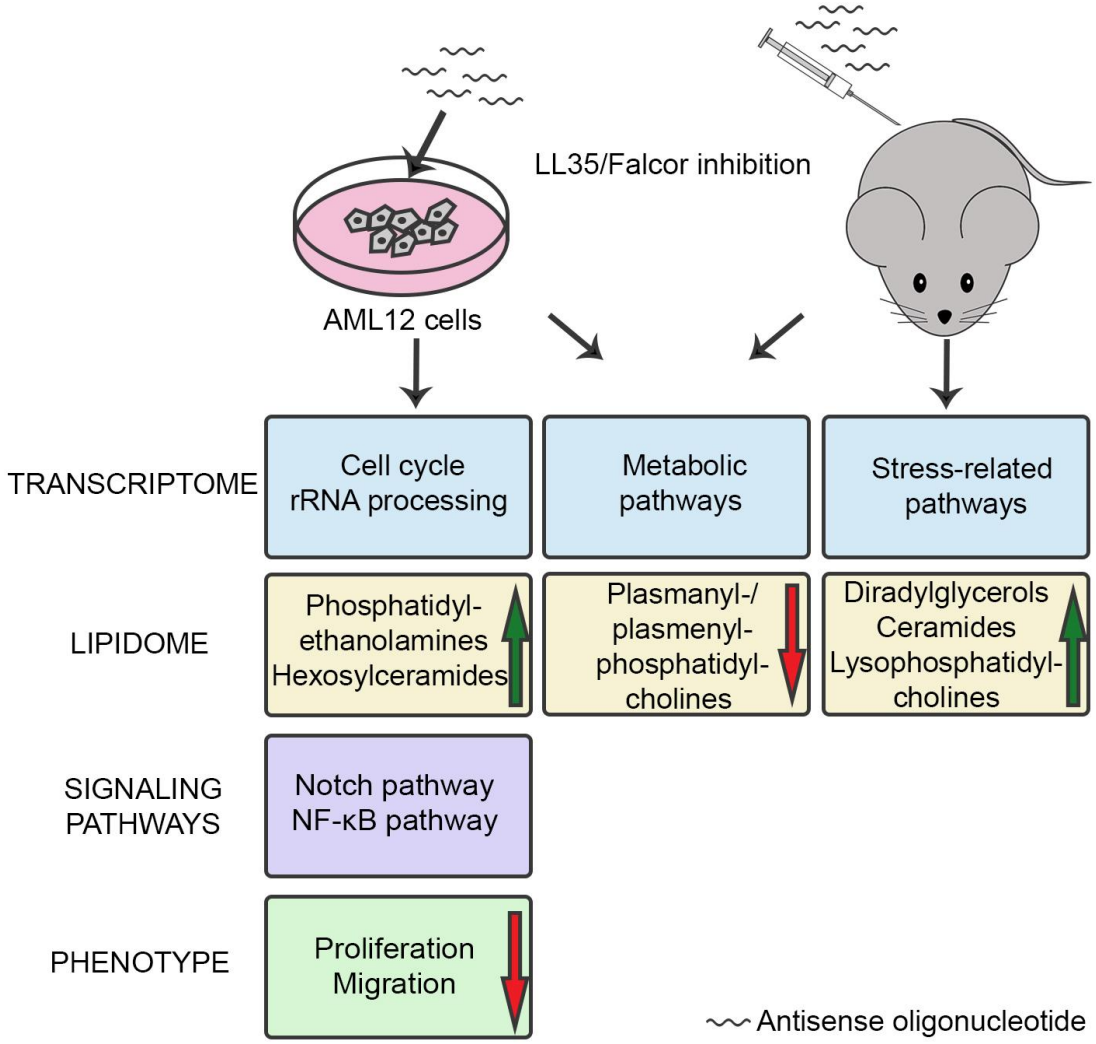

Figure 39. *Results of the LL35 depletion on the hepatocytes genotype and phenotype in vitro and in vivo.*

Summing up, we demonstrated that LL35 is a functional analog of human lncRNA DEANR1 in liver, LL35 is predominantly expressed in normal hepatocytes and

is involved in the regulation of the glycolysis and lipid biosynthesis *in vitro* and *in vivo* (**Figure 39**). We demonstrated downstream effects from LL35 depletion in normal hepatocytes on the Notch and NF-κB pathways. And all these changes of the transcriptome, lipidome, signaling pathways leads to the strong phenotype in hepatocytes – decrease of viability, migration and cell cycle stagnation (**Figure 39**). All obtained data correlate with a published one for LL35 transcriptome in lungs and for human functional analog DEANR1. Studies of species-specific lncRNA *in vivo*, which are functional analogs of human ones, may broadly highlight the involvement of lncRNAs in certain biological processes and diseases.

Our study was focused on LL35 function in normal hepatocytes, but the role of human DEANR1 is actively studied in different pathologies, mainly in cancer. Therefore, for greater clinical relevance of our study, one of the future directions from the one hand is the study of LL35 in HCC, from the other hand – investigation of DEANR1 in normal hepatocytes based on the obtained for LL35 data. Overexpression of LL35 in HCC will demonstrate its functions in cancer progression and metastasis and also possible involvement in the response to anticancer therapy. We demonstrated that depletion of LL35 in hepatocytes interferes with normal glucose and lipid metabolism, and impair response to insulin treatment. Disruption of these features in the liver leads to various diseases including diabetes, steatosis, NAFLD (non-alcoholic fatty liver disease) and others [239]. Thus, one more future direction of the research may be the study of the LL35 and DEANR1 functions in metabolic liver disorders.

Conclusions

In this study we showed that murine lncRNA LL35 is a functional analog of human lncRNA DEANR1 in the liver and described for the first time the functional significance and role of LL35 in murine hepatocytes. We demonstrated that LL35 is predominantly expressed in normal hepatocytes *in vitro* and *in vivo* compared to HCC and partial hepatectomy models. To describe the function of LL35 *in vivo* we developed a highly efficient and specific ASO-mediated knockdown of LL35 in the liver. We revealed that LL35 depletion downregulates glycolysis *in vitro* and causes decreased response to insulin treatment *in vivo.* We found that LL35 depletion causes changes in mRNA levels of genes involved in cellular metabolism both *in vitro* and *in vivo,* and in the pathways of cell cycle in the case of AML12 cells. Analysis of lipidomic changes after LL35 knockdown demonstrated the decrease of plasmanyl-/plasmenylphosphatidylcholines (O-PC/P-PC) both in AM12 cells and murine liver, while phosphatidylethanolamines (PE), hexosylceramides (HexCer) increased only in cells, and diradylglycerols (DG), ceramides (Cer;O2) and lysophosphatidylcholines (LPC) – only in the liver. Finally, in AML12 cells LL35 is essential for proper cell viability and migration and participates in regulation of Notch and NF-κB signaling pathways. Our data correlate with previously published LL35 knockout transcriptome in lungs and for LL35 human functional analog DEANR1. Thus, our investigation opens the opportunity to translate results from liver-specific LL35 knockdown in murine models to human lncRNA DEANR1 in normal liver physiology and expand the potential therapeutic role of human lncRNA.

Supplementary

Supplementary Table S1. List of ASOs for *in vitro* study.

Name	Sequence
LL35 ASO 1	ususgscscsAsTsCsAsTsGsTsTsGsTsascscsusg
LL35 ASO 2	cscscscsusCsTsCsAsGsTsGsCsTsGsgsasascsc
LL35 ASO 3	ususasgsgsTsGsGsCsAsGsTsTsCsAsgsgsasgsa
LL35 ASO 4	gsuscsgsgsTsAsTsCsAsGsTsTsGsCsasgsasgsa
LL35 ASO 5	usgsususgsusAsCsCsTsGsGsCsCsAsGsTscsasgscsusgsc
Control Luc ASO	tscsgsasasgsTsAsCsTsCsAsGscsgstsasasg

Capital letters indicate 2'-deoxynucleotides, lowercase letters indicate 2'-O-methylribonucleotides, s – phosphorothioate groups.

Supplementary Table S2. List of ASOs for *in vivo* study.

Name	Sequence
LL35 ASO 1	oUsoUsoGsoCsoCsAsTsCsAsTsGsTsTsGsTsoAsoCsoCsoUsoG3galnac
LL35 ASO 2	oCsoCsoCsoCsoUsCsTsCsAsGsTsGsCsTsGsoGsoAsoAsoCsoC3galnac
LL35 ASO 3	oUsoUsoAsoGsoGsTsGsGsCsAsGsTsTsCsAsoGsoGsoAsoGsoA3galnac
LL35 ASO 4	oGsoUsoCsoGsoGsTsAsTsCsAsGsTsTsGsCsoAsoGsoAsoGsoA3galnac
LL35 ASO 5	oAsoCsoCsoUsoGsoGsCsCsAsGsTsCsAsGsCsTsoGsoCsoUsoGsoA 3galnac
Control Luc ASO	oUsoCsoGsoAsoAsoGsTsAsCsTsCsAsGsoCsoGsoUsoAsoAsoG3galnac

Capital letters indicate 2'-deoxynucleotides, o – 2′-O-methoxyethyl (MOE), s – phosphorothioate groups, 3galnac – triple *N*-acetylgalactosamine (GalNAc) TEG.

Supplementary Table S3. List of PCR primers used in the study.

Name	Forward, 5'→3'	Reverse, 5'→3'
GAPDH	TGCACCACCAACTGCTTAGC	GGATGCAGGGATGATG
ACTB	CGGTTCCGATGCCCTGAGGCTCTT	CGTCACACTTCATGATGGAATTGA
LL35	CTCAGTGCTGGAACCCCATCTGG	CTCCAAGGCAACACAATGGGAC
HK2	ATGATCGCCTGCTTATTCACG	CGCCTAGAAATCTCCAGAAGGG
LDHA	TGTCTCCAGCAAAGACTACTGT	GACTGTACTTGACAATGTTGGGA
ENO2	AGGTGGATCTCTATACTGCCAAA	GTCCCCATCCCTTAGTTCCAG

PFKFB2	ACATGCTCATGGGCTTCCTAT	TGAGGTAGCGTGTTAGTTTCT
PFKFB3	CCCAGAGCCGGGTACAGAA	GGGGAGTTGGTCAGCTTCG
GLUT1	CAGTTCGGCTATAACACTGGTG	GCCCCCGACAGAGAAGATG
GLUT2	TCAGAAGACAAGATCACCGGA	GCTGGTGTGACTGTAAGTGGG
PDK1	AGGATCAGAAACCGGCACAAT	GTGCTGGTTGAGTAGCATTCTAA
G6PC	CTGTTTGGACAACGCCCGTAT	AGGTGACAGGGAACTGCTTTA
PEPCK	CTGCATAACGGTCTGGACTTC	CAGCAACTGCCCGTACTCC
PGC1α	TATGGAGTGACATAGAGTGTGCT	CCACTTCAATCCACCCAGAAAG
SIRT1	CATCAGCTATCGTTCGTCCAG	CCACAGCGTCATATCATCCAG
MYC	ATGCCCCTCAACGTGAACTTC	CGCAACATAGGATGGAGAGCA
EGR1	TCGGCTCCTTTCCTCACTCA	CTCATAGGGTTGTTCGCTCGG
FOXJ1	CCCTGACGACGTGGACTATG	GCCGACAGAGTGATCTTGGT
NOTCH1	CCGTGTAAGAATGCTGGAACG	AGCGACAGATGTATGAAGACTCA
NOTCH4	CTCTTGCCACTCAATTTCCCT	TTGCAGAGTTGGGTATCCCTG
HEY1	CCGACGAGACCGAATCAATAAC	TCAGGTGATCCACAGTCATCTG
HES1	CCAGCCAGTGTCAACACGA	AATGCCGGGAGCTATCTTTCT
IKBA	TGGCCAGTGTAGCAGTCTTG	GACACGTGTGGCCATTGTAG
CDH1	CAGGTCTCCTCATGGCTTTGC	CTTCCGAAAAGAAGGCTGTCC
ABCA9	TCGATAGATGCAGTGAGAGTCA	CACAAGGAGCTGAATGGTCTTT
MYOCBP1	GATCGCTACCGGAGGATTTACA	CAATGCCGCACGTTACAGTA
AGXT	AAGGCATCCAGTATGTGTTCCA	TTCCGGTTAGAAAGGAGTCCC
CDC7	AACAGCGTGATGAGGGAAACT	CGCTCTGAATCCTGGTGTG
CENPI	AGGGTTACTAGAAACTCCCAGC	GCGTGTAGAATCTTCCACTGAA
CHEK1	TTCCACCAACTCATGGCAGG	GCGTTCACGATTATTATGCCGAA
GADD45G	GGGAAAGCACTGCACGAACT	AGCACGCAAAAGGTCACATTG
GGT6	TCCTCAATCAACAGTTCCTTTGG	CAAGGTGCAAGTCATGGCTTT
GSTM2	ACACCCGCATACAGTTGGC	TGCTTGCCCAGAAACTCAGAG
GTSE1	TTTTGGGCCTGTTGGACATAAA	CTCAAGGTGCAAGGGCTACC
IL33	ATTTCCCCGGCAAAGTTCAG	AACGGAGTCTCATGCAGTAGA
MDM2	TAAAGTCCGTTGGAGCGCAAA	CTGCTGCTTCTCGTCATATAACC

PDE4D	AACACTGCACTCCTGTAATGAAG	TGCTTGTTCCAACTGTCTGAAG
PFKM	TGTGGTCCGAGTTGGTATCTT	GCACTTCCAATCACTGTGCC
PINK1	GGCTTCCGTCTGGAGGATTAT	AACCTGCCGAGATATTCCACA
PSMC6	CCTGTCAGAACAGATTCGGGA	GCAAACAGCCTTTTGGAGGTATT
RHOH	CTACAAACCCACGGTGTACGA	CCGGATACTTCTGAAGGCGT
ZFP36	CCGAATCCCTCGGAGGACTT	GAGCCAAAGGTGCAAAACCA
PCYT1B	AGACACTGTCGATACGTGGAT	TCACGGACAATTCTGGTGATG
CHPT1	CAAACTCTTGCTCTCCCTTAGG	CTGAGACGTAAGTCTGCCAATG
CEPT1	ATGAGTGGGCATCGGTCAAC	GTGGTGTCGGTAACTGAAACAA
PISD	CATACTGCTCCTGTCCGATCC	TTCCGTTCCCTGTACTTCTCATA
ETNK1	CTGTTCACAGATGGGATCACAA	CGCGGAAACTTTTCACTTCCTC
ETNK2	CGGTGGAACAGGACGACATC	AGGCCAATAGCTTGTTGGTGA
LPCAT1	AGAGCAGAGACATCCCAATCT	CCAGGTTTGAAGGTAATGAGGC
LPCAT3	CTACCCGTTGGCTCTGTTTTAC	TGAAGCACGACACATAGCAAG
PLA2G4A	CAGCACATTATAGTGGAACACCA	AGTGTCCAGCATATCGCCAAA
SMPD1	TGGGACTCCTTTGGATGGG	CGGCGCTATGGCACTGAAT
ASAH1	TCCGTGGCACACCATAAATCT	TCCACTTGGCACAAATGTATTCA

Capital letters indicate 2'-deoxynucleotides.

Supplementary Table S4. List of proteins obtained from RNA pull-down assay.

Description	Main Accession	Gene Name	#Peptides	#Validated Peptides	#Unique Peptides	#Validated Unique Peptides	Validation
Heterogeneous nuclear ribonucleoprotein H (HNRH1_MOUSE)	O35737	Hnrnph1	1	1	1	1	Doubtful
Peptidyl-prolyl cis-trans isomerase A (PPIA_MOUSE)	P17742	Ppia	1	1	1	1	Doubtful
Keratin, type II cytoskeletal 2 oral (K22O_MOUSE)	Q3UV17	Krt76	1	1	1	1	Doubtful
Actin, cytoplasmic 1 (ACTB_MOUSE)	P60710	Actb	3	3	2	2	Confident

Alpha-actinin-4 (ACTN4_MOUSE)	P57780	Actn4	1	1	1	1	Doubtful
Heterogeneous nuclear ribonucleoproteins A2/B1 (ROA2_MOUSE)	O88569	Hnrnpa2b1	3	3	3	3	Confident
Tubulin beta-4B chain (TBB4B_MOUSE)	P68372	Tubb4b	1	1	1	1	Doubtful
Histone H2A.Z (H2AZ_MOUSE)	P0C0S6	H2az1	2	2	1	1	Confident
Histone H2B type 1-F/J/L (H2B1F_MOUSE)	P10853	H2bc7	2	2	1	1	Confident
Tubulin beta-2A chain (TBB2A_MOUSE)	Q7TMM9	Tubb2a	1	1	1	1	Doubtful
Heterogeneous nuclear ribonucleoprotein F (HNRPF_MOUSE)	Q9Z2X1	Hnrnpf	1	1	1	1	Doubtful
Vimentin (VIME_MOUSE)	P20152	Vim	4	3	3	2	Confident
Pyruvate kinase PKM (KPYM_MOUSE)	P52480	Pkm	1	1	1	1	Doubtful
Histone H2A type 1-B (H2A1B_MOUSE)	C0HKE1	H2ac4	3	3	2	2	Confident
Histone H4 (H4_MOUSE)	P62806	H4c1	3	3	3	3	Confident
Histone H2A type 2-B (H2A2B_MOUSE)	Q64522	Hist2h2ab	2	2	1	1	Confident

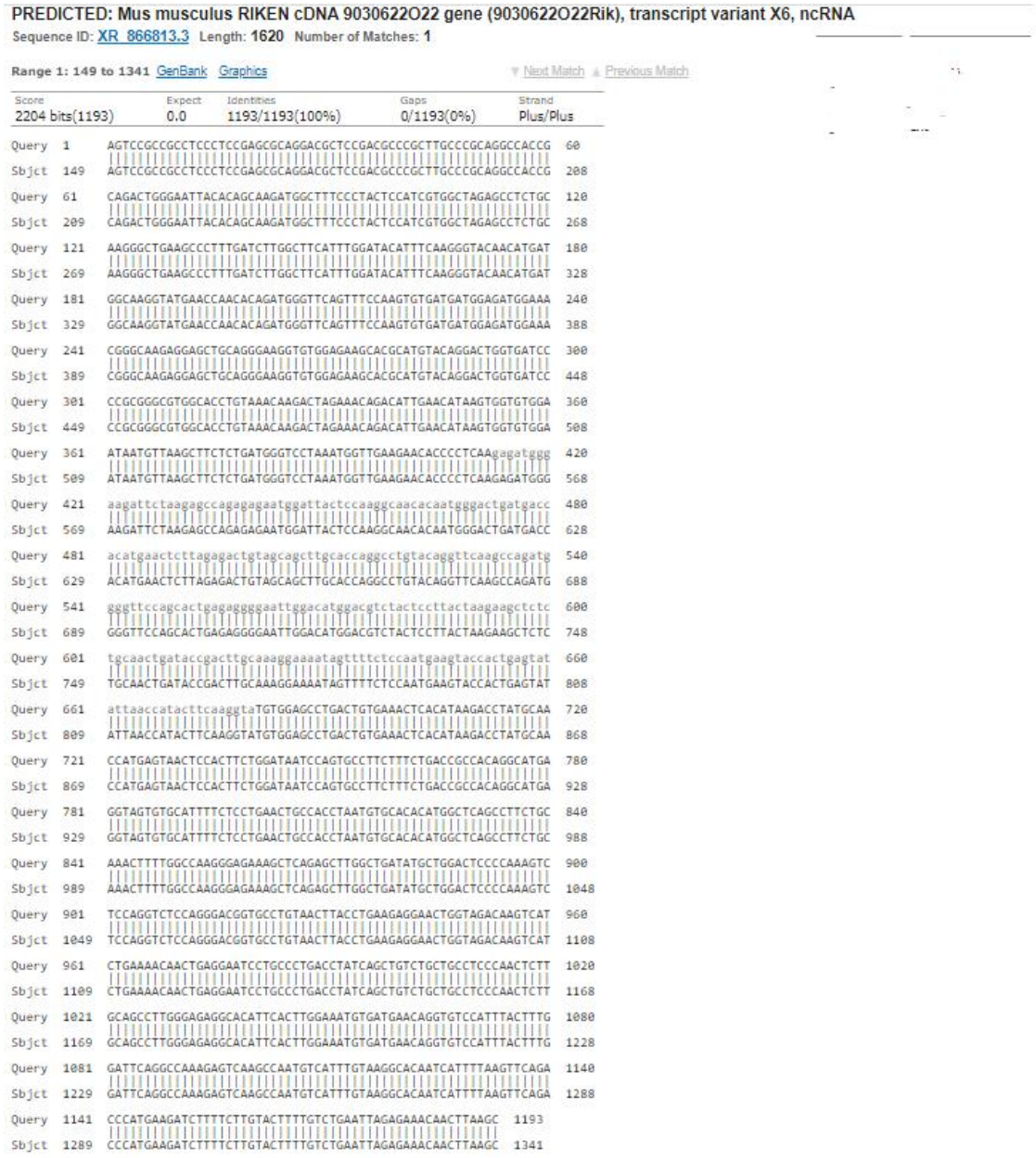

Supplementary Figure S1. *Alignment of RACE transcript, get by Sanger sequencing, with* XR_866813.3

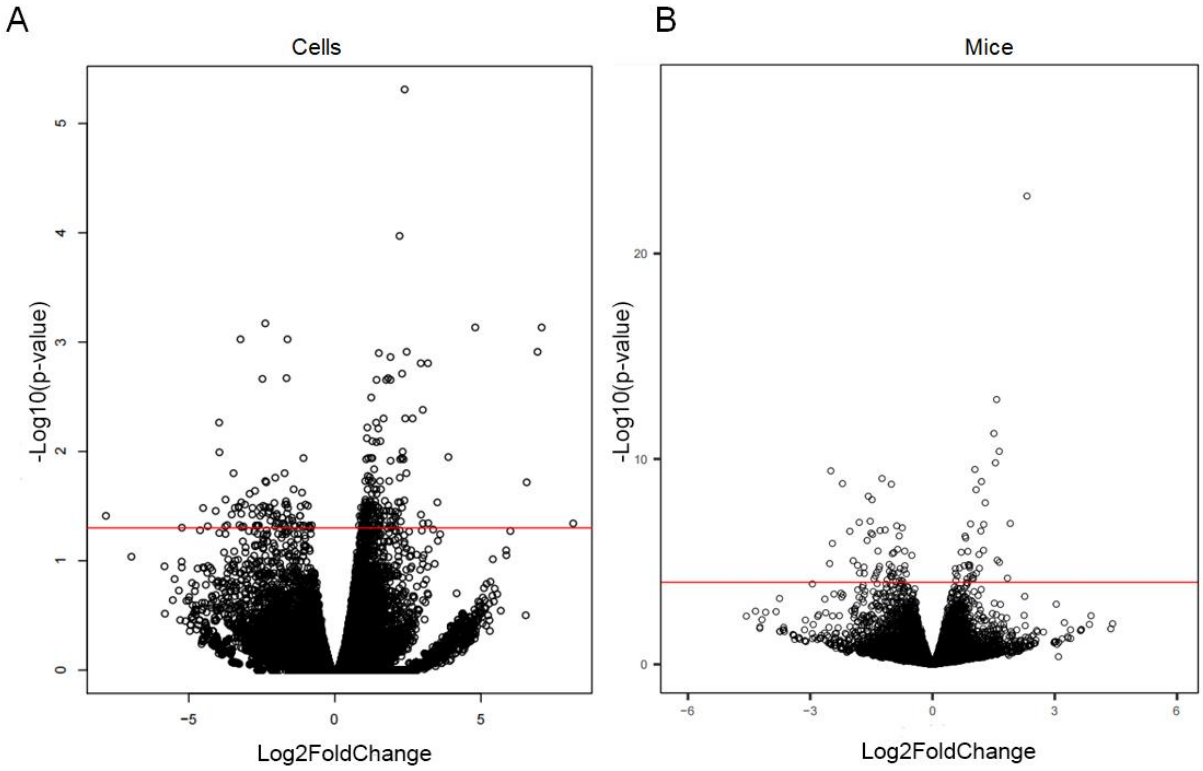

Supplementary Figure S2. Volcano plots of gene expression after LL35 depletion by ASOs mix in A. AML12 cells, day 2; B. mouse liver, day 5.

.

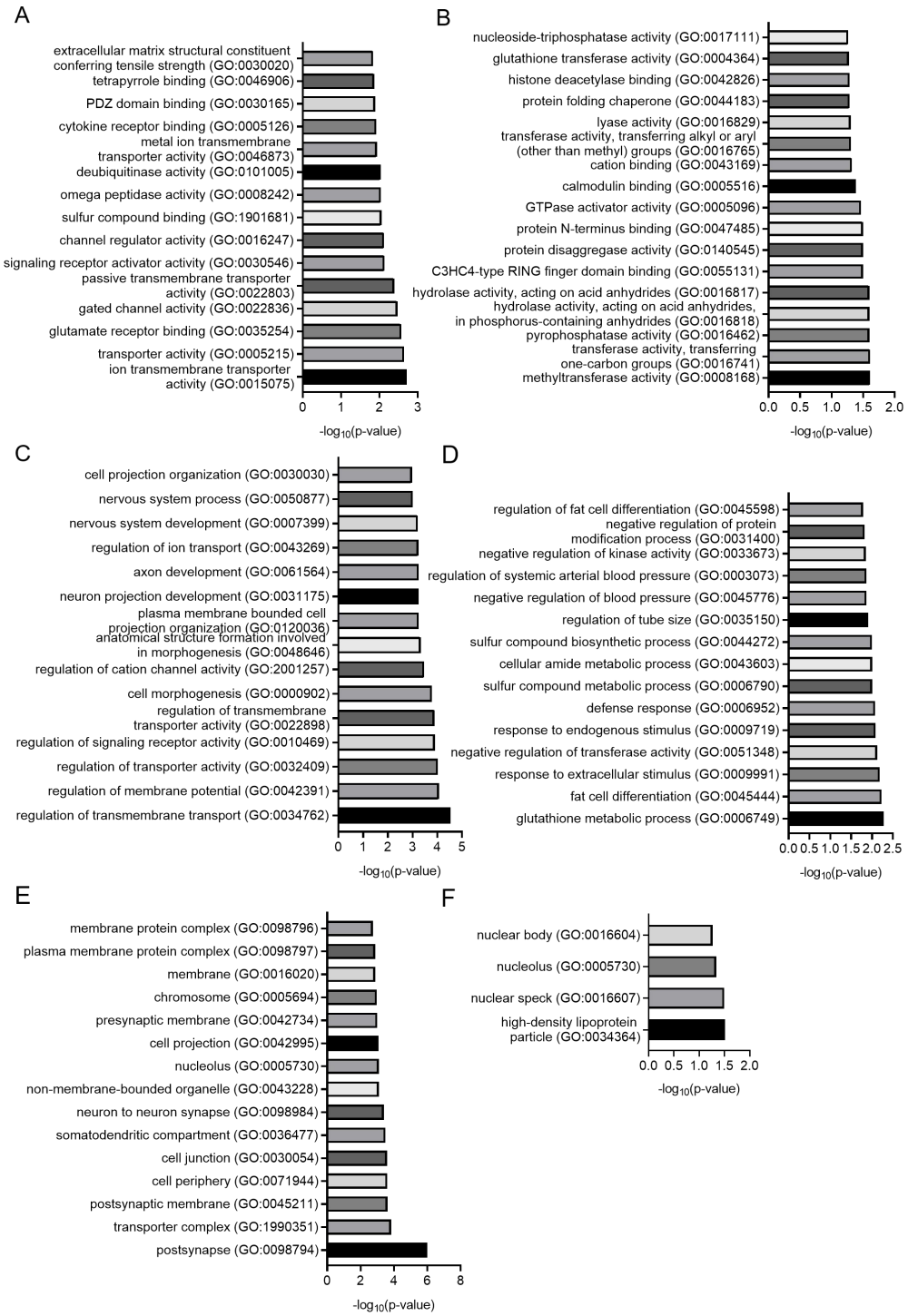

Supplementary Figure S3. Gene ontology analysis (p-value<0.05) of transcriptome data after LL35 knockdown: **A**. molecular functions MF, AML12 cells; **B**. MF, murine liver; **C**. cellular components (CC), AML12 cells; **D**. CC, murine liver; **E**. biological pathways (BP), AML12 cells; **F**. BP, murine liver

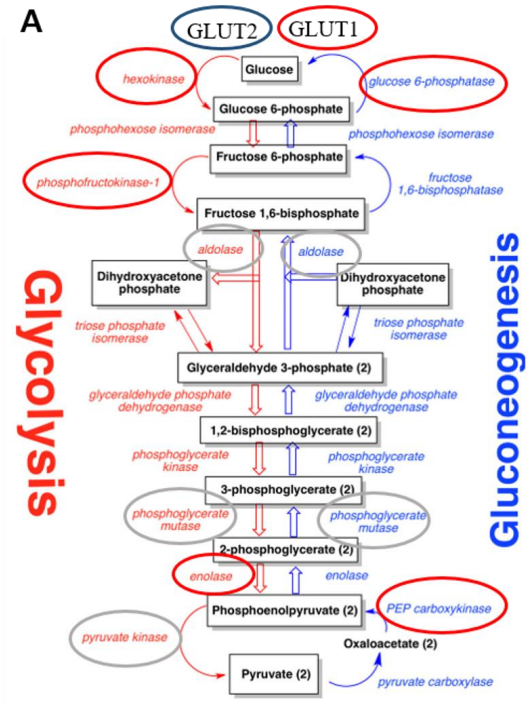

Supplementary Figure S4A. Scheme of glycolysis and gluconeogenesis (adopted from Wikipedia) with labeled enzymes, showed significant changes of their mRNA levels after LL35 depletion in AML12 cells. Red oval – upregulation, blue – downregulation, gray – no change.

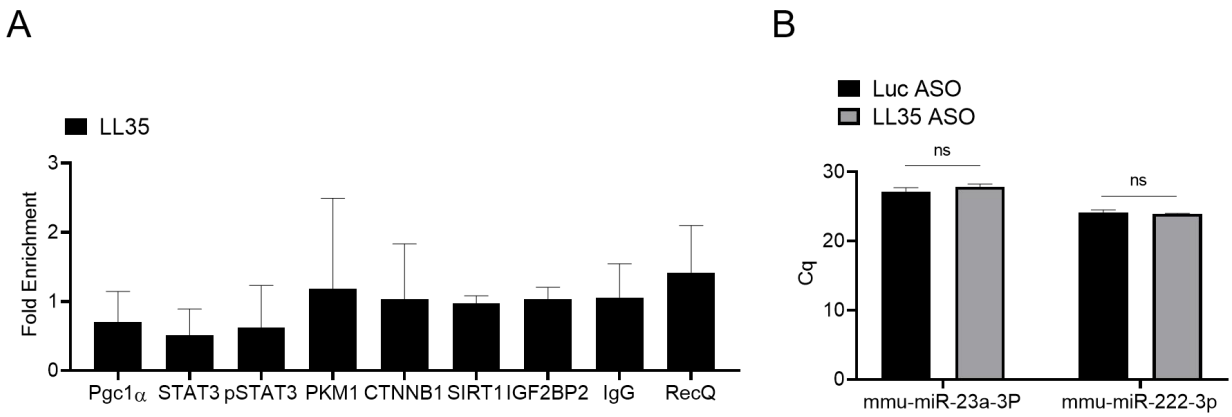

Supplementary Figure S5. A. Fold enrichment of LL35 lncRNA in the RNA immunoprecipitation assay (RIP) performed with PGC1α, STAT3, pSTAT3, PKM1, CTNNB1, SIRT1, IGFBP2 antibodies, antibodies for human RecQ and human IgG were used as controls, quantified with RT-qPCR. **B**. miRNA expression after LL35 knockdown (LL35 ASO) in AML12 cells measured by RT-qPCR, Luc ASO - control. n.s.—not significant.

Bibliography

1. Kashi, K.; Henderson, L.; Bonetti, A.; Carninci, P. Discovery and Functional Analysis of LncRNAs: Methodologies to Investigate an Uncharacterized Transcriptome. *Biochimica et Biophysica Acta (BBA) - Gene Regulatory Mechanisms* **2016**, *1859*, 3–15, doi:10.1016/j.bbagrm.2015.10.010.
2. Moore, J.B.; Uchida, S. Functional Characterization of Long Non-Coding RNAs. *Curr Opin Cardiol* **2020**, *35*, 199–206, doi:10.1097/HCO.0000000000000725.
3. Bhat, S.A.; Ahmad, S.M.; Mumtaz, P.T.; Malik, A.A.; Dar, M.A.; Urwat, U.; Shah, R.A.; Ganai, N.A. Long Non-Coding RNAs: Mechanism of Action and Functional Utility. *Non-coding RNA Research* **2016**, *1*, 43–50, doi:10.1016/j.ncrna.2016.11.002.
4. Sauvageau, M.; Goff, L.A.; Lodato, S.; Bonev, B.; Groff, A.F.; Gerhardinger, C.; Sanchez-Gomez, D.B.; Hacisuleyman, E.; Li, E.; Spence, M.; et al. Multiple Knockout Mouse Models Reveal LincRNAs Are Required for Life and Brain Development. *eLife* **2013**, *2*, e01749, doi:10.7554/eLife.01749.
5. Swarr, D.T.; Herriges, M.; Li, S.; Morley, M.; Fernandes, S.; Sridharan, A.; Zhou, S.; Garcia, B.A.; Stewart, K.; Morrisey, E.E. The Long Noncoding RNA Falcor Regulates Foxa2 Expression to Maintain Lung Epithelial Homeostasis and Promote Regeneration. *Genes Dev* **2019**, *33*, 656–668, doi:10.1101/gad.320523.118.
6. Wu, H.; Liu, J.; Li, W.; Liu, G.; Li, Z. LncRNA-HOTAIR Promotes TNF-α Production in Cardiomyocytes of LPS-Induced Sepsis Mice by Activating NF-KB

Pathway. *Biochemical and Biophysical Research Communications* **2016**, *471*, 240–246, doi:10.1016/j.bbrc.2016.01.117.

7. Chen, Z.; Xiang, L.; Hu, Z.; Ou, H.; Liu, X.; Yu, L.; Chen, W.; Jiang, L.; Yu, Q.; Fang, Y.; et al. Epigenetically Silenced Linc00261 Contributes to the Metastasis of Hepatocellular Carcinoma via Inducing the Deficiency of FOXA2 Transcription. *Am J Cancer Res* **2021**, *11*, 277–296.
8. Li, Y.; Li, H.; Wei, X. Long Noncoding RNA LINC00261 Suppresses Prostate Cancer Tumorigenesis through Upregulation of GATA6-Mediated DKK3. *Cancer Cell Int* **2020**, *20*, 474, doi:10.1186/s12935-020-01484-5.
9. Guo, C.; Shi, H.; Shang, Y.; Zhang, Y.; Cui, J.; Yu, H. LncRNA LINC00261 Overexpression Suppresses the Growth and Metastasis of Lung Cancer via Regulating MiR-1269a/FOXO1 Axis. *Cancer Cell International* **2020**, *20*, 1–15, doi:10.1186/s12935-020-01332-6.
10. Zhai, S.; Xu, Z.; Xie, J.; Zhang, J.; Wang, X.; Peng, C.; Li, H.; Chen, H.; Shen, B.; Deng, X. Epigenetic Silencing of LncRNA LINC00261 Promotes C-Myc-Mediated Aerobic Glycolysis by Regulating MiR-222-3p/HIPK2/ERK Axis and Sequestering IGF2BP1. *Oncogene* **2021**, *40*, 277–291, doi:10.1038/s41388-020-01525-3.
11. Wang, H.; Sha, L.; Huang, L.; Yang, S.; Zhou, Q.; Luo, X.; Shi, B. LINC00261 Functions as a Competing Endogenous RNA to Regulate BCL2L11 Expression by Sponging MiR-132-3p in Endometriosis. *Am J Transl Res* **2019**, *11*, 2269–2279.

12. Zhang, M.; Gao, F.; Yu, X.; Zhang, Q.; Sun, Z.; He, Y.; Guo, W. LINC00261: A Burgeoning Long Noncoding RNA Related to Cancer. *Cancer Cell International* **2021**, *21*, 274, doi:10.1186/s12935-021-01988-8.

13. Shi, J.; Ma, H.; Wang, H.; Zhu, W.; Jiang, S.; Dou, R.; Yan, B. Overexpression of LINC00261 Inhibits Non–Small Cell Lung Cancer Cells Progression by Interacting with MiR-522-3p and Suppressing Wnt Signaling. *Journal of Cellular Biochemistry* **2019**, *120*, 18378–18387, doi:10.1002/jcb.29149.

14. Gao, J.; Qin, W.; Kang, P.; Xu, Y.; Leng, K.; Li, Z.; Huang, L.; Cui, Y.; Zhong, X. Up-Regulated LINC00261 Predicts a Poor Prognosis and Promotes a Metastasis by EMT Process in Cholangiocarcinoma. *Pathol Res Pract* **2020**, *216*, 152733, doi:10.1016/j.prp.2019.152733.

15. Guo, G.; Dai, S.; Chen, Q. Long Noncoding RNA LINC00261 Reduces Proliferation and Migration of Breast Cancer Cells via the NME1-EMT Pathway. *Cancer Manag Res* **2020**, *12*, 3081–3089, doi:10.2147/CMAR.S237197.

16. Wang, Z.K.; Yang, L.; Wu, L.L.; Mao, H.; Zhou, Y.H.; Zhang, P.F.; Dai, G.H. Long Non-Coding RNA LINC00261 Sensitizes Human Colon Cancer Cells to Cisplatin Therapy. *Braz J Med Biol Res* **2017**, *51*, e6793, doi:10.1590/1414-431X20176793.

17. Sergeeva, O.V.; Korinfskaya, S.A.; Kurochkin, I.I.; Zatsepin, T.S. Long Noncoding RNA LL35/Falcor Regulates Expression of Transcription Factor Foxa2 in Hepatocytes in Normal and Fibrotic Mouse Liver. *Acta Naturae* **2019**, *11*, 66–74, doi:10.32607/20758251-2019-11-3-66-74.

18. Zhang, X.; Wang, W.; Zhu, W.; Dong, J.; Cheng, Y.; Yin, Z.; Shen, F. Mechanisms and Functions of Long Non-Coding RNAs at Multiple Regulatory Levels. *Int J Mol Sci* **2019**, *20*, 5573, doi:10.3390/ijms20225573.

19. Derrien, T.; Johnson, R.; Bussotti, G.; Tanzer, A.; Djebali, S.; Tilgner, H.; Guernec, G.; Martin, D.; Merkel, A.; Knowles, D.G.; et al. The GENCODE v7 Catalog of Human Long Noncoding RNAs: Analysis of Their Gene Structure, Evolution, and Expression. *Genome Res* **2012**, *22*, 1775–1789, doi:10.1101/gr.132159.111.

20. Taniue, K.; Akimitsu, N. The Functions and Unique Features of LncRNAs in Cancer Development and Tumorigenesis. *Int J Mol Sci* **2021**, *22*, 632, doi:10.3390/ijms22020632.

21. Noviello, T.M.R.; Di Liddo, A.; Ventola, G.M.; Spagnuolo, A.; D'Aniello, S.; Ceccarelli, M.; Cerulo, L. Detection of Long Non–Coding RNA Homology, a Comparative Study on Alignment and Alignment–Free Metrics. *BMC Bioinformatics* **2018**, *19*, 407, doi:10.1186/s12859-018-2441-6.

22. Jiang, W.; Liu, Y.; Liu, R.; Zhang, K.; Zhang, Y. LncRNA DEANR1 Facilitates Human Endoderm Differentiation by Activating FOXA2 Expression. *Cell Rep* **2015**, *11*, 137–148, doi:10.1016/j.celrep.2015.03.008.

23. Chen, X.; Xu, Y.; Zhao, D.; Chen, T.; Gu, C.; Yu, G.; Chen, K.; Zhong, Y.; He, J.; Liu, S.; et al. LncRNA-AK012226 Is Involved in Fat Accumulation in Db/Db Mice Fatty Liver and Non-Alcoholic Fatty Liver Disease Cell Model. *Front Pharmacol* **2018**, *9*, 888, doi:10.3389/fphar.2018.00888.

24. Choong, O.K.; Chen, C.Y.; Lin, J.H.; Lin, P.J.; Zhang, J.H.; Kamp, T.J.; Hsieh, P.C.H.; (*) 264The Long Noncoding RNA H19 Modulates Cardiac Remodeling after Infarction. *European Heart Journal* **2019**, *40*, ehz747.0080, doi:10.1093/eurheartj/ehz747.0080.

25. Morlando, M.; Ballarino, M.; Fatica, A. Long Non-Coding RNAs: New Players in Hematopoiesis and Leukemia. *Front Med (Lausanne)* **2015**, *2*, 23, doi:10.3389/fmed.2015.00023.

26. Akhade, V.S.; Pal, D.; Kanduri, C. Long Noncoding RNA: Genome Organization and Mechanism of Action. In *Long Non Coding RNA Biology*; Rao, M.R.S., Ed.; Advances in Experimental Medicine and Biology; Springer: Singapore, 2017; pp. 47–74 ISBN 978-981-10-5203-3.

27. Sims, R.J.; Nishioka, K.; Reinberg, D. Histone Lysine Methylation: A Signature for Chromatin Function. *Trends in Genetics* **2003**, *19*, 629–639, doi:10.1016/j.tig.2003.09.007.

28. Hu, J.; Shan, Y.; Ma, J.; Pan, Y.; Zhou, H.; Jiang, L.; Jia, L. LncRNA ST3Gal6-AS1/ST3Gal6 Axis Mediates Colorectal Cancer Progression by Regulating α-2,3 Sialylation via PI3K/Akt Signaling. *Int J Cancer* **2019**, *145*, 450–460, doi:10.1002/ijc.32103.

29. Liu, Y.; Xia, R.; Lu, K.; Xie, M.; Yang, F.; Sun, M.; De, W.; Wang, C.; Ji, G. LincRNAFEZF1-AS1 Represses P21 Expression to Promote Gastric Cancer Proliferation through LSD1-Mediated H3K4me2 Demethylation. *Mol Cancer* **2017**, *16*, 39, doi:10.1186/s12943-017-0588-9.

30. Lavarone, E.; Barbieri, C.M.; Pasini, D. Dissecting the Role of H3K27 Acetylation and Methylation in PRC2 Mediated Control of Cellular Identity. *Nat Commun* **2019**, *10*, 1679, doi:10.1038/s41467-019-09624-w.

31. da Rocha, S.T.; Boeva, V.; Escamilla-Del-Arenal, M.; Ancelin, K.; Granier, C.; Matias, N.R.; Sanulli, S.; Chow, J.; Schulz, E.; Picard, C.; et al. Jarid2 Is Implicated in the Initial Xist-Induced Targeting of PRC2 to the Inactive X Chromosome. *Mol Cell* **2014**, *53*, 301–316, doi:10.1016/j.molcel.2014.01.002.

32. Marín-Béjar, O.; Marchese, F.P.; Athie, A.; Sánchez, Y.; González, J.; Segura, V.; Huang, L.; Moreno, I.; Navarro, A.; Monzó, M.; et al. Pint LincRNA Connects the P53 Pathway with Epigenetic Silencing by the Polycomb Repressive Complex 2. *Genome Biology 2013 14:9* **2013**, *14*, 1–17, doi:10.1186/GB-2013-14-9-R104.

33. Marín-Béjar, O.; Marchese, F.P.; Athie, A.; Sánchez, Y.; González, J.; Segura, V.; Huang, L.; Moreno, I.; Navarro, A.; Monzó, M.; et al. Pint LincRNA Connects the P53 Pathway with Epigenetic Silencing by the Polycomb Repressive Complex 2. *Genome Biol* **2013**, *14*, R104, doi:10.1186/gb-2013-14-9-r104.

34. Rinn, J.L.; Kertesz, M.; Wang, J.K.; Squazzo, S.L.; Xu, X.; Brugmann, S.A.; Goodnough, H.; Helms, J.A.; Farnham, P.J.; Segal, E.; et al. Functional Demarcation of Active and Silent Chromatin Domains in Human HOX Loci by Non-Coding RNAs. *Cell* **2007**, *129*, 1311–1323, doi:10.1016/j.cell.2007.05.022.

35. Jain, A.K.; Xi, Y.; McCarthy, R.; Allton, K.; Akdemir, K.C.; Patel, L.R.; Aronow, B.; Lin, C.; Li, W.; Yang, L.; et al. LncPRESS1 Is a P53-Regulated LncRNA That

Safeguards Pluripotency by Disrupting SIRT6 Mediated de-Acetylation of Histone H3K56. *Mol Cell* **2016**, *64*, 967–981, doi:10.1016/j.molcel.2016.10.039.

36. Sun, T.-T.; He, J.; Liang, Q.; Ren, L.-L.; Yan, T.-T.; Yu, T.-C.; Tang, J.-Y.; Bao, Y.-J.; Hu, Y.; Lin, Y.; et al. LncRNA GClnc1 Promotes Gastric Carcinogenesis and May Act as a Modular Scaffold of WDR5 and KAT2A Complexes to Specify the Histone Modification Pattern. *Cancer Discov* **2016**, *6*, 784–801, doi:10.1158/2159-8290.CD-15-0921.

37. Song, C.; Xiong, Y.; Liao, W.; Meng, L.; Yang, S. Long Noncoding RNA ATB Participates in the Development of Renal Cell Carcinoma by Downregulating P53 via Binding to DNMT1. *J Cell Physiol* **2019**, *234*, 12910–12917, doi:10.1002/jcp.27957.

38. Zhao, X.; Hu, X. Downregulated Long Noncoding RNA LINC00313 Inhibits the Epithelial-Mesenchymal Transition, Invasion, and Migration of Thyroid Cancer Cells through Inhibiting the Methylation of ALX4. *J Cell Physiol* **2019**, *234*, 20992–21004, doi:10.1002/jcp.28703.

39. Li, B.; Chen, P.; Qu, J.; Shi, L.; Zhuang, W.; Fu, J.; Li, J.; Zhang, X.; Sun, Y.; Zhuang, W. Activation of LTBP3 Gene by a Long Noncoding RNA (LncRNA) MALAT1 Transcript in Mesenchymal Stem Cells from Multiple Myeloma. *J Biol Chem* **2014**, *289*, 29365–29375, doi:10.1074/jbc.M114.572693.

40. Ai, B.; Kong, X.; Wang, X.; Zhang, K.; Yang, X.; Zhai, J.; Gao, R.; Qi, Y.; Wang, J.; Wang, Z.; et al. LINC01355 Suppresses Breast Cancer Growth through

FOXO3-Mediated Transcriptional Repression of CCND1. *Cell Death & Disease* **2019**, *10*, 502, doi:10.1038/s41419-019-1741-8.

41. Lee, Y.; Rio, D.C. Mechanisms and Regulation of Alternative Pre-MRNA Splicing. *Annu Rev Biochem* **2015**, *84*, 291–323, doi:10.1146/annurev-biochem-060614-034316.

42. Tripathi, V.; Ellis, J.D.; Shen, Z.; Song, D.Y.; Pan, Q.; Watt, A.T.; Freier, S.M.; Bennett, C.F.; Sharma, A.; Bubulya, P.A.; et al. The Nuclear-Retained Noncoding RNA MALAT1 Regulates Alternative Splicing by Modulating SR Splicing Factor Phosphorylation. *Mol Cell* **2010**, *39*, 925–938, doi:10.1016/j.molcel.2010.08.011.

43. Fefilova, A.; Melnikov, P.; Prikazchikova, T.; Abakumova, T.; Kurochkin, I.; Mazin, P.V.; Ziganshin, R.; Sergeeva, O.; Zatsepin, T.S. Murine Long Noncoding RNA Morrbid Contributes in the Regulation of NRAS Splicing in Hepatocytes In Vitro. *Int J Mol Sci* **2020**, *21*, 5605, doi:10.3390/ijms21165605.

44. O'Brien, J.; Hayder, H.; Zayed, Y.; Peng, C. Overview of MicroRNA Biogenesis, Mechanisms of Actions, and Circulation. *Front Endocrinol (Lausanne)* **2018**, *9*, 402, doi:10.3389/fendo.2018.00402.

45. Jarroux, J.; Morillon, A.; Pinskaya, M. History, Discovery, and Classification of LncRNAs. *Adv Exp Med Biol* **2017**, *1008*, 1–46, doi:10.1007/978-981-10-5203-3_1.

46. Zhang, M.; Li, F.; Sun, J.; Li, D.; Li, W.; Jiang, R.; Li, Z.; Liu, X.; Han, R.; Li, G.; et al. LncRNA IMFNCR Promotes Intramuscular Adipocyte Differentiation by

Sponging MiR-128-3p and MiR-27b-3p. *Front Genet* **2019**, *10*, 42, doi:10.3389/fgene.2019.00042.

47. Xiao, J.; Lin, L.; Luo, D.; Shi, L.; Chen, W.; Fan, H.; Li, Z.; Ma, X.; Ni, P.; Yang, L.; et al. Long Noncoding RNA TRPM2-AS Acts as a MicroRNA Sponge of MiR-612 to Promote Gastric Cancer Progression and Radioresistance. *Oncogenesis* **2020**, *9*, 29, doi:10.1038/s41389-020-0215-2.

48. Gong, C.; Maquat, L.E. LncRNAs Transactivate Staufen1-Mediated MRNA Decay by Duplexing with 3'UTRs via Alu Elements. *Nature* **2011**, *470*, 284–288, doi:10.1038/nature09701.

49. Zhang, L.; Yang, Z.; Trottier, J.; Barbier, O.; Wang, L. LncRNA MEG3 Induces Cholestatic Liver Injury by Interaction with PTBP1 to Facilitate Shp MRNA Decay. *Hepatology* **2017**, *65*, 604–615, doi:10.1002/hep.28882.

50. Anderson, D.M.; Anderson, K.M.; Chang, C.-L.; Makarewich, C.A.; Nelson, B.R.; McAnally, J.R.; Kasaragod, P.; Shelton, J.M.; Liou, J.; Bassel-Duby, R.; et al. A Micropeptide Encoded by a Putative Long Non-Coding RNA Regulates Muscle Performance. *Cell* **2015**, *160*, 595–606, doi:10.1016/j.cell.2015.01.009.

51. Chugunova, A.; Loseva, E.; Mazin, P.; Mitina, A.; Navalayeu, T.; Bilan, D.; Vishnyakova, P.; Marey, M.; Golovina, A.; Serebryakova, M.; et al. LINC00116 Codes for a Mitochondrial Peptide Linking Respiration and Lipid Metabolism. *Proc Natl Acad Sci U S A* **2019**, *116*, 4940–4945, doi:10.1073/pnas.1809105116.

52. Yoon, J.-H.; Abdelmohsen, K.; Srikantan, S.; Yang, X.; Martindale, J.L.; De, S.; Huarte, M.; Zhan, M.; Becker, K.G.; Gorospe, M. LincRNA-P21 Suppresses

Target MRNA Translation. *Mol Cell* **2012**, *47*, 648–655, doi:10.1016/j.molcel.2012.06.027.

53. Hu, G.; Lou, Z.; Gupta, M. The Long Non-Coding RNA GAS5 Cooperates with the Eukaryotic Translation Initiation Factor 4E to Regulate c-Myc Translation. *PLoS One* **2014**, *9*, e107016, doi:10.1371/journal.pone.0107016.

54. Jia, X.; Shi, L.; Wang, X.; Luo, L.; Ling, L.; Yin, J.; Song, Y.; Zhang, Z.; Qiu, N.; Liu, H.; et al. KLF5 Regulated LncRNA RP1 Promotes the Growth and Metastasis of Breast Cancer via Repressing P27kip1 Translation. *Cell Death Dis* **2019**, *10*, 373, doi:10.1038/s41419-019-1566-5.

55. Gumireddy, K.; Li, A.; Yan, J.; Setoyama, T.; Johannes, G.J.; Orom, U.A.; Tchou, J.; Liu, Q.; Zhang, L.; Speicher, D.W.; et al. Identification of a Long Non-Coding RNA-Associated RNP Complex Regulating Metastasis at the Translational Step. *EMBO J* **2013**, *32*, 2672–2684, doi:10.1038/emboj.2013.188.

56. Wang, P.; Xue, Y.; Han, Y.; Lin, L.; Wu, C.; Xu, S.; Jiang, Z.; Xu, J.; Liu, Q.; Cao, X. The STAT3-Binding Long Noncoding RNA Lnc-DC Controls Human Dendritic Cell Differentiation. *Science* **2014**, *344*, 310–313, doi:10.1126/science.1251456.

57. Li, D.; Liu, X.; Zhou, J.; Hu, J.; Zhang, D.; Liu, J.; Qiao, Y.; Zhan, Q. Long Noncoding RNA HULC Modulates the Phosphorylation of YB-1 through Serving as a Scaffold of Extracellular Signal-Regulated Kinase and YB-1 to Enhance Hepatocarcinogenesis. *Hepatology* **2017**, *65*, 1612–1627, doi:10.1002/hep.29010.

58. Yoon, J.-H.; Abdelmohsen, K.; Kim, J.; Yang, X.; Martindale, J.L.; Tominaga-Yamanaka, K.; White, E.J.; Orjalo, A.V.; Rinn, J.L.; Kreft, S.G.; et al. Scaffold Function of Long Non-Coding RNA HOTAIR in Protein Ubiquitination. *Nat Commun* **2013**, *4*, 2939, doi:10.1038/ncomms3939.

59. Ni, W.; Zhang, Y.; Zhan, Z.; Ye, F.; Liang, Y.; Huang, J.; Chen, K.; Chen, L.; Ding, Y. A Novel LncRNA Uc.134 Represses Hepatocellular Carcinoma Progression by Inhibiting CUL4A-Mediated Ubiquitination of LATS1. *J Hematol Oncol* **2017**, *10*, 91, doi:10.1186/s13045-017-0449-4.

60. Chen, R.; Liu, Y.; Zhuang, H.; Yang, B.; Hei, K.; Xiao, M.; Hou, C.; Gao, H.; Zhang, X.; Jia, C.; et al. Quantitative Proteomics Reveals That Long Non-Coding RNA MALAT1 Interacts with DBC1 to Regulate P53 Acetylation. *Nucleic Acids Res* **2017**, *45*, 9947–9959, doi:10.1093/nar/gkx600.

61. Lin, W.; Zhou, Q.; Wang, C.-Q.; Zhu, L.; Bi, C.; Zhang, S.; Wang, X.; Jin, H. LncRNAs Regulate Metabolism in Cancer. *Int J Biol Sci* **2020**, *16*, 1194–1206, doi:10.7150/ijbs.40769.

62. Lin, Y.-H. Crosstalk of LncRNA and Cellular Metabolism and Their Regulatory Mechanism in Cancer. *Int J Mol Sci* **2020**, *21*, 2947, doi:10.3390/ijms21082947.

63. Zhao, X.-Y.; Lin, J.D. Long Noncoding RNAs: A New Regulatory Code in Metabolic Control. *Trends Biochem Sci* **2015**, *40*, 586–596, doi:10.1016/j.tibs.2015.08.002.

64. Rui, L. Energy Metabolism in the Liver. *Compr Physiol* **2014**, *4*, 177–197, doi:10.1002/cphy.c130024.

65. Alves-Bezerra, M.; Cohen, D.E. Triglyceride Metabolism in the Liver. *Compr Physiol* **2017**, *8*, 1–8, doi:10.1002/cphy.c170012.

66. Santoro, N.; Zhang, C.K.; Zhao, H.; Pakstis, A.J.; Kim, G.; Kursawe, R.; Dykas, D.J.; Bale, A.E.; Giannini, C.; Pierpont, B.; et al. Variant in the Glucokinase Regulatory Protein (GCKR) Gene Is Associated with Fatty Liver in Obese Children and Adolescents. *Hepatology* **2012**, *55*, 781–789, doi:10.1002/hep.24806.

67. Oosterveer, M.H.; Mataki, C.; Yamamoto, H.; Harach, T.; Moullan, N.; van Dijk, T.H.; Ayuso, E.; Bosch, F.; Postic, C.; Groen, A.K.; et al. LRH-1-Dependent Glucose Sensing Determines Intermediary Metabolism in Liver. *J Clin Invest* **2012**, *122*, 2817–2826, doi:10.1172/JCI62368.

68. van der Veen, J.N.; Kennelly, J.P.; Wan, S.; Vance, J.E.; Vance, D.E.; Jacobs, R.L. The Critical Role of Phosphatidylcholine and Phosphatidylethanolamine Metabolism in Health and Disease. *Biochimica et Biophysica Acta (BBA) - Biomembranes* **2017**, *1859*, 1558–1572, doi:10.1016/j.bbamem.2017.04.006.

69. Walker, A.K.; Jacobs, R.L.; Watts, J.L.; Rottiers, V.; Jiang, K.; Finnegan, D.M.; Shioda, T.; Hansen, M.; Yang, F.; Niebergall, L.J.; et al. A Conserved SREBP-1/Phosphatidylcholine Feedback Circuit Regulates Lipogenesis in Metazoans. *Cell* **2011**, *147*, 840–852, doi:10.1016/j.cell.2011.09.045.

70. DeLong, C.J.; Shen, Y.J.; Thomas, M.J.; Cui, Z. Molecular Distinction of Phosphatidylcholine Synthesis between the CDP-Choline Pathway and Phosphatidylethanolamine Methylation Pathway. *J Biol Chem* **1999**, *274*, 29683–29688, doi:10.1074/jbc.274.42.29683.

71. Law, S.-H.; Chan, M.-L.; Marathe, G.K.; Parveen, F.; Chen, C.-H.; Ke, L.-Y. An Updated Review of Lysophosphatidylcholine Metabolism in Human Diseases. *Int J Mol Sci* **2019**, *20*, 1149, doi:10.3390/ijms20051149.

72. Kitatani, K.; Idkowiak-Baldys, J.; Hannun, Y.A. The Sphingolipid Salvage Pathway in Ceramide Metabolism and Signaling. *Cell Signal* **2008**, *20*, 1010–1018, doi:10.1016/j.cellsig.2007.12.006.

73. Pagadala, M.; Kasumov, T.; McCullough, A.J.; Zein, N.N.; Kirwan, J.P. Role of Ceramides in Nonalcoholic Fatty Liver Disease. *Trends Endocrinol Metab* **2012**, *23*, 365–371, doi:10.1016/j.tem.2012.04.005.

74. Lu, W.; Cao, F.; Wang, S.; Sheng, X.; Ma, J. LncRNAs: The Regulator of Glucose and Lipid Metabolism in Tumor Cells. *Front Oncol* **2019**, *9*, 1099, doi:10.3389/fonc.2019.01099.

75. Lu, C.; Ma, J.; Cai, D. Increased HAGLR Expression Promotes Non-Small Cell Lung Cancer Proliferation and Invasion via Enhanced de Novo Lipogenesis. *Tumour Biol* **2017**, *39*, 1010428317697574, doi:10.1177/1010428317697574.

76. Ma, D.-D.; Yuan, L.-L.; Lin, L.-Q. LncRNA HOTAIR Contributes to the Tumorigenesis of Nasopharyngeal Carcinoma via Up-Regulating FASN. *Eur Rev Med Pharmacol Sci* **2017**, *21*, 5143–5152, doi:10.26355/eurrev_201711_13831.

77. Zhou, Q.; Chen, F.; Zhao, J.; Li, B.; Liang, Y.; Pan, W.; Zhang, S.; Wang, X.; Zheng, D. Long Non-Coding RNA PVT1 Promotes Osteosarcoma Development by Acting as a Molecular Sponge to Regulate MiR-195. *Oncotarget* **2016**, *7*, 82620–82633, doi:10.18632/oncotarget.13012.

78. Zhang, X.; Wu, J.; Wu, C.; Chen, W.; Lin, R.; Zhou, Y.; Huang, X. The LINC01138 Interacts with PRMT5 to Promote SREBP1-Mediated Lipid Desaturation and Cell Growth in Clear Cell Renal Cell Carcinoma. *Biochem Biophys Res Commun* **2018**, *507*, 337–342, doi:10.1016/j.bbrc.2018.11.036.

79. Liu, X.; Liang, Y.; Song, R.; Yang, G.; Han, J.; Lan, Y.; Pan, S.; Zhu, M.; Liu, Y.; Wang, Y.; et al. Long Non-Coding RNA NEAT1-Modulated Abnormal Lipolysis via ATGL Drives Hepatocellular Carcinoma Proliferation. *Mol Cancer* **2018**, *17*, 90, doi:10.1186/s12943-018-0838-5.

80. Cui, M.; Xiao, Z.; Wang, Y.; Zheng, M.; Song, T.; Cai, X.; Sun, B.; Ye, L.; Zhang, X. Long Noncoding RNA HULC Modulates Abnormal Lipid Metabolism in Hepatoma Cells through an MiR-9-Mediated RXRA Signaling Pathway. *Cancer Res* **2015**, *75*, 846–857, doi:10.1158/0008-5472.CAN-14-1192.

81. Yang, L.; Li, P.; Yang, W.; Ruan, X.; Kiesewetter, K.; Zhu, J.; Cao, H. Integrative Transcriptome Analyses of Metabolic Responses in Mice Define Pivotal LncRNA Metabolic Regulators. *Cell Metabolism* **2016**, *24*, 627–639, doi:10.1016/j.cmet.2016.08.019.

82. Mazar, J.; Zhao, W.; Khalil, A.M.; Lee, B.; Shelley, J.; Govindarajan, S.S.; Yamamoto, F.; Ratnam, M.; Aftab, M.N.; Collins, S.; et al. The Functional Characterization of Long Noncoding RNA SPRY4-IT1 in Human Melanoma Cells. *Oncotarget* **2014**, *5*, 8959–8969, doi:10.18632/oncotarget.1863.

83. Lu, M.-C.; Yu, H.-C.; Yu, C.-L.; Huang, H.-B.; Koo, M.; Tung, C.-H.; Lai, N.-S. Increased Expression of Long Noncoding RNAs LOC100652951 and

LOC100506036 in T Cells from Patients with Rheumatoid Arthritis Facilitates the Inflammatory Responses. *Immunol Res* **2016**, *64*, 576–583, doi:10.1007/s12026-015-8756-8.

84. Zeng, Y.; Ren, K.; Zhu, X.; Zheng, Z.; Yi, G. Chapter One - Long Noncoding RNAs: Advances in Lipid Metabolism. In *Advances in Clinical Chemistry*; Makowski, G.S., Ed.; Advances in Clinical Chemistry; Elsevier, 2018; Vol. 87, pp. 1–36.

85. Lin, A.; Hu, Q.; Li, C.; Xing, Z.; Ma, G.; Wang, C.; Li, J.; Ye, Y.; Yao, J.; Liang, K.; et al. The LINK-A LncRNA Interacts with PtdIns(3,4,5)P(3) to Hyperactivate AKT and Confer Resistance to AKT Inhibitors. *Nat Cell Biol* **2017**, *19*, 238–251, doi:10.1038/ncb3473.

86. Bechmann, L.P.; Hannivoort, R.A.; Gerken, G.; Hotamisligil, G.S.; Trauner, M.; Canbay, A. The Interaction of Hepatic Lipid and Glucose Metabolism in Liver Diseases. *Journal of Hepatology* **2012**, *56*, 952–964, doi:10.1016/j.jhep.2011.08.025.

87. Towle, H.C.; Kaytor, E.N.; Shih, H.M. Regulation of the Expression of Lipogenic Enzyme Genes by Carbohydrate. *Annu Rev Nutr* **1997**, *17*, 405–433, doi:10.1146/annurev.nutr.17.1.405.

88. Nordlie, R.C.; Foster, J.D.; Lange, A.J. Regulation of Glucose Production by the Liver. *Annu Rev Nutr* **1999**, *19*, 379–406, doi:10.1146/annurev.nutr.19.1.379.

89. Han, H.-S.; Kang, G.; Kim, J.S.; Choi, B.H.; Koo, S.-H. Regulation of Glucose Metabolism from a Liver-Centric Perspective. *Exp Mol Med* **2016**, *48*, e218, doi:10.1038/emm.2015.122.

90. Vekemans, K.; Braet, F. Structural and Functional Aspects of the Liver and Liver Sinusoidal Cells in Relation to Colon Carcinoma Metastasis. *World J Gastroenterol* **2005**, *11*, 5095–5102, doi:10.3748/wjg.v11.i33.5095.

91. Zhang, T.; Wang, S.; Lin, Y.; Xu, W.; Ye, D.; Xiong, Y.; Zhao, S.; Guan, K.-L. Acetylation Negatively Regulates Glycogen Phosphorylase by Recruiting Protein Phosphatase 1. *Cell Metab* **2012**, *15*, 75–87, doi:10.1016/j.cmet.2011.12.005.

92. Kir, S.; Beddow, S.A.; Samuel, V.T.; Miller, P.; Previs, S.F.; Suino-Powell, K.; Xu, H.E.; Shulman, G.I.; Kliewer, S.A.; Mangelsdorf, D.J. FGF19 as a Postprandial, Insulin-Independent Activator of Hepatic Protein and Glycogen Synthesis. *Science* **2011**, *331*, 1621–1624, doi:10.1126/science.1198363.

93. Shimano, H.; Yahagi, N.; Amemiya-Kudo, M.; Hasty, A.H.; Osuga, J.; Tamura, Y.; Shionoiri, F.; Iizuka, Y.; Ohashi, K.; Harada, K.; et al. Sterol Regulatory Element-Binding Protein-1 as a Key Transcription Factor for Nutritional Induction of Lipogenic Enzyme Genes. *J Biol Chem* **1999**, *274*, 35832–35839, doi:10.1074/jbc.274.50.35832.

94. Yamashita, H.; Takenoshita, M.; Sakurai, M.; Bruick, R.K.; Henzel, W.J.; Shillinglaw, W.; Arnot, D.; Uyeda, K. A Glucose-Responsive Transcription Factor That Regulates Carbohydrate Metabolism in the Liver. *Proc Natl Acad Sci U S A* **2001**, *98*, 9116–9121, doi:10.1073/pnas.161284298.

95. Mitro, N.; Mak, P.A.; Vargas, L.; Godio, C.; Hampton, E.; Molteni, V.; Kreusch, A.; Saez, E. The Nuclear Receptor LXR Is a Glucose Sensor. *Nature* **2007**, *445*, 219–223, doi:10.1038/nature05449.

96. Denechaud, P.-D.; Bossard, P.; Lobaccaro, J.-M.A.; Millatt, L.; Staels, B.; Girard, J.; Postic, C. ChREBP, but Not LXRs, Is Required for the Induction of Glucose-Regulated Genes in Mouse Liver. *J Clin Invest* **2008**, *118*, 956–964, doi:10.1172/JCI34314.

97. Jeoung, N.H.; Wu, P.; Joshi, M.A.; Jaskiewicz, J.; Bock, C.B.; Depaoli-Roach, A.A.; Harris, R.A. Role of Pyruvate Dehydrogenase Kinase Isoenzyme 4 (PDHK4) in Glucose Homoeostasis during Starvation. *Biochem J* **2006**, *397*, 417–425, doi:10.1042/BJ20060125.

98. Zhao, S.; Xu, W.; Jiang, W.; Yu, W.; Lin, Y.; Zhang, T.; Yao, J.; Zhou, L.; Zeng, Y.; Li, H.; et al. Regulation of Cellular Metabolism by Protein Lysine Acetylation. *Science* **2010**, *327*, 1000–1004, doi:10.1126/science.1179689.

99. Jiang, W.; Wang, S.; Xiao, M.; Lin, Y.; Zhou, L.; Lei, Q.; Xiong, Y.; Guan, K.-L.; Zhao, S. Acetylation Regulates Gluconeogenesis by Promoting PEPCK1 Degradation via Recruiting the UBR5 Ubiquitin Ligase. *Mol Cell* **2011**, *43*, 33–44, doi:10.1016/j.molcel.2011.04.028.

100. Kwok, R.P.; Laurance, M.E.; Lundblad, J.R.; Goldman, P.S.; Shih, H.; Connor, L.M.; Marriott, S.J.; Goodman, R.H. Control of CAMP-Regulated Enhancers by the Viral Transactivator Tax through CREB and the Co-Activator CBP. *Nature* **1996**, *380*, 642–646, doi:10.1038/380642a0.

101. MJ, P.; J, B.-M.; M, C.; T, H.; NE, S.; S, S.; K, S.-P.; HE, X.; RD, G.; BN, F.; et al. FGF15/19 Regulates Hepatic Glucose Metabolism by Inhibiting the CREB-PGC-1α Pathway. *Cell metabolism* **2011**, *13*, 729–738, doi:10.1016/J.CMET.2011.03.019.

102. Zhang, X.; Yang, S.; Chen, J.; Su, Z. Unraveling the Regulation of Hepatic Gluconeogenesis. *Front Endocrinol (Lausanne)* **2019**, *9*, 802–802, doi:10.3389/fendo.2018.00802.

103. Zhang, W.; Patil, S.; Chauhan, B.; Guo, S.; Powell, D.R.; Le, J.; Klotsas, A.; Matika, R.; Xiao, X.; Franks, R.; et al. FoxO1 Regulates Multiple Metabolic Pathways in the Liver: Effects on Gluconeogenic, Glycolytic, and Lipogenic Gene Expression. *J Biol Chem* **2006**, *281*, 10105–10117, doi:10.1074/jbc.M600272200.

104. Lee, M.-W.; Chanda, D.; Yang, J.; Oh, H.; Kim, S.S.; Yoon, Y.-S.; Hong, S.; Park, K.-G.; Lee, I.-K.; Choi, C.S.; et al. Regulation of Hepatic Gluconeogenesis by an ER-Bound Transcription Factor, CREBH. *Cell Metab* **2010**, *11*, 331–339, doi:10.1016/j.cmet.2010.02.016.

105. Herzig, S.; Long, F.; Jhala, U.S.; Hedrick, S.; Quinn, R.; Bauer, A.; Rudolph, D.; Schutz, G.; Yoon, C.; Puigserver, P.; et al. CREB Regulates Hepatic Gluconeogenesis through the Coactivator PGC-1. *Nature* **2001**, *413*, 179–183, doi:10.1038/35093131.

106. Ravnskjaer, K.; Hogan, M.F.; Lackey, D.; Tora, L.; Dent, S.Y.R.; Olefsky, J.; Montminy, M. Glucagon Regulates Gluconeogenesis through KAT2B- and

WDR5-Mediated Epigenetic Effects. *J Clin Invest* **2013**, *123*, 4318–4328, doi:10.1172/JCI69035.

107. Wang, Y.; Vera, L.; Fischer, W.H.; Montminy, M. The CREB Coactivator CRTC2 Links Hepatic ER Stress and Fasting Gluconeogenesis. *Nature* **2009**, *460*, 534–537, doi:10.1038/nature08111.

108. De Meyts, P. Insulin and Its Receptor: Structure, Function and Evolution. *Bioessays* **2004**, *26*, 1351–1362, doi:10.1002/bies.20151.

109. Morán, I.; Akerman, I.; van de Bunt, M.; Xie, R.; Benazra, M.; Nammo, T.; Arnes, L.; Nakić, N.; García-Hurtado, J.; Rodríguez-Seguí, S.; et al. Human β Cell Transcriptome Analysis Uncovers LncRNAs That Are Tissue-Specific, Dynamically Regulated, and Abnormally Expressed in Type 2 Diabetes. *Cell Metab* **2012**, *16*, 435–448, doi:10.1016/j.cmet.2012.08.010.

110. Sanchez-Parra, C.; Jacovetti, C.; Dumortier, O.; Lee, K.; Peyot, M.-L.; Guay, C.; Prentki, M.; Laybutt, D.R.; Van Obberghen, E.; Regazzi, R. Contribution of the Long Noncoding RNA H19 to β-Cell Mass Expansion in Neonatal and Adult Rodents. *Diabetes* **2018**, *67*, 2254–2267, doi:10.2337/db18-0201.

111. Arnes, L.; Akerman, I.; Balderes, D.A.; Ferrer, J.; Sussel, L. Blinc1 Encodes a Long Noncoding RNA That Regulates Islet β-Cell Formation and Function. *Genes Dev* **2016**, *30*, 502–507, doi:10.1101/gad.273821.115.

112. Zhang, T.-N.; Wang, W.; Yang, N.; Huang, X.-M.; Liu, C.-F. Regulation of Glucose and Lipid Metabolism by Long Non-Coding RNAs: Facts and Research

Progress. *Front Endocrinol (Lausanne)* **2020**, *11*, 457–457, doi:10.3389/fendo.2020.00457.

113. Wang, N.; Zhu, Y.; Xie, M.; Wang, L.; Jin, F.; Li, Y.; Yuan, Q.; De, W. Long Noncoding RNA Meg3 Regulates Mafa Expression in Mouse Beta Cells by Inactivating Rad21, Smc3 or Sin3α. *Cell Physiol Biochem* **2018**, *45*, 2031–2043, doi:10.1159/000487983.

114. Zhao, X.; Rong, C.; Pan, F.; Xiang, L.; Wang, X.; Hu, Y. Expression Characteristics of Long Noncoding RNA Uc.322 and Its Effects on Pancreatic Islet Function. *J Cell Biochem* **2018**, *119*, 9239–9248, doi:10.1002/jcb.27191.

115. Yin, D.; Zhang, E.; You, L.; Wang, N.; Wang, L.; Jin, F.; Zhu, Y.; Cao, L.; Yuan, Q.; De, W.; et al. Downregulation of LncRNA TUG1 Affects Apoptosis and Insulin Secretion in Mouse Pancreatic β Cells. *Cell Physiol Biochem* **2015**, *35*, 1892–1904, doi:10.1159/000373999.

116. Ruan, X.; Li, P.; Cangelosi, A.; Yang, L.; Cao, H. A Long Non-Coding RNA, LncLGR, Regulates Hepatic Glucokinase Expression and Glycogen Storage during Fasting. *Cell Rep* **2016**, *14*, 1867–1875, doi:10.1016/j.celrep.2016.01.062.

117. Liu, X.; Gan, B. LncRNA NBR2 Modulates Cancer Cell Sensitivity to Phenformin through GLUT1. *Cell Cycle* **2016**, *15*, 3471–3481, doi:10.1080/15384101.2016.1249545.

118. Ellis, B.C.; Graham, L.D.; Molloy, P.L. CRNDE, a Long Non-Coding RNA Responsive to Insulin/IGF Signaling, Regulates Genes Involved in Central

Metabolism. *Biochim Biophys Acta* **2014**, *1843*, 372–386, doi:10.1016/j.bbamcr.2013.10.016.

119. Chen, S.; Xu, X.; Lu, S.; Hu, B. Long Non-Coding RNA HAND2-AS1 Targets Glucose Metabolism and Inhibits Cancer Cell Proliferation in Osteosarcoma. *Oncol Lett* **2019**, *18*, 1323–1329, doi:10.3892/ol.2019.10445.

120. Wang, Y.; Zhang, X.; Wang, Z.; Hu, Q.; Wu, J.; Li, Y.; Ren, X.; Wu, T.; Tao, X.; Chen, X.; et al. LncRNA-P23154 Promotes the Invasion-Metastasis Potential of Oral Squamous Cell Carcinoma by Regulating Glut1-Mediated Glycolysis. *Cancer Lett* **2018**, *434*, 172–183, doi:10.1016/j.canlet.2018.07.016.

121. Chang, L.; Xu, W.; Zhang, Y.; Gong, F. Long Non-Coding RNA-NEF Targets Glucose Transportation to Inhibit the Proliferation of Non-Small-Cell Lung Cancer Cells. *Oncol Lett* **2019**, *17*, 2795–2801, doi:10.3892/ol.2019.9919.

122. Wei, S.; Fan, Q.; Yang, L.; Zhang, X.; Ma, Y.; Zong, Z.; Hua, X.; Su, D.; Sun, H.; Li, H.; et al. Promotion of Glycolysis by HOTAIR through GLUT1 Upregulation via MTOR Signaling. *Oncol Rep* **2017**, *38*, 1902–1908, doi:10.3892/or.2017.5840.

123. Zhao, Y.; Liu, Y.; Lin, L.; Huang, Q.; He, W.; Zhang, S.; Dong, S.; Wen, Z.; Rao, J.; Liao, W.; et al. The LncRNA MACC1-AS1 Promotes Gastric Cancer Cell Metabolic Plasticity via AMPK/Lin28 Mediated MRNA Stability of MACC1. *Mol Cancer* **2018**, *17*, 69, doi:10.1186/s12943-018-0820-2.

124. Fan, C.; Tang, Y.; Wang, J.; Xiong, F.; Guo, C.; Wang, Y.; Zhang, S.; Gong, Z.; Wei, F.; Yang, L.; et al. Role of Long Non-Coding RNAs in Glucose Metabolism in Cancer. *Molecular Cancer* **2017**, *16*, 130, doi:10.1186/s12943-017-0699-3.

125. Li, N.; Zhan, X.; Zhan, X. The LncRNA SNHG3 Regulates Energy Metabolism of Ovarian Cancer by an Analysis of Mitochondrial Proteomes. *Gynecol Oncol* **2018**, *150*, 343–354, doi:10.1016/j.ygyno.2018.06.013.

126. Liu, C.; Zhang, Y.; She, X.; Fan, L.; Li, P.; Feng, J.; Fu, H.; Liu, Q.; Liu, Q.; Zhao, C.; et al. A Cytoplasmic Long Noncoding RNA LINC00470 as a New AKT Activator to Mediate Glioblastoma Cell Autophagy. *Journal of Hematology & Oncology* **2018**, *11*, 77, doi:10.1186/s13045-018-0619-z.

127. Lin, Y.-H.; Wu, M.-H.; Huang, Y.-H.; Yeh, C.-T.; Cheng, M.-L.; Chi, H.-C.; Tsai, C.-Y.; Chung, I.-H.; Chen, C.-Y.; Lin, K.-H. Taurine Up-Regulated Gene 1 Functions as a Master Regulator to Coordinate Glycolysis and Metastasis in Hepatocellular Carcinoma. *Hepatology* **2018**, *67*, 188–203, doi:10.1002/hep.29462.

128. Han, X.; Yang, Y.; Sun, Y.; Qin, L.; Yang, Y. LncRNA TUG1 Affects Cell Viability by Regulating Glycolysis in Osteosarcoma Cells. *Gene* **2018**, *674*, 87–92, doi:10.1016/j.gene.2018.06.085.

129. Song, J.; Wu, X.; Liu, F.; Li, M.; Sun, Y.; Wang, Y.; Wang, C.; Zhu, K.; Jia, X.; Wang, B.; et al. Long Non-Coding RNA PVT1 Promotes Glycolysis and Tumor Progression by Regulating MiR-497/HK2 Axis in Osteosarcoma. *Biochem Biophys Res Commun* **2017**, *490*, 217–224, doi:10.1016/j.bbrc.2017.06.024.

130. Chen, J.; Yu, Y.; Li, H.; Hu, Q.; Chen, X.; He, Y.; Xue, C.; Ren, F.; Ren, Z.; Li, J.; et al. Long Non-Coding RNA PVT1 Promotes Tumor Progression by Regulating the MiR-143/HK2 Axis in Gallbladder Cancer. *Mol Cancer* **2019**, *18*, 33, doi:10.1186/s12943-019-0947-9.

131. Ma, J.; Fan, Y.; Feng, T.; Chen, F.; Xu, Z.; Li, S.; Lin, Q.; He, X.; Shi, W.; Liu, Y.; et al. HOTAIR Regulates HK2 Expression by Binding Endogenous MiR-125 and MiR-143 in Oesophageal Squamous Cell Carcinoma Progression. *Oncotarget* **2017**, *8*, 86410–86422, doi:10.18632/oncotarget.21195.

132. Xing, Z.; Zhang, Y.; Liang, K.; Yan, L.; Xiang, Y.; Li, C.; Hu, Q.; Jin, F.; Putluri, V.; Putluri, N.; et al. Expression of Long Noncoding RNA YIYA Promotes Glycolysis in Breast Cancer. *Cancer Res* **2018**, *78*, 4524–4532, doi:10.1158/0008-5472.CAN-17-0385.

133. Bian, Z.; Zhang, J.; Li, M.; Feng, Y.; Wang, X.; Zhang, J.; Yao, S.; Jin, G.; Du, J.; Han, W.; et al. LncRNA-FEZF1-AS1 Promotes Tumor Proliferation and Metastasis in Colorectal Cancer by Regulating PKM2 Signaling. *Clin Cancer Res* **2018**, *24*, 4808–4819, doi:10.1158/1078-0432.CCR-17-2967.

134. Zheng, Y.-L.; Li, L.; Jia, Y.-X.; Zhang, B.-Z.; Li, J.-C.; Zhu, Y.-H.; Li, M.-Q.; He, J.-Z.; Zeng, T.-T.; Ban, X.-J.; et al. LINC01554-Mediated Glucose Metabolism Reprogramming Suppresses Tumorigenicity in Hepatocellular Carcinoma via Downregulating PKM2 Expression and Inhibiting Akt/MTOR Signaling Pathway. *Theranostics* **2019**, *9*, 796–810, doi:10.7150/thno.28992.

135. Chen, H.; Pei, H.; Hu, W.; Ma, J.; Zhang, J.; Mao, W.; Nie, J.; Xu, C.; Li, B.; Hei, T.K.; et al. Long Non-Coding RNA CRYBG3 Regulates Glycolysis of Lung Cancer Cells by Interacting with Lactate Dehydrogenase A. *J Cancer* **2018**, *9*, 2580–2588, doi:10.7150/jca.24896.

136. Hu, R.; Zhong, P.; Xiong, L.; Duan, L. Long Noncoding RNA Cancer Susceptibility Candidate 8 Suppresses the Proliferation of Bladder Cancer Cells via Regulating Glycolysis. *DNA Cell Biol* **2017**, *36*, 767–774, doi:10.1089/dna.2017.3785.

137. Zhao, L.; Ji, G.; Le, X.; Wang, C.; Xu, L.; Feng, M.; Zhang, Y.; Yang, H.; Xuan, Y.; Yang, Y.; et al. Long Noncoding RNA LINC00092 Acts in Cancer-Associated Fibroblasts to Drive Glycolysis and Progression of Ovarian Cancer. *Cancer Res* **2017**, *77*, 1369–1382, doi:10.1158/0008-5472.CAN-16-1615.

138. Kino, T.; Hurt, D.E.; Ichijo, T.; Nader, N.; Chrousos, G.P. Noncoding RNA Gas5 Is a Growth Arrest- and Starvation-Associated Repressor of the Glucocorticoid Receptor. *Sci Signal* **2010**, *3*, ra8, doi:10.1126/scisignal.2000568.

139. Ma, M.-Z.; Zhang, Y.; Weng, M.-Z.; Wang, S.-H.; Hu, Y.; Hou, Z.-Y.; Qin, Y.-Y.; Gong, W.; Zhang, Y.-J.; Kong, X.; et al. Long Noncoding RNA GCASPC, a Target of MiR-17-3p, Negatively Regulates Pyruvate Carboxylase-Dependent Cell Proliferation in Gallbladder Cancer. *Cancer Res* **2016**, *76*, 5361–5371, doi:10.1158/0008-5472.CAN-15-3047.

140. Liberti, M.V.; Locasale, J.W. The Warburg Effect: How Does It Benefit Cancer Cells? *Trends Biochem Sci* **2016**, *41*, 211–218, doi:10.1016/j.tibs.2015.12.001.

141. Yang, F.; Zhang, H.; Mei, Y.; Wu, M. Reciprocal Regulation of HIF-1α and LincRNA-P21 Modulates the Warburg Effect. *Mol Cell* **2014**, *53*, 88–100, doi:10.1016/j.molcel.2013.11.004.

142. Luo, F.; Liu, X.; Ling, M.; Lu, L.; Shi, L.; Lu, X.; Li, J.; Zhang, A.; Liu, Q. The LncRNA MALAT1, Acting through HIF-1α Stabilization, Enhances Arsenite-Induced Glycolysis in Human Hepatic L-02 Cells. *Biochim Biophys Acta* **2016**, *1862*, 1685–1695, doi:10.1016/j.bbadis.2016.06.004.

143. Yang, F.; Huo, X.; Yuan, S.; Zhang, L.; Zhou, W.; Wang, F.; Sun, S. Repression of the Long Noncoding RNA-LET by Histone Deacetylase 3 Contributes to Hypoxia-Mediated Metastasis. *Mol Cell* **2013**, *49*, 1083–1096, doi:10.1016/j.molcel.2013.01.010.

144. Lin, A.; Li, C.; Xing, Z.; Hu, Q.; Liang, K.; Han, L.; Wang, C.; Hawke, D.H.; Wang, S.; Zhang, Y.; et al. The LINK-A LncRNA Activates Normoxic HIF1α Signalling in Triple-Negative Breast Cancer. *Nat Cell Biol* **2016**, *18*, 213–224, doi:10.1038/ncb3295.

145. Takahashi, K.; Yan, I.K.; Haga, H.; Patel, T. Modulation of Hypoxia-Signaling Pathways by Extracellular Linc-RoR. *J Cell Sci* **2014**, *127*, 1585–1594, doi:10.1242/jcs.141069.

146. van Dam, E.M.; Govers, R.; James, D.E. Akt Activation Is Required at a Late Stage of Insulin-Induced GLUT4 Translocation to the Plasma Membrane. *Mol Endocrinol* **2005**, *19*, 1067–1077, doi:10.1210/me.2004-0413.

147. Poliseno, L.; Salmena, L.; Zhang, J.; Carver, B.; Haveman, W.J.; Pandolfi, P.P. A Coding-Independent Function of Gene and Pseudogene MRNAs Regulates Tumour Biology. *Nature* **2010**, *465*, 1033–1038, doi:10.1038/nature09144.

148. Li, D.; Feng, J.; Wu, T.; Wang, Y.; Sun, Y.; Ren, J.; Liu, M. Long Intergenic Noncoding RNA HOTAIR Is Overexpressed and Regulates PTEN Methylation in Laryngeal Squamous Cell Carcinoma. *Am J Pathol* **2013**, *182*, 64–70, doi:10.1016/j.ajpath.2012.08.042.

149. Zou, Z.W.; Ma, C.; Medoro, L.; Chen, L.; Wang, B.; Gupta, R.; Liu, T.; Yang, X.Z.; Chen, T.T.; Wang, R.Z.; et al. LncRNA ANRIL Is Up-Regulated in Nasopharyngeal Carcinoma and Promotes the Cancer Progression via Increasing Proliferation, Reprograming Cell Glucose Metabolism and Inducing Side-Population Stem-like Cancer Cells. *Oncotarget* **2016**, *7*, 61741–61754, doi:10.18632/oncotarget.11437.

150. Gao, Y.; Wu, F.; Zhou, J.; Yan, L.; Jurczak, M.J.; Lee, H.-Y.; Yang, L.; Mueller, M.; Zhou, X.-B.; Dandolo, L.; et al. The H19/Let-7 Double-Negative Feedback Loop Contributes to Glucose Metabolism in Muscle Cells. *Nucleic Acids Res* **2014**, *42*, 13799–13811, doi:10.1093/nar/gku1160.

151. Inoki, K.; Zhu, T.; Guan, K.-L. TSC2 Mediates Cellular Energy Response to Control Cell Growth and Survival. *Cell* **2003**, *115*, 577–590, doi:10.1016/s0092-8674(03)00929-2.

152. Shackelford, D.B.; Vasquez, D.S.; Corbeil, J.; Wu, S.; Leblanc, M.; Wu, C.-L.; Vera, D.R.; Shaw, R.J. MTOR and HIF-1alpha-Mediated Tumor Metabolism in an LKB1 Mouse Model of Peutz-Jeghers Syndrome. *Proc Natl Acad Sci U S A* **2009**, *106*, 11137–11142, doi:10.1073/pnas.0900465106.

153. Chen, Z.; Li, J.-L.; Lin, S.; Cao, C.; Gimbrone, N.T.; Yang, R.; Fu, D.A.; Carper, M.B.; Haura, E.B.; Schabath, M.B.; et al. CAMP/CREB-Regulated LINC00473 Marks LKB1-Inactivated Lung Cancer and Mediates Tumor Growth. *J Clin Invest* **2016**, *126*, 2267–2279, doi:10.1172/JCI85250.

154. Liu, X.; Xiao, Z.-D.; Han, L.; Zhang, J.; Lee, S.-W.; Wang, W.; Lee, H.; Zhuang, L.; Chen, J.; Lin, H.-K.; et al. LncRNA NBR2 Engages a Metabolic Checkpoint by Regulating AMPK under Energy Stress. *Nat Cell Biol* **2016**, *18*, 431–442, doi:10.1038/ncb3328.

155. Lee, S.Y.; Jeon, H.M.; Ju, M.K.; Kim, C.H.; Yoon, G.; Han, S.I.; Park, H.G.; Kang, H.S. Wnt/Snail Signaling Regulates Cytochrome C Oxidase and Glucose Metabolism. *Cancer Res* **2012**, *72*, 3607–3617, doi:10.1158/0008-5472.CAN-12-0006.

156. Yuan, Z.; Yu, X.; Ni, B.; Chen, D.; Yang, Z.; Huang, J.; Wang, J.; Chen, D.; Wang, L. Overexpression of Long Non-Coding RNA-CTD903 Inhibits Colorectal Cancer Invasion and Migration by Repressing Wnt/β-Catenin Signaling and Predicts Favorable Prognosis. *Int J Oncol* **2016**, *48*, 2675–2685, doi:10.3892/ijo.2016.3447.

157. Xiao, C.; Wu, C.-H.; Hu, H.-Z. LncRNA UCA1 Promotes Epithelial-Mesenchymal Transition (EMT) of Breast Cancer Cells via Enhancing Wnt/Beta-Catenin Signaling Pathway. *Eur Rev Med Pharmacol Sci* **2016**, *20*, 2819–2824.

158. Rupaimoole, R.; Lee, J.; Haemmerle, M.; Ling, H.; Previs, R.A.; Pradeep, S.; Wu, S.Y.; Ivan, C.; Ferracin, M.; Dennison, J.B.; et al. Long Noncoding RNA

Ceruloplasmin Promotes Cancer Growth by Altering Glycolysis. *Cell Rep* **2015**, *13*, 2395–2402, doi:10.1016/j.celrep.2015.11.047.

159. Li, Z.; Li, X.; Wu, S.; Xue, M.; Chen, W. Long Non-Coding RNA UCA1 Promotes Glycolysis by Upregulating Hexokinase 2 through the MTOR–STAT3/MicroRNA143 Pathway. *Cancer Sci* **2014**, *105*, 951–955, doi:10.1111/cas.12461.

160. Wu, M.; An, J.; Zheng, Q.; Xin, X.; Lin, Z.; Li, X.; Li, H.; Lu, D. Double Mutant P53 (N340Q/L344R) Promotes Hepatocarcinogenesis through Upregulation of Pim1 Mediated by PKM2 and LncRNA CUDR. *Oncotarget* **2016**, *7*, 66525–66539, doi:10.18632/oncotarget.9089.

161. Huarte, M.; Guttman, M.; Feldser, D.; Garber, M.; Koziol, M.J.; Kenzelmann-Broz, D.; Khalil, A.M.; Zuk, O.; Amit, I.; Rabani, M.; et al. A Large Intergenic Noncoding RNA Induced by P53 Mediates Global Gene Repression in the P53 Response. *Cell* **2010**, *142*, 409–419, doi:10.1016/j.cell.2010.06.040.

162. Tripathi, V.; Shen, Z.; Chakraborty, A.; Giri, S.; Freier, S.M.; Wu, X.; Zhang, Y.; Gorospe, M.; Prasanth, S.G.; Lal, A.; et al. Long Noncoding RNA MALAT1 Controls Cell Cycle Progression by Regulating the Expression of Oncogenic Transcription Factor B-MYB. *PLoS Genet* **2013**, *9*, e1003368, doi:10.1371/journal.pgen.1003368.

163. Kim, J.; Gao, P.; Liu, Y.-C.; Semenza, G.L.; Dang, C.V. Hypoxia-Inducible Factor 1 and Dysregulated c-Myc Cooperatively Induce Vascular Endothelial Growth

Factor and Metabolic Switches Hexokinase 2 and Pyruvate Dehydrogenase Kinase 1. *Mol Cell Biol* **2007**, *27*, 7381–7393, doi:10.1128/MCB.00440-07.

164. Hung, C.-L.; Wang, L.-Y.; Yu, Y.-L.; Chen, H.-W.; Srivastava, S.; Petrovics, G.; Kung, H.-J. A Long Noncoding RNA Connects C-Myc to Tumor Metabolism. *Proc Natl Acad Sci U S A* **2014**, *111*, 18697–18702, doi:10.1073/pnas.1415669112.

165. Zhang, P.; Cao, L.; Fan, P.; Mei, Y.; Wu, M. LncRNA-MIF, a c-Myc-Activated Long Non-Coding RNA, Suppresses Glycolysis by Promoting Fbxw7-Mediated c-Myc Degradation. *EMBO Rep* **2016**, *17*, 1204–1220, doi:10.15252/embr.201642067.

166. Li, Y.; Wu, C. LINC00261/MicroRNA-550a-3p/SDPR Axis Affects the Biological Characteristics of Breast Cancer Stem Cells. *IUBMB Life* **2021**, *73*, 188–201, doi:10.1002/iub.2416.

167. Wang, X.; Gao, X.; Tian, J.; Zhang, R.; Qiao, Y.; Hua, X.; Shi, G. LINC00261 Inhibits Progression of Pancreatic Cancer by Down-Regulating MiR-23a-3p. *Arch Biochem Biophys* **2020**, *689*, 108469, doi:10.1016/j.abb.2020.108469.

168. Fang, Q.; Sang, L.; Du, S. Long Noncoding RNA LINC00261 Regulates Endometrial Carcinoma Progression by Modulating MiRNA/FOXO1 Expression. *Cell Biochem Funct* **2018**, *36*, 323–330, doi:10.1002/cbf.3352.

169. Li, X.; Li, J.; Lu, P.; Li, M. LINC00261 Relieves the Progression of Sepsis-Induced Acute Kidney Injury by Inhibiting NF-KB Activation through Targeting the MiR-654-5p/SOCS3 Axis. *J Bioenerg Biomembr* **2021**, *53*, 129–137, doi:10.1007/s10863-021-09874-8.

170. Zou, L.; He, H.; Li, Z.; Chen, O.; Jia, X.; Zhang, H. Long Noncoding RNA LINC00261 Upregulates ITIH5 to Impair Tumorigenic Ability of Pancreatic Cancer Stem Cells. *Cell Death Discov* **2021**, *7*, 220, doi:10.1038/s41420-021-00575-0.

171. Liu, S.; Zheng, Y.; Zhang, Y.; Zhang, J.; Xie, F.; Guo, S.; Gu, J.; Yang, J.; Zheng, P.; Lai, J.; et al. Methylation-Mediated LINC00261 Suppresses Pancreatic Cancer Progression by Epigenetically Inhibiting c-Myc Transcription. *Theranostics* **2020**, *10*, 10634–10651, doi:10.7150/thno.44278.

172. Chen, T.; Lei, S.; Zeng, Z.; Zhang, J.; Xue, Y.; Sun, Y.; Lan, J.; Xu, S.; Mao, D.; Guo, B. Linc00261 Inhibits Metastasis and the WNT Signaling Pathway of Pancreatic Cancer by Regulating a MiR-552-5p/FOXO3 Axis. *Oncol Rep* **2020**, *43*, 930–942, doi:10.3892/or.2020.7480.

173. Cheng, D.; Jiang, S.; Chen, J.; Li, J.; Ao, L.; Zhang, Y. Upregulated Long Noncoding RNA Linc00261 in Pre-Eclampsia and Its Effect on Trophoblast Invasion and Migration via Regulating MiR-558/TIMP4 Signaling Pathway. *J Cell Biochem* **2019**, *120*, 13243–13253, doi:10.1002/jcb.28598.

174. Ma, D.; Wei, J.; Chen, S.; Wang, H.; Ning, L.; Luo, S.-H.; Liu, C.-L.; Song, G.; Yao, Q. Fucoidan Inhibits the Progression of Hepatocellular Carcinoma via Causing LncRNA LINC00261 Overexpression. *Front Oncol* **2021**, *11*, 653902, doi:10.3389/fonc.2021.653902.

175. Yang, B.; Ma, H.; Bian, Y. LINC00261 Inhibits Esophageal Cancer Radioresistance by Down-Regulating MicroRNA-552-3p and Promoting DIRAS1. *Cancer Manag Res* **2021**, *13*, 8559–8573, doi:10.2147/CMAR.S332640.

176. Jiang, C.; Zhao, Q.; Wang, C.; Peng, M.; Hao, G.; Liu, Z.; Fu, W.; Zhao, K. Downregulation of Long Noncoding RNA LINC00261 Attenuates Myocardial Infarction through the MiR-522-3p/Trinucleotide Repeat-Containing Gene 6a (TNRC6A) Axis. *Cardiovasc Ther* **2021**, *2021*, 6628194, doi:10.1155/2021/6628194.

177. Yan, D.; Liu, W.; Liu, Y.; Luo, M. LINC00261 Suppresses Human Colon Cancer Progression via Sponging MiR-324-3p and Inactivating the Wnt/β-Catenin Pathway. *J Cell Physiol* **2019**, *234*, 22648–22656, doi:10.1002/jcp.28831.

178. Wang, L.; Wang, X.; Yan, P.; Liu, Y.; Jiang, X. LINC00261 Suppresses Cisplatin Resistance of Esophageal Squamous Cell Carcinoma Through MiR-545-3p/MT1M Axis. *Front Cell Dev Biol* **2021**, *9*, 687788, doi:10.3389/fcell.2021.687788.

179. Han, G.; Guo, Q.; Ma, N.; Bi, W.; Xu, M.; Jia, J. Apatinib Inhibits Cell Proliferation and Migration of Osteosarcoma via Activating LINC00261/MiR-620/PTEN Axis. *Cell Cycle* **2021**, *20*, 1785–1798, doi:10.1080/15384101.2021.1949132.

180. Zhang, R.; Li, Y.; Liu, X.; Qin, S.; Guo, B.; Chang, L.; Huang, L.; Liu, S. FOXO3a-Mediated Long Non-Coding RNA LINC00261 Resists Cardiomyocyte Hypoxia/Reoxygenation Injury via Targeting MiR23b-3p/NRF2 Axis. *J Cell Mol Med* **2020**, *24*, 8368–8378, doi:10.1111/jcmm.15292.

181. Zou, J.; Pei, X.; Xing, D.; Wu, X.; Chen, S. LINC00261 Elevation Inhibits Angiogenesis and Cell Cycle Progression of Pancreatic Cancer Cells by Upregulating SCP2 via Targeting FOXP3. *J Cell Mol Med* **2021**, *25*, 9826–9836, doi:10.1111/jcmm.16930.

182. Llovet, J.M.; Kelley, R.K.; Villanueva, A.; Singal, A.G.; Pikarsky, E.; Roayaie, S.; Lencioni, R.; Koike, K.; Zucman-Rossi, J.; Finn, R.S. Hepatocellular Carcinoma. *Nat Rev Dis Primers* **2021**, *7*, 1–28, doi:10.1038/s41572-020-00240-3.

183. Smekalova, E.M.; Kotelevtsev, Y.V.; Leboeuf, D.; Shcherbinina, E.Y.; Fefilova, A.S.; Zatsepin, T.S.; Koteliansky, V. LncRNA in the Liver: Prospects for Fundamental Research and Therapy by RNA Interference. *Biochimie* **2016**, *131*, 159–172, doi:10.1016/j.biochi.2016.06.007.

184. Zhang, H.-F.; Li, W.; Han, Y.-D. LINC00261 Suppresses Cell Proliferation, Invasion and Notch Signaling Pathway in Hepatocellular Carcinoma. *Cancer Biomark* **2018**, *21*, 575–582, doi:10.3233/CBM-170471.

185. Sui, J.; Miao, Y.; Han, J.; Nan, H.; Shen, B.; Zhang, X.; Zhang, Y.; Wu, Y.; Wu, W.; Liu, T.; et al. Systematic Analyses of a Novel LncRNA-Associated Signature as the Prognostic Biomarker for Hepatocellular Carcinoma. *Cancer Med* **2018**, *7*, 3240–3256, doi:10.1002/cam4.1541.

186. Chen, Z.; Xiang, L.; Huang, Y.; Fang, Y.; Li, X.; Yang, D. Expression of long noncoding RNA linc00261 in hepatocellular carcinoma and its association with postoperative outcomes. *Nan Fang Yi Ke Da Xue Xue Bao* **2018**, *38*, 1179–1186, doi:10.3969/j.issn.1673-4254.2018.10.05.

187. Jiang, W.; Liu, Y.; Liu, R.; Zhang, K.; Zhang, Y. The LncRNA DEANR1 Facilitates Human Endoderm Differentiation by Activating FOXA2 Expression. *Cell Rep* **2015**, *11*, 137–148, doi:10.1016/j.celrep.2015.03.008.

188. Kuo, C.-C.; Hänzelmann, S.; Sentürk Cetin, N.; Frank, S.; Zajzon, B.; Derks, J.-P.; Akhade, V.S.; Ahuja, G.; Kanduri, C.; Grummt, I.; et al. Detection of RNA-DNA Binding Sites in Long Noncoding RNAs. *Nucleic Acids Res* **2019**, *47*, e32, doi:10.1093/nar/gkz037.

189. Bülow, M.H.; Aebersold, R.; Pankratz, M.J.; Jünger, M.A. The Drosophila FoxA Ortholog Fork Head Regulates Growth and Gene Expression Downstream of Target of Rapamycin. *PLoS One* **2010**, *5*, e15171, doi:10.1371/journal.pone.0015171.

190. Mazin, P.; Xiong, J.; Liu, X.; Yan, Z.; Zhang, X.; Li, M.; He, L.; Somel, M.; Yuan, Y.; Phoebe Chen, Y.-P.; et al. Widespread Splicing Changes in Human Brain Development and Aging. *Mol Syst Biol* **2013**, *9*, 633, doi:10.1038/msb.2012.67.

191. Ulashchik, E.A.; Martynenko-Makaev, Y.V.; Akhlamionok, T.P.; Melnik, D.M.; Shmanai, V.V.; Zatsepin, T.S. Synthesis of GalNAc-Oligonucleotide Conjugates Using GalNAc Phosphoramidite and Triple-GalNAc CPG Solid Support. In *Design and Delivery of SiRNA Therapeutics*; Ditzel, H.J., Tuttolomondo, M., Kauppinen, S., Eds.; Methods in Molecular Biology; Springer US: New York, NY, 2021; pp. 101–118 ISBN 978-1-07-161298-9.

192. Bogorad, R.L.; Yin, H.; Zeigerer, A.; Nonaka, H.; Ruda, V.M.; Zerial, M.; Anderson, D.G.; Koteliansky, V. Nanoparticle-Formulated SiRNA Targeting

Integrins Inhibits Hepatocellular Carcinoma Progression in Mice. *Nat Commun* **2014**, *5*, 3869, doi:10.1038/ncomms4869.

193. Mitchell, C.; Willenbring, H. A Reproducible and Well-Tolerated Method for 2/3 Partial Hepatectomy in Mice. *Nat Protoc* **2008**, *3*, 1167–1170, doi:10.1038/nprot.2008.80.
194. Kramer, M.F. Stem-Loop RT-QPCR for MiRNAs. *Curr Protoc Mol Biol* **2011**, *Chapter 15*, Unit 15.10, doi:10.1002/0471142727.mb1510s95.
195. Ferreira, T.; Rasband, W. ImageJ User Guide. 198.
196. PANTHER Available online: http://www.pantherdb.org/ (accessed on 11 May 2022).
197. Kulak, N.A.; Pichler, G.; Paron, I.; Nagaraj, N.; Mann, M. Minimal, Encapsulated Proteomic-Sample Processing Applied to Copy-Number Estimation in Eukaryotic Cells. *Nat Methods* **2014**, *11*, 319–324, doi:10.1038/nmeth.2834.
198. Kovalchuk, S.I.; Jensen, O.N.; Rogowska-Wrzesinska, A. FlashPack: Fast and Simple Preparation of Ultrahigh-Performance Capillary Columns for LC-MS*. *Mol Cell Proteomics* **2019**, *18*, 383–390, doi:10.1074/mcp.TIR118.000953.
199. Tyanova, S.; Temu, T.; Cox, J. The MaxQuant Computational Platform for Mass Spectrometry-Based Shotgun Proteomics. *Nat Protoc* **2016**, *11*, 2301–2319, doi:10.1038/nprot.2016.136.
200. Tyanova, S.; Temu, T.; Sinitcyn, P.; Carlson, A.; Hein, M.Y.; Geiger, T.; Mann, M.; Cox, J. The Perseus Computational Platform for Comprehensive Analysis of (Prote)Omics Data. *Nat Methods* **2016**, *13*, 731–740, doi:10.1038/nmeth.3901.

201. LIPID MAPS Available online: https://www.lipidmaps.org/ (accessed on 15 June 2022).

202. Human Metabolome Database Available online: https://hmdb.ca/ (accessed on 15 June 2022).

203. Goracci, L.; Tortorella, S.; Tiberi, P.; Pellegrino, R.M.; Di Veroli, A.; Valeri, A.; Cruciani, G. Lipostar, a Comprehensive Platform-Neutral Cheminformatics Tool for Lipidomics. *Anal. Chem.* **2017**, *89*, 6257–6264, doi:10.1021/acs.analchem.7b01259.

204. Korotkevich, G.; Sukhov, V.; Sergushichev, A. Fast Gene Set Enrichment Analysis. *bioRxiv* **2019**, doi:10.1101/060012,.

205. Kanehisa, M.; Goto, S. KEGG: Kyoto Encyclopedia of Genes and Genomes. *Nucleic Acids Research* **2000**, *28*, 27–30, doi:10.1093/nar/28.1.27.

206. Frolkis, A.; Knox, C.; Lim, E.; Jewison, T.; Law, V.; Hau, D.D.; Liu, P.; Gautam, B.; Ly, S.; Guo, A.C.; et al. SMPDB: The Small Molecule Pathway Database. *Nucleic Acids Research* **2010**, *38*, D480–D487, doi:10.1093/nar/gkp1002.

207. Xia, J.; Psychogios, N.; Young, N.; Wishart, D.S. MetaboAnalyst: A Web Server for Metabolomic Data Analysis and Interpretation. *Nucleic Acids Research* **2009**, *37*, W652–W660, doi:10.1093/nar/gkp356.

208. Zou, H.; Hastie, T.; Tibshirani, R. Sparse Principal Component Analysis. *Journal of Computational and Graphical Statistics* **2006**, *15*, 265–286, doi:10.1198/106186006X113430.

209. Rohart, F.; Gautier, B.; Singh, A.; Lê Cao, K.-A. MixOmics: An R Package for 'omics Feature Selection and Multiple Data Integration. *PLoS Comput Biol* **2017**, *13*, e1005752–e1005752, doi:10.1371/journal.pcbi.1005752.

210. Addgene: Plasmid Cloning by Restriction Enzyme Digest (with Protocols) Available online: https://www.addgene.org/protocols/subcloning/ (accessed on 7 July 2022).

211. Oliveros, J.C. Venny. An Interactive Tool for Comparing Lists with Venn's Diagrams. Available online: https://bioinfogp.cnb.csic.es/tools/venny/ (accessed on 11 May 2022).

212. Sergeeva, O.; Sviridov, E.; Zatsepin, T. Noncoding RNA in Liver Regeneration—From Molecular Mechanisms to Clinical Implications. *Semin Liver Dis* **2020**, *40*, 70–83, doi:10.1055/s-0039-1693513.

213. Mus Musculus Annotation Report Available online: https://www.ncbi.nlm.nih.gov/genome/annotation_euk/Mus_musculus/109/ (accessed on 15 June 2022).

214. Mus_musculus - Ensembl Genome Browser 106 Available online: https://www.ensembl.org/Mus_musculus/Info/Index?db=core (accessed on 15 June 2022).

215. Fausto, N.; Campbell, J.S. The Role of Hepatocytes and Oval Cells in Liver Regeneration and Repopulation. *Mechanisms of Development* **2003**, *120*, 117–130, doi:10.1016/S0925-4773(02)00338-6.

216. Mehlem, A.; Hagberg, C.E.; Muhl, L.; Eriksson, U.; Falkevall, A. Imaging of Neutral Lipids by Oil Red O for Analyzing the Metabolic Status in Health and Disease. *Nat Protoc* **2013**, *8*, 1149–1154, doi:10.1038/nprot.2013.055.

217. Chen, L.; Chen, X.-W.; Huang, X.; Song, B.-L.; Wang, Y.; Wang, Y. Regulation of Glucose and Lipid Metabolism in Health and Disease. *Sci. China Life Sci.* **2019**, *62*, 1420–1458, doi:10.1007/s11427-019-1563-3.

218. Norton, L.; Shannon, C.; Gastaldelli, A.; DeFronzo, R.A. Insulin: The Master Regulator of Glucose Metabolism. *Metabolism* **2022**, *129*, 155142, doi:10.1016/j.metabol.2022.155142.

219. Gallagher, E.J.; LeRoith, D. The Proliferating Role of Insulin and Insulin-like Growth Factors in Cancer. *Trends Endocrinol Metab* **2010**, *21*, 610–618, doi:10.1016/j.tem.2010.06.007.

220. Ge, D.; Dauchy, R.T.; Liu, S.; Zhang, Q.; Mao, L.; Dauchy, E.M.; Blask, D.E.; Hill, S.M.; Rowan, B.G.; Brainard, G.C.; et al. Insulin and IGF1 Enhance IL-17-Induced Chemokine Expression through a GSK3B-Dependent Mechanism: A New Target for Melatonin's Anti-Inflammatory Action. *Journal of Pineal Research* **2013**, *55*, 377–387, doi:10.1111/jpi.12084.

221. Wang, B.; Hsu, S.; Frankel, W.; Ghoshal, K.; Jacob, S.T. Stat3-Mediated Activation of MiR-23a Suppresses Gluconeogenesis in Hepatocellular Carcinoma by Downregulating G6PC and PGC-1α. *Hepatology* **2012**, *56*, 186–197, doi:10.1002/hep.25632.

222. Manokawinchoke, J.; Nattasit, P.; Thongngam, T.; Pavasant, P.; Tompkins, K.A.; Egusa, H.; Osathanon, T. Indirect Immobilized Jagged1 Suppresses Cell Cycle Progression and Induces Odonto/Osteogenic Differentiation in Human Dental Pulp Cells. *Scientific Reports* **2017**, *7*, 10124, doi:10.1038/s41598-017-10638-x.

223. Pancewicz Joanna; Taylor John M.; Datta Abhik; Baydoun Hicham H.; Waldmann Thomas A.; Hermine Olivier; Nicot Christophe Notch Signaling Contributes to Proliferation and Tumor Formation of Human T-Cell Leukemia Virus Type 1–Associated Adult T-Cell Leukemia. *Proceedings of the National Academy of Sciences* **2010**, *107*, 16619–16624, doi:10.1073/pnas.1010722107.

224. Luedde, T.; Schwabe, R.F. NF-KB in the Liver—Linking Injury, Fibrosis and Hepatocellular Carcinoma. *Nat Rev Gastroenterol Hepatol* **2011**, *8*, 108–118, doi:10.1038/nrgastro.2010.213.

225. Nagarajan, S.R.; Paul-Heng, M.; Krycer, J.R.; Fazakerley, D.J.; Sharland, A.F.; Hoy, A.J. Lipid and Glucose Metabolism in Hepatocyte Cell Lines and Primary Mouse Hepatocytes: A Comprehensive Resource for in Vitro Studies of Hepatic Metabolism. *American Journal of Physiology-Endocrinology and Metabolism* **2019**, *316*, E578–E589, doi:10.1152/ajpendo.00365.2018.

226. Liang, X.-H.; Sun, H.; Nichols, J.G.; Crooke, S.T. RNase H1-Dependent Antisense Oligonucleotides Are Robustly Active in Directing RNA Cleavage in Both the Cytoplasm and the Nucleus. *Mol Ther* **2017**, *25*, 2075–2092, doi:10.1016/j.ymthe.2017.06.002.

227. Debacker, A.J.; Voutila, J.; Catley, M.; Blakey, D.; Habib, N. Delivery of Oligonucleotides to the Liver with GalNAc: From Research to Registered Therapeutic Drug. *Mol Ther* **2020**, *28*, 1759–1771, doi:10.1016/j.ymthe.2020.06.015.

228. Gupta, R.; Schrooders, Y.; Hauser, D.; van Herwijnen, M.; Albrecht, W.; Ter Braak, B.; Brecklinghaus, T.; Castell, J.V.; Elenschneider, L.; Escher, S.; et al. Comparing in Vitro Human Liver Models to in Vivo Human Liver Using RNA-Seq. *Arch Toxicol* **2021**, *95*, 573–589, doi:10.1007/s00204-020-02937-6.

229. Sergeeva, O.; Abakumova, T.; Kurochkin, I.; Ialchina, R.; Kosyreva, A.; Prikazchikova, T.; Varlamova, V.; Shcherbinina, E.; Zatsepin, T. Level of Murine DDX3 RNA Helicase Determines Phenotype Changes of Hepatocytes In Vitro and In Vivo. *International Journal of Molecular Sciences* **2021**, *22*, 6958, doi:10.3390/ijms22136958.

230. Abike, R.R. Fructose Metabolism and Health Risks. *J Obes Weight Loss Ther* **2015**, *05*, doi:10.4172/2165-7904.1000245.

231. Khitan, Z.; Kim, D.H. Fructose: A Key Factor in the Development of Metabolic Syndrome and Hypertension. *Journal of Nutrition and Metabolism* **2013**, *2013*, 682673, doi:10.1155/2013/682673.

232. Barra, J.; Leucci, E. Probing Long Non-Coding RNA-Protein Interactions. *Frontiers in Molecular Biosciences* **2017**, *4*.

233. Kim, I.; Kwak, H.; Lee, H.K.; Hyun, S.; Jeong, S. β-Catenin Recognizes a Specific RNA Motif in the Cyclooxygenase-2 MRNA 3′-UTR and Interacts with HuR in

Colon Cancer Cells. *Nucleic Acids Res* **2012**, *40*, 6863–6872, doi:10.1093/nar/gks331.

234. Li, X.; Tian, B.-M.; Deng, D.-K.; Liu, F.; Zhou, H.; Kong, D.-Q.; Qu, H.-L.; Sun, L.-J.; He, X.-T.; Chen, F.-M. LncRNA GACAT2 Binds with Protein PKM1/2 to Regulate Cell Mitochondrial Function and Cementogenesis in an Inflammatory Environment. *Bone Res* **2022**, *10*, 29, doi:10.1038/s41413-022-00197-x.

235. Tavares, C.D.J.; Aigner, S.; Sharabi, K.; Sathe, S.; Mutlu, B.; Yeo, G.W.; Puigserver, P. Transcriptome-Wide Analysis of PGC-1α–Binding RNAs Identifies Genes Linked to Glucagon Metabolic Action. *Proc Natl Acad Sci U S A* **2020**, *117*, 22204–22213, doi:10.1073/pnas.2000643117.

236. Wang, Y.; Lu, J.-H.; Wu, Q.-N.; Jin, Y.; Wang, D.-S.; Chen, Y.-X.; Liu, J.; Luo, X.-J.; Meng, Q.; Pu, H.-Y.; et al. LncRNA LINRIS Stabilizes IGF2BP2 and Promotes the Aerobic Glycolysis in Colorectal Cancer. *Mol Cancer* **2019**, *18*, 174, doi:10.1186/s12943-019-1105-0.

237. Lan, X.; Yan, J.; Ren, J.; Zhong, B.; Li, J.; Li, Y.; Liu, L.; Yi, J.; Sun, Q.; Yang, X.; et al. A Novel Long Noncoding RNA Lnc-HC Binds HnRNPA2B1 to Regulate Expressions of Cyp7a1 and Abca1 in Hepatocytic Cholesterol Metabolism. *Hepatology* **2016**, *64*, 58–72, doi:10.1002/hep.28391.

238. Wang, Y.; Xue, K.; Guan, Y.; Jin, Y.; Liu, S.; Wang, Y.; Liu, S.; Wang, L.; Han, L. Long Noncoding RNA LINC00261 Suppresses Cell Proliferation and Invasion and Promotes Cell Apoptosis in Human Choriocarcinoma. *Oncol Res* **2017**, *25*, 733–742, doi:10.3727/096504016X14772362173376.

239. Jones, J.G. Hepatic Glucose and Lipid Metabolism. *Diabetologia* **2016**, *59*, 1098–1103, doi:10.1007/s00125-016-3940-5.